

**COUPLED THERMAL-  
HYDROLOGICAL-MECHANICAL  
PROCESSES IN SALT: HOT  
GRANULAR SALT  
CONSOLIDATION, CONSTITUTIVE  
MODEL AND MICROMECHANICS**

**Fuel Cycle Research & Development**

*Prepared for*  
*US Department of Energy*  
*UFD Campaign*  
*F.D. Hansen, S.J. Bauer,*  
*S.T. Broome*  
*Sandia National Laboratories*  
*G.D. Callahan*  
*RESPEC*  
*November 15, 2012*  
*FCRD-UFD-2012-000422*  
*SAND2012-9893P*



**DISCLAIMER**

This information was prepared as an account of work sponsored by an agency of the U.S. Government. Neither the U.S. Government nor any agency thereof, nor any of their employees, makes any warranty, expressed or implied, or assumes any legal liability or responsibility for the accuracy, completeness, or usefulness, of any information, apparatus, product, or process disclosed, or represents that its use would not infringe privately owned rights. References herein to any specific commercial product, process, or service by trade name, trade mark, manufacturer, or otherwise, does not necessarily constitute or imply its endorsement, recommendation, or favoring by the U.S. Government or any agency thereof. The views and opinions of authors expressed herein do not necessarily state or reflect those of the U.S. Government or any agency thereof.

Sandia National Laboratories is a multi-program laboratory managed and operated by Sandia Corporation, a wholly owned subsidiary of Lockheed Martin Corporation, for the U.S. Department of Energy's National Nuclear Security Administration under contract DE-AC04-94AL85000.

**FCT Quality Assurance Program Document**

**Appendix E  
FCT Document Cover Sheet**

Name/Title of Deliverable/Milestone Work Package Title and Number Work Package WBS Number Responsible Work Package Manager	M2FT-12SN0806081 Coupled Thermal-Hydrological-Mechanical Processes in Salt: Hot Granular Salt Consolidation, Constitutive Model and Micromechanics DR Salt R&D FT-13SN081803 1.02.08.18 Christi Leigh <i>Robert MacKinnon for</i> (Name/Signature)
---	--

Date Submitted November 15, 2012

Quality Rigor Level for Deliverable/Milestone	<input checked="" type="checkbox"/> QRL-3	<input type="checkbox"/> QRL-2	<input type="checkbox"/> QRL-1 <input type="checkbox"/> Nuclear Data	<input type="checkbox"/> N/A*
---	---	--------------------------------	---	-------------------------------

This deliverable was prepared in accordance with Sandia National Laboratories  
(Participant/National Laboratory Name)

QA program which meets the requirements of  
 DOE Order 414.1     NQA-1-2000

**This Deliverable was subjected to:**

Technical Review

**Technical Review (TR)**

**Review Documentation Provided**

- Signed TR Report or,
- Signed TR Concurrence Sheet or,
- Signature of TR Reviewer(s) below

**Name and Signature of Reviewers**

Robert J. MacKinnon, Manager, SNL

*Robert MacKinnon*

Peer Review

**Peer Review (PR)**

**Review Documentation Provided**

- Signed PR Report or,
- Signed PR Concurrence Sheet or,
- Signature of PR Reviewer(s) below

\*Note: In some cases there may be a milestone where an item is being fabricated, maintenance is being performed on a facility, or a document is being issued through a formal document control process where it specifically calls out a formal review of the document. In these cases, documentation (e.g., inspection report, maintenance request, work planning package documentation or the documented review of the issued document through the document control process) of the completion of the activity along with the Document Cover Sheet is sufficient to demonstrate achieving the milestone. QRL for such milestones may be also be marked N/A in the work package provided the work package clearly specifies the requirement to use the Document Cover Sheet and provide supporting documentation.

## SUMMARY

Design, analysis and performance assessment of potential salt repositories for heat-generating nuclear waste require knowledge of thermal, mechanical, and fluid transport properties of reconsolidating granular salt. Mechanical properties of crushed salt are functions of porosity which decreases as the surrounding salt creeps inward and compresses granular salt within the rooms, drifts or shafts. These central phenomena have been documented extensively at ambient temperatures but only limited data include excursions to 100°C. Heat-generating nuclear waste is anticipated to result in higher temperatures, necessitating extension of both the database and model capabilities to elevated temperature regimes. The research reported here addresses granular salt reconsolidation from three vantage points: laboratory testing, modeling, and petrofabrics. The experimental data 1) provide greater insight and understanding into the role of elevated temperature and pressure regimes on physical properties of reconsolidated crushed salt, 2) can supplement an existing database used to develop a reconsolidation constitutive model and 3) provide data for model evaluation. The constitutive model discussed in this report accounts for the effects of moisture through pressure solution and dislocation creep, with both terms dependent on effective stress to account for the effects of porosity. Microscopy techniques were used to examine the substructures after consolidation to identify the micro-mechanisms activated at these temperatures and pressures. This research provides significant insight into granular salt consolidation at elevated temperature.

In the laboratory, mine-run salt from the Waste Isolation Pilot Program was first dried at 105°C until no further weight loss occurred. Right-circular cylindrical sample assemblies of unconsolidated granular salt with initial porosities of ~ 40%, nominally 10 cm in diameter and 17.5 cm in length, were jacketed in malleable lead tubing. Samples were placed in a pressure vessel and maintained at test temperatures of 100, 175 or 250°C. Samples were vented to the atmosphere during the entire test procedure to minimize or prevent build-up of pore pressure. In hydrostatic tests, confining pressure was increased to 20 Mega Pascal with periodic unload/reload loops implemented to determine bulk modulus. Volume strain increased with increasing temperature. In shear tests, axial stress was superimposed so that the granular salt was subjected to a differential stress. As axial load was applied, periodic unload/reload loops were conducted and used to determine elastic modulus and lateral strain ratio. At predetermined differential stress levels, conditions were held constant to measure creep consolidation. At these test conditions the creep rate (rate of deformation under constant stress) increased with increasing temperature and stress and decreased as porosity decreased.

To model the mechanical behavior of reconsolidating granular salt in a repository setting, a constitutive model was developed to capture the major deformation components. The constitutive model includes nonlinear elastic and creep consolidation components. Upon complete consolidation, the crushed-salt model reproduces the multimechanism deformation model typically used for intact salt. Parameter values for the model were determined through nonlinear least-squares model fitting to the experimental database. Using the fitted parameter values, the constitutive model was validated against constant strain-rate tests, which is a load path outside of the laboratory experimental database. The database encompasses predominately room temperature tests; however, eight short duration isostatic/hydrostatic (both terms are used synonymously in this document) tests were conducted up to temperatures of 100°C. Additional

isostatic and shear consolidation tests such as those conducted here, will allow a more complete evaluation of this model at temperatures up to 250°C.

Microstructural observations were made on several of the reconsolidated granular salt specimens deformed at 250°C under hydrostatic-quasistatic, shear-quasistatic, and creep conditions. These test specimens were consolidated from ~40% to approximately 10% porosity, which was estimated from random point counting and mechanical test data. Deformation mechanisms were inferred from microstructural observations made using optical and electron microscopy on fragments of a tested specimen, and polished thin sections and etched cleavage chips from multiple specimens. Extensive deformation was exhibited in the final, low porosity states. Initial porosity was removed by grain boundary sliding with attendant comminution at grain boundaries. Widespread crystal plasticity was manifested in elongated and sinuous grain fabric. Etching techniques highlight heavily deformed grains that exhibit wavy slip band microstructures, and climb recovery processes with an associated minute subgrain size. Free dislocation density was sparse in the highly deformed grains. Despite massive tangles of substructure and hence potentially high internal strain energy, only minor dynamic recrystallization was observed. In addition, despite drying the granular salt to a typically accepted dry condition, sufficient brine apparently remained within the crystal lattice as fluid inclusions to facilitate fluid-assisted diffusional transfer. This research has significant implications for use and performance of granular salt in repository barriers.

## CONTENTS

SUMMARY .....	iv
CONTENTS.....	vi
FIGURES .....	vii
TABLES .....	viii
1 INTRODUCTION.....	4
2 LABORATORY RESULTS .....	7
2.1 Background and Techniques .....	7
2.1.1 Isostatic tests .....	13
2.1.2 Multistage Hydrostatic and Shear (Quasistatic and Creep) Tests .....	15
2.2 Summary and Conclusions.....	21
3 CONSTITUTIVE MODELING .....	22
3.1 Model Temperature Dependencies .....	23
3.2 Comparison with Experiments .....	30
4 MICROMECHANICS .....	34
4.1 Background .....	34
4.1.1 WIPP Shaft Seal Technological Advances .....	35
4.1.2 BAMBUS II Evidence .....	37
4.2 Observational Techniques.....	39
5 RECOMMENDATIONS AND CONCLUSIONS .....	45
6 REFERENCES .....	47
APPENDIX A: Mechanical Property Test Results .....	A-1
FCT-CS-HQ-100-02 .....	A-2
FCT-CS-HQ-175-01 .....	A-3
FCT-CS-HQ-250-02 .....	A-4
FCT-CS-SQ-250-01 .....	A-5
FCT-CS-SQ-250-02 .....	A-7
FCT-CS-CR-250-01 .....	A-8
FCT-CS-CR-175-01 .....	A-9
FCT-CS-CR-175-02 .....	A-11
FCT-CS-CR-100-01 .....	A-12
FCT-CS-CR-250-05 .....	A-14
FCT-CS-CR-100-02 .....	A-15
FCT-CS-CR-100-03 .....	A-17
FCT-CS-HQ-ALL-01 .....	A-18
FCT-CS-HQ-ALL-02 .....	A-19

## FIGURES

Figure 2-1. Schematic of Test Arrangement. ....	9
Figure 2-2. Instrumented Specimen Assembly Pretest.....	10
Figure 2-3. Test Apparatus with Reconsolidated Sample. ....	10
Figure 2-4. Specimen Post Test.....	11
Figure 2-5. Application of Copper Jacket (Left) and After Test (Right).....	12
Figure 2-6. Brine Exiting the Pore Pressure Port at 250°C.....	13
Figure 2-7. Volume Strain Versus Hydrostatic Confining Pressure ( $\sigma_3$ ). ....	14
Figure 2-8. Normalized Density Versus Hydrostatic Confining Pressure ( $\sigma_3$ ).....	14
Figure 2-9. Fractional Density Versus Bulk Modulus, $K$ . ....	15
Figure 2-10. True Lateral Strain Versus Hydrostatic Pressure.....	16
Figure 2-11. Stress-Strain Response for a Typical 250°C Test. ....	17
Figure 2-12. True Strain Versus Time (a) 100°C, (b) 175°C, (c) 250°C.....	19
Figure 2-13. Fractional Density Versus Normalized Young's Modulus. ....	20
Figure 3-1. Normalized Creep Consolidation Temperature Functions. ....	24
Figure 3-2. Normalized M-D Transient Temperature Function. ....	25
Figure 3-3. Log Normalized M-D Steady-State Temperature Functions. ....	27
Figure 3-4. Normalized M-D Transient Temperature Function. ....	27
Figure 3-5. Contributions to the Total Steady-State Strain Rate by Each Mechanism as a Function of Temperature for Effective Stresses of 5, 10, 20, and 25 MPa. ....	29

Figure 3-6. Comparison of Model Predictions to Isostatic Laboratory Test Numbers 2 (100°C), 4 (250°C), and 6 (250°C).....	31
Figure 3-7. Comparison of Model Prediction to the Shear Stages of Laboratory Test Number 18 at 100°C.....	32
Figure 3-8. Comparison of Model Prediction to the Shear Stages of Laboratory Creep Consolidation Test Number 16 at 250°C.....	33
Figure 4-1. Volumetric Strain and Brine Flow Measurements on Reconsolidating Granular Salt.....	36
Figure 4-2. Photograph of the BAMBUS II E Re-excavation.....	38
Figure 4-3. Reconsolidated Salt with 20.7% Porosity.....	39
Figure 4-4. Sawn Samples and an Optical Thick-Thin Section.....	40
Figure 4-5. Extensive Grain Deformation During Reconsolidation at 250°C.....	41
Figure 4-6. Glide of Fluid Inclusions Along Slip Planes 250°C.....	42
Figure 4-7. Etched Cleavage Chips from Samples Consolidated at 250°C.....	42
Figure 4-8. Plasticity Coupled Pressure Solution.....	43
Figure 4-9. Recrystallization.....	44

## TABLES

Table 2-1. Test Matrix for Salt Reconsolidation at Elevated Temperature <sup>1</sup> .....	8
Table 2-2. Summary of Tests Completed.....	12
Table 3-1. Test Matrix for Salt Reconsolidation at Elevated Temperature.....	30

## ACRONYMS

{100}	Miller Indices
BAMBUS	Backfilling and Sealing of Underground Repositories for Radioactive Waste in Salt
FCT	Fuel Cycle Technology
M-D	Multimechanism Deformation
MPa	Mega Pascal
SEM	Scanning Electron Microscopy
TSDE	Thermal Simulation of Drift Emplacement
US	United States
WIPP	Waste Isolation Pilot Plant

# COUPLED THERMAL-HYDROLOGICAL-MECHANICAL PROCESSES IN SALT: HOT GRANULAR SALT CONSOLIDATION, CONSTITUTIVE MODEL AND MICROMECHANICS

## 1 INTRODUCTION

Understanding and predicting the reconsolidation behavior of granular crushed salt is vital to backfilling or sealing nuclear waste repositories in salt. Significant research efforts have attempted to address this recognized need resulting in a long history of crushed salt backfill testing for salt repository applications. Callahan (1999) summarized the constitutive model for room temperature consolidation with application to the shaft seal system at the Waste Isolation Pilot Plant (WIPP). Over the years, salt reconsolidation has been a topic of great interest to international salt repository studies as exemplified by recurring symposia (for example: Aubertin and Hardy, 1996 and Wallner et al., 2007). A preponderance of these studies focused on room temperature experiments, with only a few tests conducted at elevated temperatures up to 100°C. Today there is a renewed national and international interest in salt reconsolidation at elevated temperature, particularly as applied to disposal of heat-generating nuclear waste.

In recognition of the need for this essential research, the United States (US) Department of Energy supported investigations to explore and solidify our understanding of reconsolidation of granular salt under high temperatures. For this purpose, a new experimental procedure for a laboratory study of reconsolidation of salt aggregate was developed, emphasizing testing at elevated temperature. The primary purpose of these experiments is to quantitatively evaluate consolidation as a function of stress and temperature and determine if the results fit the existing constitutive model. An equally important but secondary purpose is to establish the deformational processes by which the salt reconsolidates. Successful completion of these experiments under challenging pressure and temperature regimes required development of advanced geomechanics techniques.

Salt consolidation testing as discussed in this Milestone Report is part of a larger, sequential testing and modeling effort called Salt Disposal Investigations (DOE, 2011). Therefore, this work is closely related to other research tasks including measurements of thermal conductivity as a function of porosity and advanced modeling of thermal-mechanical-hydrological phenomena. These combined efforts are prerequisite studies for high level waste salt repository design, analysis and performance. Indeed, this work will guide planning and interpretation of future field-scale testing or demonstrations that may be pursued.

The following objectives were identified in the test plan (Bauer, 2012) for this research:

- Develop test techniques for geomechanics experiments above 100°C
- Acquire consolidation data for mine-run salt for temperatures up to 250°C
- Assess the impact of dryness on the consolidation process
- Evaluate the micromechanical deformation processes through optical microscopy and scanning electron microscopy (SEM)

- Compare laboratory results at elevated temperature to the well-developed ambient consolidation model

This research accomplished these goals and unveiled some new discoveries, as will be discussed in the subsequent sections.

The salt used in these experiments is called “mine-run,” which means the aggregate was produced during normal mining operations at WIPP (with aggregate pieces greater than 9.5 mm removed). The laboratory studies provide data representing consolidation behavior as a function of stress state and temperatures up to 250<sup>o</sup>C. Observational microscopy techniques were used to document deformational processes for some of the tested samples after completion of testing.

The laboratory test procedures used both hydrostatic (isostatic) and shear stresses to consolidate the mine-run salt. Hydrostatic refers to the application of a uniform or isotropic stress state, while shear stresses involve the superposition of an additional axial stress. Consolidation under shear stress more realistically represents conditions expected in a disposal concept where the roof-to-floor closure would be faster than the rib-to-rib closure.

The laboratory test data were used to evaluate a model for reconsolidation of mine-run granular salt subjected to elevated temperature and repository-relevant stress states. In addition to elevated temperature, hydrostatic pressures up to 20 Mega Pascal (MPa) and stress differences up to 10 MPa were applied. The stresses correspond to in situ stresses encountered at commercial salt mining operations as well as WIPP.

Because of the high temperatures and venting of the samples, the prospect was that the effective pressure-solution redeposition process would be minimized because available and accessible water would be driven off. Further, it was hypothesized that the negative-crystal fluid inclusions within the crystal structure would remain trapped. As will be discussed later in this report, neither hypothesis proved correct, which is a key finding of this research. The idea that drying would occur with an accompanying change of consolidation mechanisms is a potentially important hypothesis relevant to crushed salt in a heat-generating salt repository. Such experimental work was identified to be of great interest to national and international salt repository programs (Hansen and Leigh, 2011).

The reconsolidation model developed by Callahan (1999) is quite sophisticated. It accounts for the effects of moisture through pressure solution and dislocation creep, with both terms dependent on effective stress to account for the effects of porosity. At the limit of zero moisture content, the pressure solution term contributes nothing to the strain rate and at the limit of zero porosity the dislocation creep term becomes equal to the WIPP model for intact salt.

Experimental testing, constitutive modeling, and substructural observations have been completed successfully while managing the high degree of complexity associated with the laboratory investigations. The next three Chapters will summarize results obtained to date. Chapter 2 reports the laboratory procedures, including the challenges associated with this first-of-its-kind testing, and quantitative test results. Chapter 3 discusses the new laboratory results in the context of the current model for salt reconsolidation. Chapter 4 presents perspectives of the reconsolidation mechanisms of this study and other relevant granular salt microstructural evidence. Chapter 5 provides a summary of conclusions and recommendations, with particular emphasis on application to repository science. As with much cutting-edge science, there remain certain areas where additional research could add value. For example, loading variations,

differing stress paths and some repeated load cycles could help quantify results. Additional substructural microscopy could illuminate governing deformational processes at intermediate temperatures. However, the research reported here substantially advances our understanding of granular salt reconsolidation at high temperatures.

## 2 LABORATORY RESULTS

The physical properties of reconsolidating mine-run granular salt are foundational to the science behind generic salt repository design, operation and performance. As noted, there is a renewed national and international interest in salt reconsolidation at elevated temperature, particularly as applied to disposal of heat-generating nuclear waste. Most previous salt reconsolidation studies focused on room temperature deformation, with only a few tests conducted at temperatures up to 100°C. A laboratory test plan (Bauer, 2012) was developed under the Fuel Cycle Technology (FCT) Program to expand our knowledge base. The test plan presents an experimental procedure for a laboratory study of reconsolidation of granular salt, emphasizing testing at elevated temperature. All of the test data discussed in this section is plotted individually in Appendix A. Activities were conducted in accordance with the requirements specified in the FCT Quality Assurance Program Document.

### 2.1 Background and Techniques

A suite of experiments was designed to systematically evaluate the consolidation of crushed salt as a function of stress ( $\sigma$ ) and temperature (T) conditions. Laboratory studies provide consolidation behavior for temperature to 250°C and stress to 20 MPa. Selected tested samples were examined microscopically to document deformational processes by which the salt reconsolidates. Microstructural forensics was applied through optical and scanning electron microscopic techniques to illuminate the deformed substructures.

The test matrix is summarized in Table 1, which lists the test type, stress, temperature conditions, and other test information. Three test types used in this test series are isostatic, shear and shear in combination with creep of right circular cylindrical specimens. Most of the tests had multiple stages, for example, an initial isostatic segment followed by one or more shear and creep consolidation portions. The experimental stages of temperature, pressure, and shear were chosen in that order to successfully parameterize and provide a means to evaluate the constitutive model using a minimum number of tests that still explored the full range of desired temperature, pressure and stress space.

For all tests, jacketed specimens of crushed mine-run salt from the WIPP were dried at 105°C until no further weight loss occurred. Undeformed right-circular cylindrical specimen assemblies of unconsolidated granular salt with initial porosities of ~ 40%, nominally 10 cm in diameter and 17.5 cm in length, were jacketed in malleable soldered lead tubes. Samples were placed in a pressure vessel and kept at test temperatures of 100°, 175° or 250°C and vented to the atmosphere during the entire test procedure.

In isostatic tests, confining pressure is slowly increased at pressurization rates ranging from ~ 0.0005 MPa/sec at the beginning of the test to ~0.0422 MPa/sec near the end of pressurization by pumping at rates of 9.46 mL/min or by advancing the actuator at a rate of 0.00254 cm/sec into the pressure vessel (both pressurization methods increased pressure at equivalent but non-uniform rates). During pressurization, pressure and sample displacement (used to determine strain) are recorded. During the test, at predetermined pressure levels, pressurization is reversed to  $\frac{1}{3}$  to  $\frac{1}{2}$  the previous maximum level, then loading is resumed. This is termed an unload/reload loop; from such a loop the bulk modulus may be determined.

In shear tests, after an isostatic pressure increase to a predetermined level, the axial piston housed in the loading frame is advanced in a quasistatic manner (slowly at a rate of 0.00127

cm/sec actuator displacement rate equivalent to  $\sim 8E-5$ /sec strain rate on a 15.49 cm long sample) until a predetermined stress level (Table 2-1) is attained. At predetermined axial stress levels, axial loading is reversed to  $1/3$  to  $1/2$  the starting differential stress level, then loading is resumed. In this type of unload/reload loop, the elastic Young's modulus and Poisson's ratio may be determined. The specimen is typically held at constant differential stress and allowed to creep until approximately 5% additional axial strain accrues through creep consolidation. At that point, the axial piston is advanced in a quasistatic manner until the second predetermined stress level (Table 2-1) is attained (accompanied by unload/reload loops during loading). The specimen is allowed to creep (and further consolidate) at the higher stress level until approximately 5% additional axial strain is experienced. Then the axial load is reduced to zero, the confining pressure is reduced to zero, and the heating elements are turned off allowing the specimen to cool to ambient temperature.

**Table 2-1. Test Matrix for Salt Reconsolidation at Elevated Temperature<sup>1</sup>**

Test Number	Test Type	T (°C)	Maximum Isostatic Confining Pressure (MPa)	Stress Difference (MPa)	Axial Stress (MPa)	Mean Stress (MPa)	Description
7	Isostatic	250	20.0	0.0	20.0	20.0	Quasistatic
8/9	Isostatic/Shear	250	10.0	10.0	20.0	13.33	Quasistatic
1/10-16	Isostatic/Shear	100	2.5	2.50/5.0	5.0/7.5	3.33/4.17	Quasistatic-Creep
2/11-17	Isostatic/Shear	100	5.0	2.50/5.0	7.5/10.0	5.83/6.67	Quasistatic-Creep
3/12-18	Isostatic/Shear	175	2.5	2.50/5.0	5.0/7.5	3.33/4.17	Quasistatic-Creep
4/13-19	Isostatic/Shear	175	5.0	2.50/5.0	7.5/10.0	5.83/6.67	Quasistatic-Creep
5/14-20	Isostatic/Shear	250	2.5	2.50/5.0	5.0/7.5	3.33/4.17	Quasistatic-Creep
6/15-21	Isostatic/Shear	250	5.0	2.50/5.0	7.5/10.0	5.83/6.67	Quasistatic-Creep

<sup>1</sup>Components of the test number are color keyed to the test type and description.

The experimental process is presented in Bauer (2012) and is briefly outlined herein. The specimen assembly (Figure 2-1) consists of a right circular cylinder of unconsolidated granular salt, nominally 10 cm in diameter and 17.5 cm in length, constrained vertically between specially machined aluminum end caps. The machining of the outer diameter of the end caps enables a metal-metal seal of an outer lead jacket to the end cap. The upper end cap is vented to the atmosphere during the test to prevent buildup of pore pressure. Beveled end plates are placed between the end caps and salt to accommodate the diameter change for the unconsolidated salt portion of the assembly and allow space for the inner lead jacket. A porous metal frit shown in the figure as porous felt metal, is placed below the top end cap to allow fluid migration and venting across the entire specimen top surface area. The outer lead jacket, a soldered lead tube, laterally contains the entire assemble from top to bottom, and isolates the inner lead jacket and

the end caps from the confining medium. The lead is highly malleable and conforms to the shape of the specimen when hydrostatic pressure is applied.

Each assembly is fitted with two high temperature lateral deformation gages (Figure 2-2) affixed near the specimen mid height and oriented approximately orthogonal to one another. The specimen is placed in the pressure vessel (Figure 2-3) by lowering the vessel over the specimen assembly. (Figure 2-3 shows a specimen upon test completion below the pressure vessel.) The pressure vessel is then filled with confining fluid, heated to the test temperature at about 1°C/min to minimize temperature gradients and allow uniform thermal expansion of the unconstrained specimen, and held at test temperature overnight at ambient pressure. At the initiation of the loading portion of the test, the isostatic pressure is increased as described above, followed by the axial force/stress being increased as described above for the shear/creep portion of the test. A reconsolidated specimen in posttest condition is shown in Figure 2-4. Note the significant dimpling of the lead jacket, caused by the presence of local voids and undulations in the granulated salt surface coupled with malleability of the lead jacketing material.

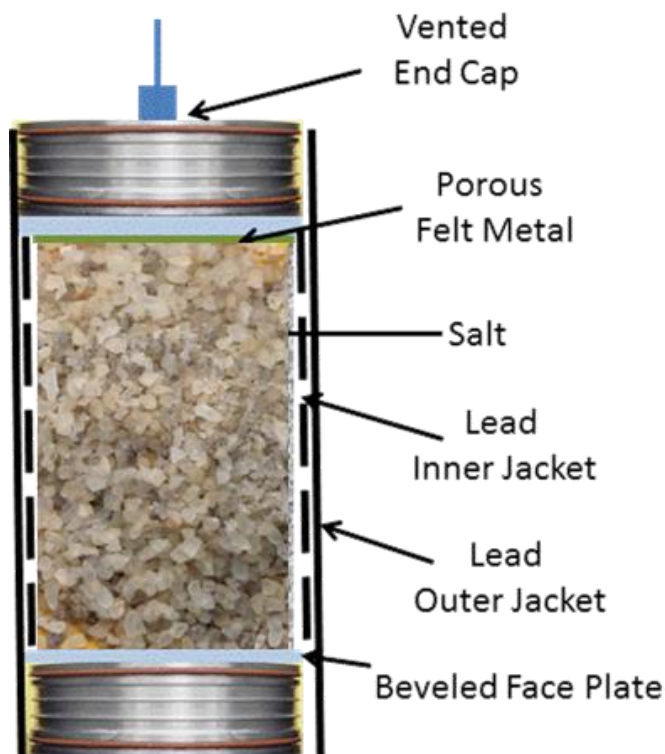
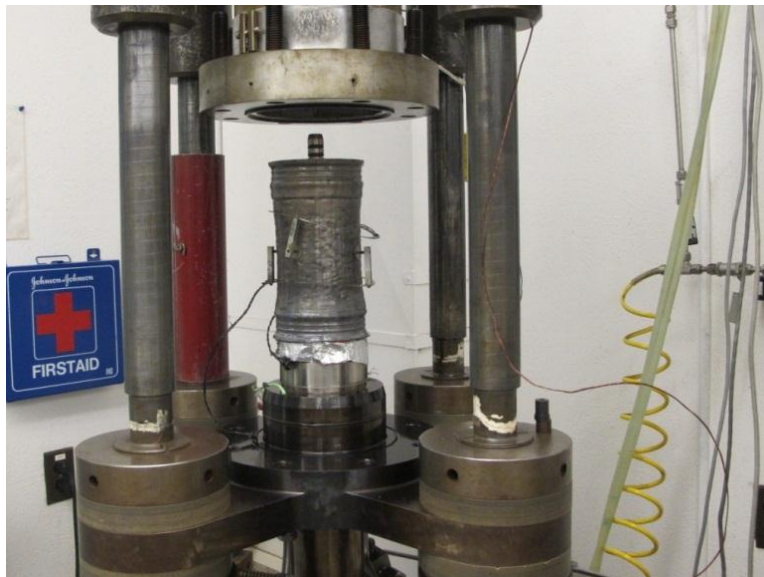


Figure 2-1. Schematic of Test Arrangement.



**Figure 2-2. Instrumented Specimen Assembly Pretest.**



**Figure 2-3. Test Apparatus with Reconsolidated Sample.**



**Figure 2-4. Specimen Post Test.**

Jacket leaks were problematic at 250°C because of extreme consolidation, large volumetric strains, and further softening of the lead jackets. To successfully mitigate the potential for jacket puncture, an intermediate thin copper sheet was placed between lead jackets for 250°C tests as shown in Figure 2-5.

Table 2-2 provides a list of all laboratory tests completed and shows the correspondence of each test with the experimental matrix shown in Table 2-1. The experiments are numbered chronologically and identified with a unique identification number; the total volume strain, normalized density, and confining pressure are presented.

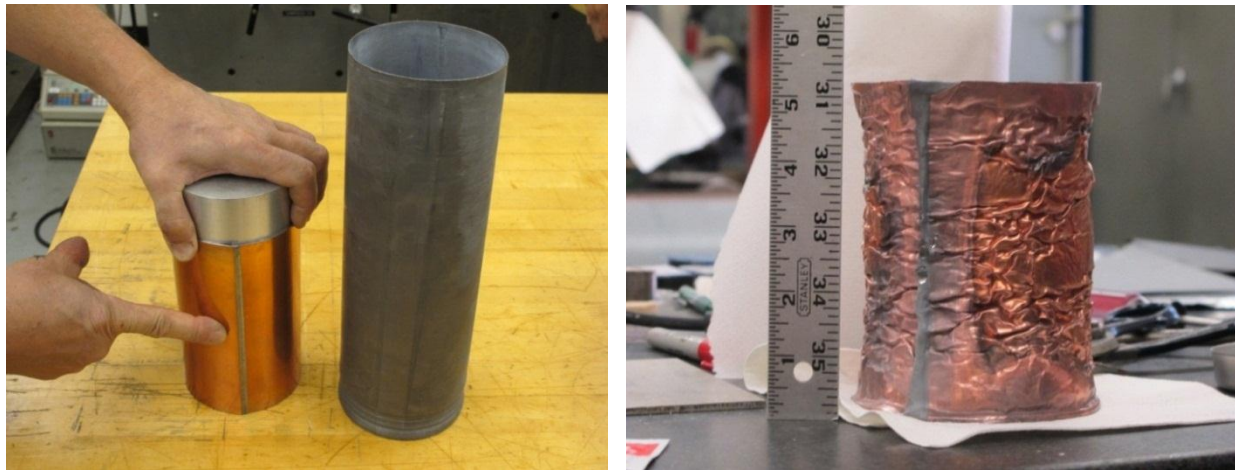


Figure 2-5. Application of Copper Jacket (Left) and After Test (Right).

Table 2-2. Summary of Tests Completed

Test number (Scientific Notebook number sequence)	Date of test	Sample ID	Total Volumetric strain $\varepsilon_v$ (%)	Normalized Density (% of theoretical)	Isostatic Confining pressure obtained (MPa)	Tests satisfied from test matrix (Table 2-1)			
2	6/28/2011	FCT-CS-HQ-100-02	28	79	20	1,2			
3	7/6/2011	FCT-CS-HQ-250-01	29, Leak	78, Leak	5.5	5,6			
4	7/12/2011	FCT-CS-HQ-175-01	35	87	16.6	3,4			
5	1/19/2012	FCT-CS-HQ-175-02	Actuator piston contacted sample at $\sigma_c = 10.3$ MPa						
6	3/15/2012	FCT-CS-HQ-250-02	37	93	20	5,6,7,8			
7	4/4/2012	FCT-CS-SQ-250-01	31, $\sigma_c^*$	84, $\sigma_c^*$	10	8			
8	5/1/2012	FCT-CS-SQ-250-02	37	93	10	9			
9	5/8/2012	FCT-CS-CR-250-01	33	86	2.5	14,20			
10	5/23/2012	FCT-CS-CR-250-02	N/A (breach of confining medium into sample)						
11	6/19/2012	FCT-CS-CR-250-03							
12	6/27/2012	FCT-CS-CR-250-04							
13	7/3/2012	FCT-CS-CR-175-01	31	86	2.5	12,18			
14	7/11/2012	FCT-CS-CR-175-02	32	85	5	13,19			
15	7/23/2012	FCT-CS-CR-100-01	19	73	2.5	10,16 ( $\sigma_D = 2.5$ MPa only)			
16	7/24/2012	FCT-CS-CR-250-05	40	94	5	15,21			
17	7/27/2012	FCT-CS-CR-100-02	26	77	2.5	10,16			
18	8/9/2012	FCT-CS-CR-100-03	33	86	5	11,17			
19	8/22/2012	FCT-CS-CR-175-03	N/A**	N/A**	2.5	12,18 ( $\sigma_D = 5.0$ MPa only)			
20	9/12/2012	FCT-CS-HQ-ALL-01	39	97	20	1,2			
21	10/31/2012	FCT-CS-HQ-ALL-02	35	90	20	3,4			

\*Values obtained after hydrostatic compaction and are not available after the shear stage.

\*\*Data not available at this time.

A noteworthy, perhaps unexpected observation during these tests was the production of brine from the pore pressure port during 250°C tests (Figure 2-6). This occurred during the heating phase of these tests, when the specimen was unconfined.



**Figure 2-6. Brine Exiting the Pore Pressure Port at 250°C.**

### **2.1.1 Isostatic tests**

After the test temperature had stabilized overnight, pressure was increased to 20 MPa and specimen volume change was recorded either through dilatometry or using “on specimen” gages. At all temperatures, the specimens consolidate irreversibly with increasing pressure; the compacting specimen stiffens with increasing pressure. This is clearly shown in Figure 2-7 where volume strain is compared to applied hydrostatic pressure for three tests at successively greater temperatures. As shown, increasing temperature facilitates compaction; i.e. more compaction is observed at a given pressure for greater temperatures. As the crushed salt is forced to compact, its normalized density increases (Figure 2-8). The normalized density is the calculated density during the test divided by the theoretical density of solid salt.

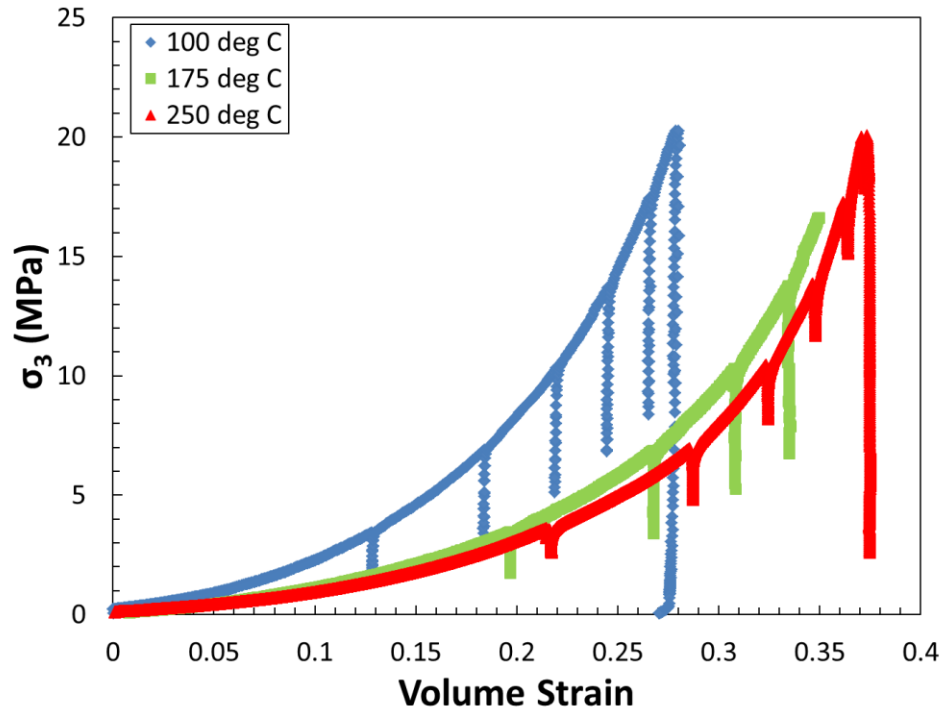


Figure 2-7. Volume Strain Versus Hydrostatic Confining Pressure ( $\sigma_3$ ).

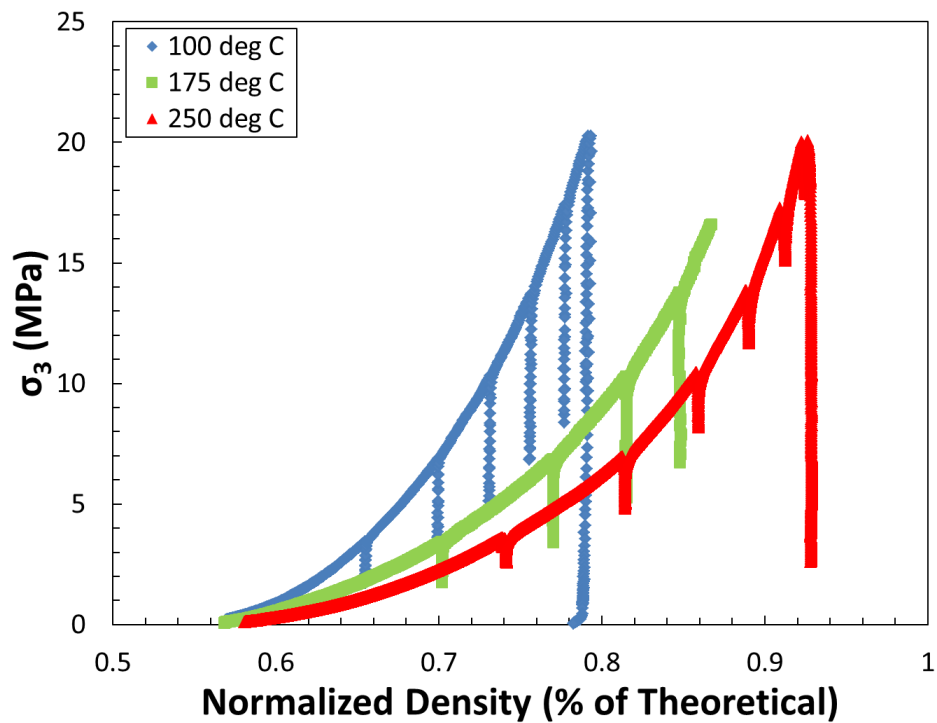


Figure 2-8. Normalized Density Versus Hydrostatic Confining Pressure ( $\sigma_3$ ).

The unload reload loops conducted during each test facilitate determinations of the bulk modulus ( $K$ ) at intervals during the deformation. In Figure 2-9,  $K$  is plotted against the fractional density (the % of theoretical density [2.165 g/cc]).  $K$  is low and insensitive to fractional density increases until a fractional density of ~75% is attained. Near this value of fractional density,  $K$  begins increasing with increasing fractional density to the maximum level observed. These data imply that  $K$  is primarily dependent on fractional density and less dependent on temperature. The maximal values of  $K$ 's are greater than the  $K$  of intact salt, which is a recognized and unresolved issue. The unreasonable calculated values are perhaps the result of the new experimental technique developed during the test series. Also, the rate of unloading/reloading affected the calculated results because the crushed salt was always creeping. Additional data would improve our confidence in the experimental relationships developed.

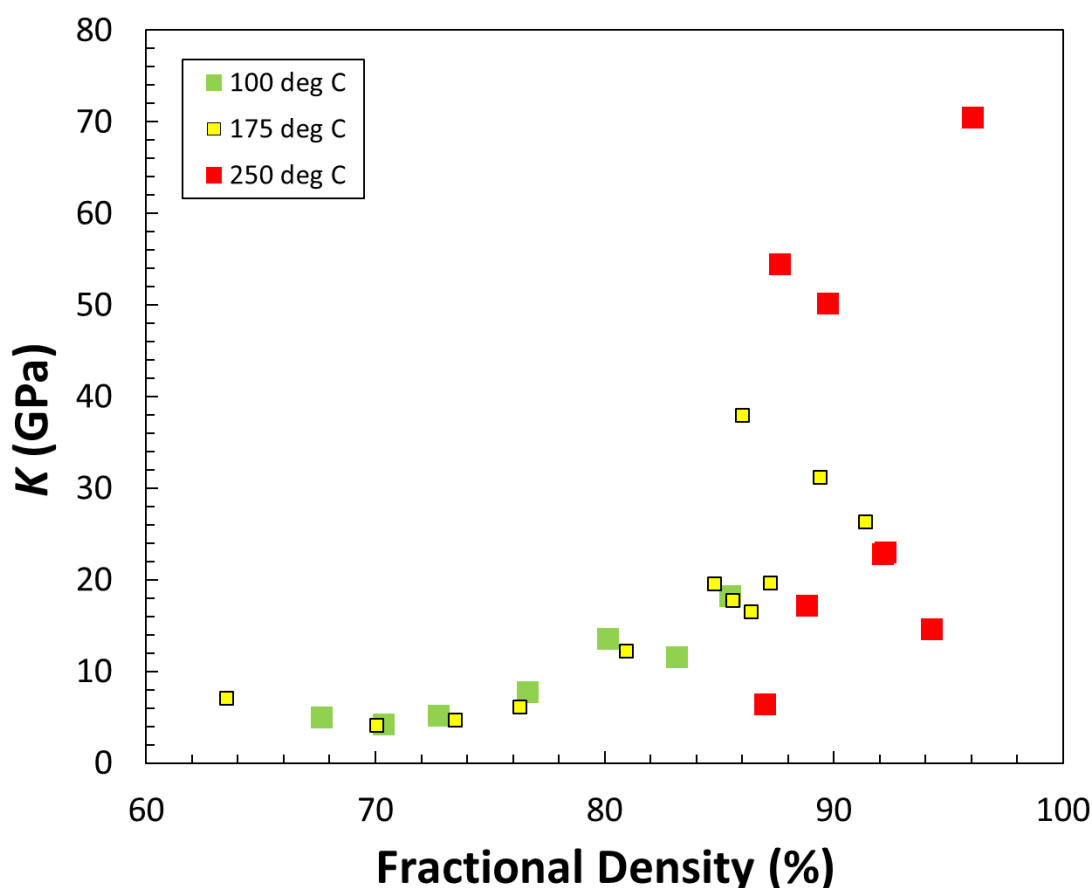


Figure 2-9. Fractional Density Versus Bulk Modulus,  $K$ .

### 2.1.2 Multistage Hydrostatic and Shear (Quasistatic and Creep) Tests

In this section examples of data from multistage tests are presented. After application of hydrostatic confining pressure, axial stress was increased in a quasistatic manner (slowly). Axial and radial displacement measurements were measured for each specimen as a function of time. This allowed axial, lateral and volume strain to be determined. Figure 2-10 shows a lateral strain

versus hydrostatic confining pressure record from a 250°C test. As confining pressure increases, the crushed salt compacts. In all tests, pressure was held constant for a brief time while preparing to apply axial force. This resulted in a small amount of isostatic creep compaction, about 1% in this test.

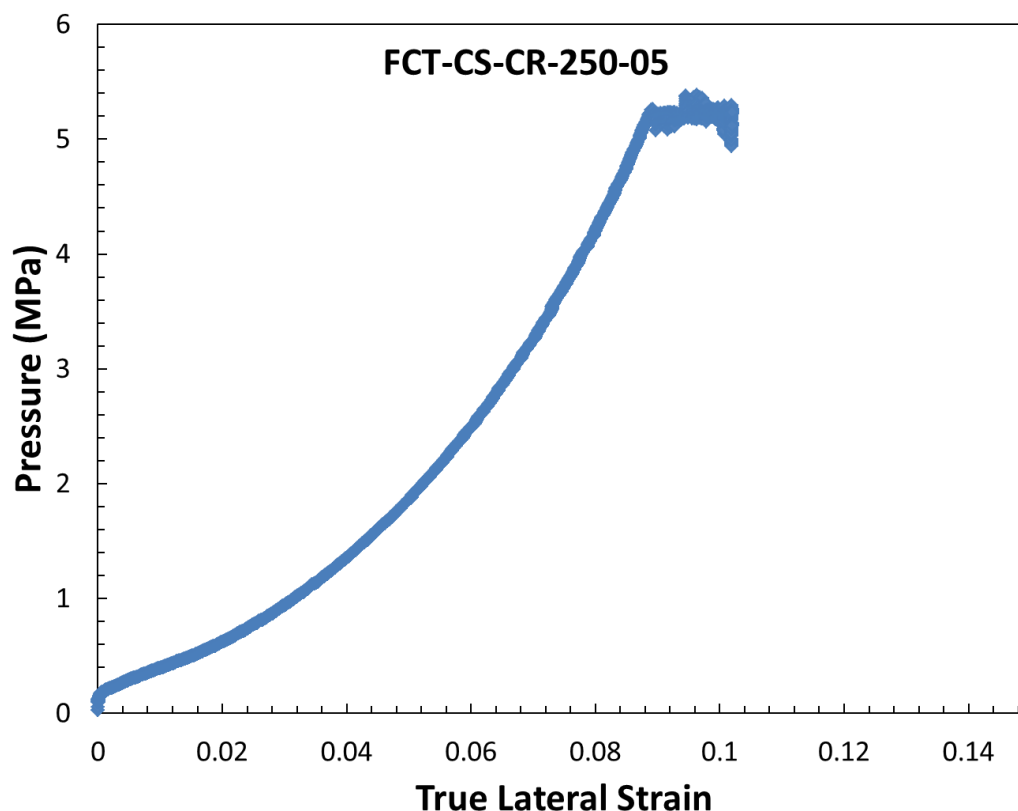


Figure 2-10. True Lateral Strain Versus Hydrostatic Pressure.

In Figure 2-11, the detailed stress-strain response for the differential stress portion of this 250°C test is presented. During the initial axial loading, unload/reload loops are evident; as indicated, elastic moduli and Poisson's ratio are deduced from the axial and lateral strains measured during this portion of the test. This is accomplished through fitting of the unload/reload loops with a best fit line through the unload/reload loop. The zoom view provides insight into data quality, quantity and fidelity. Upon reaching the creep stress, stress levels are held constant. True strains are used due to the large deformations.

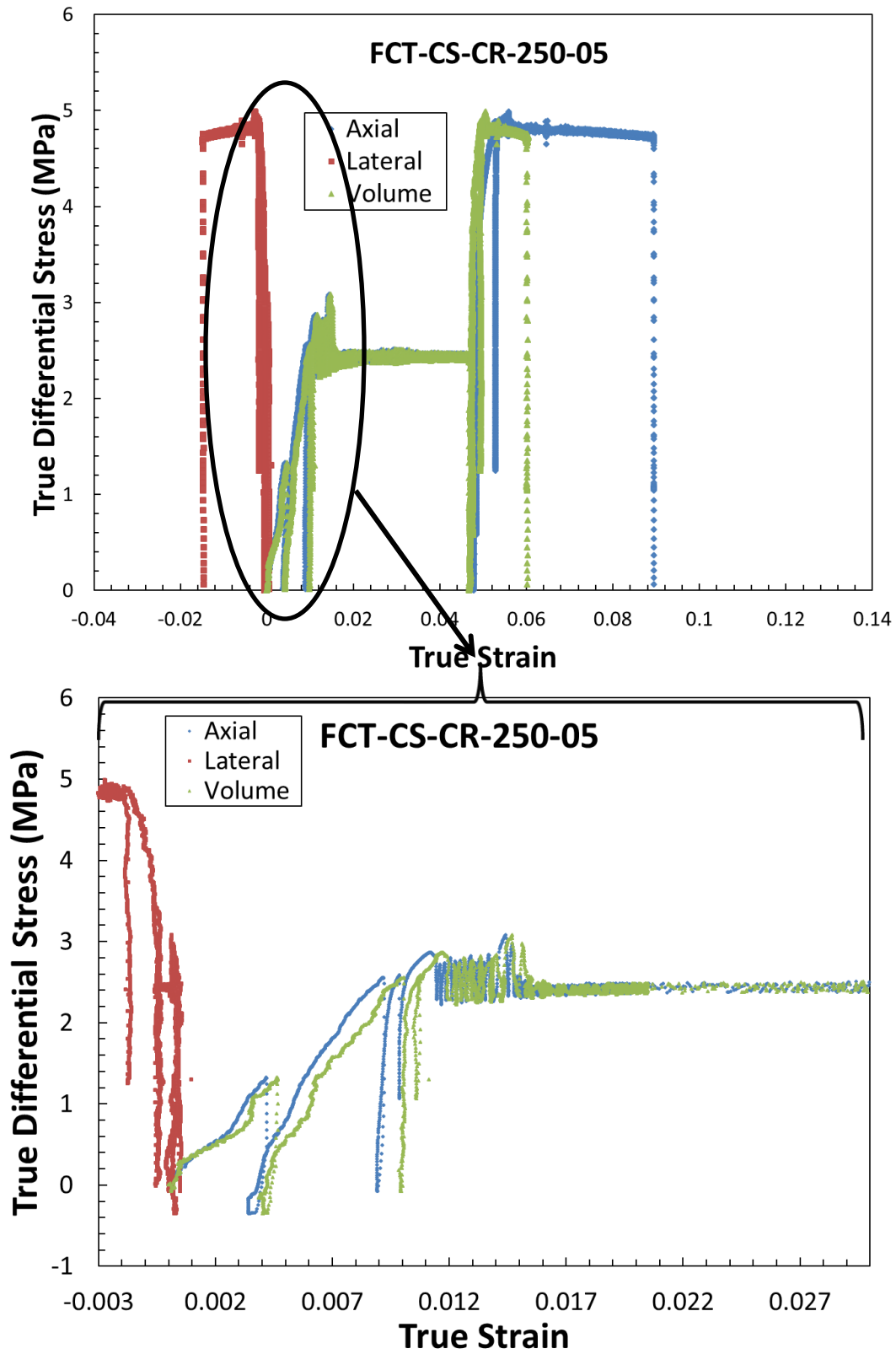
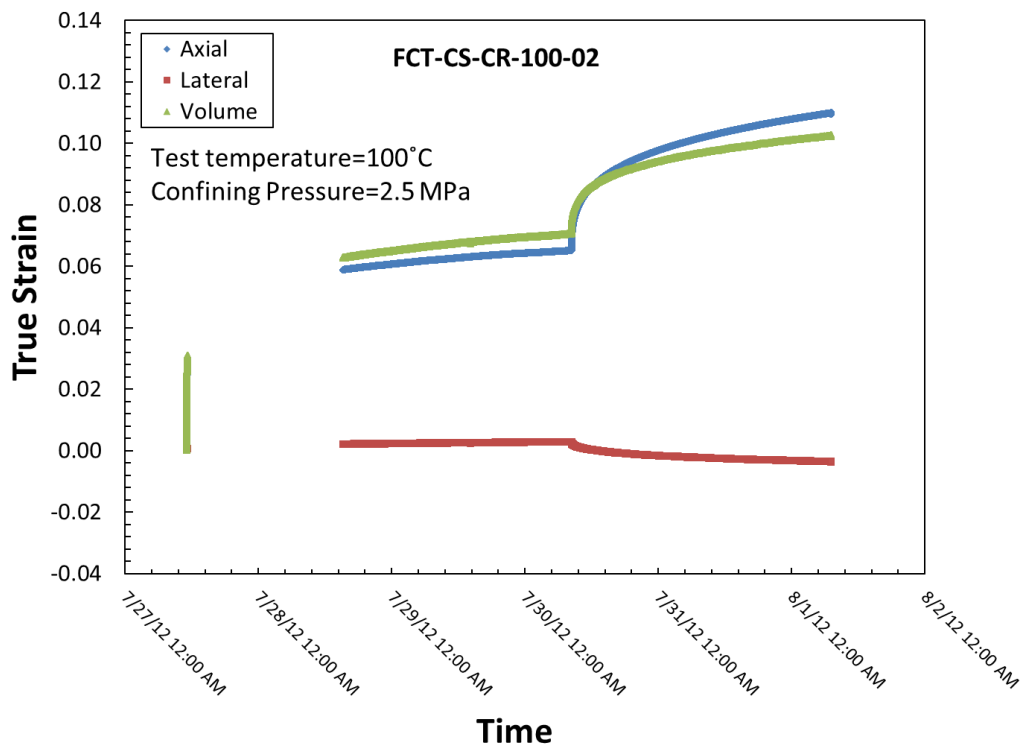
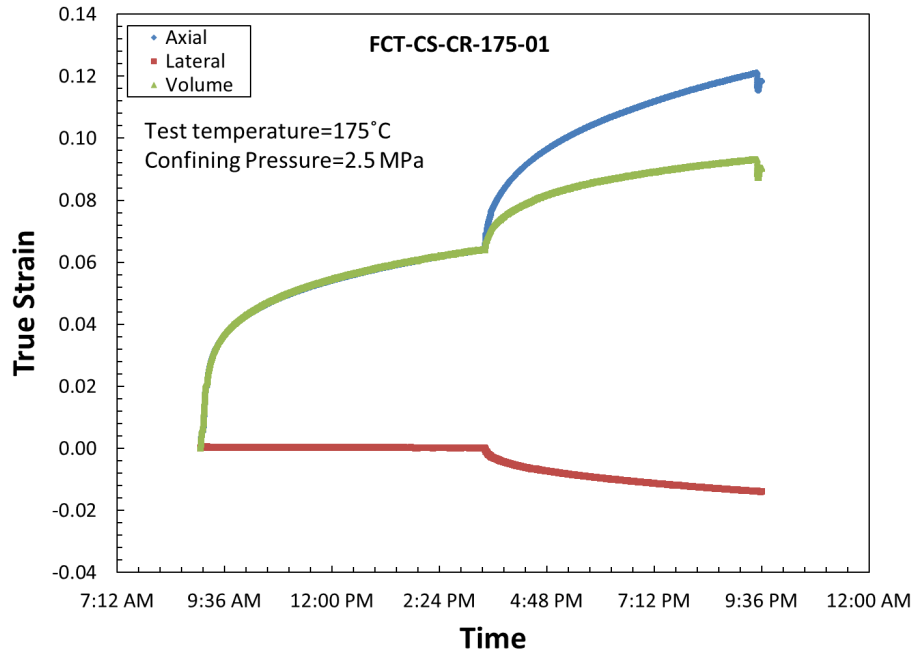


Figure 2-11. Stress-Strain Response for a Typical 250°C Test.

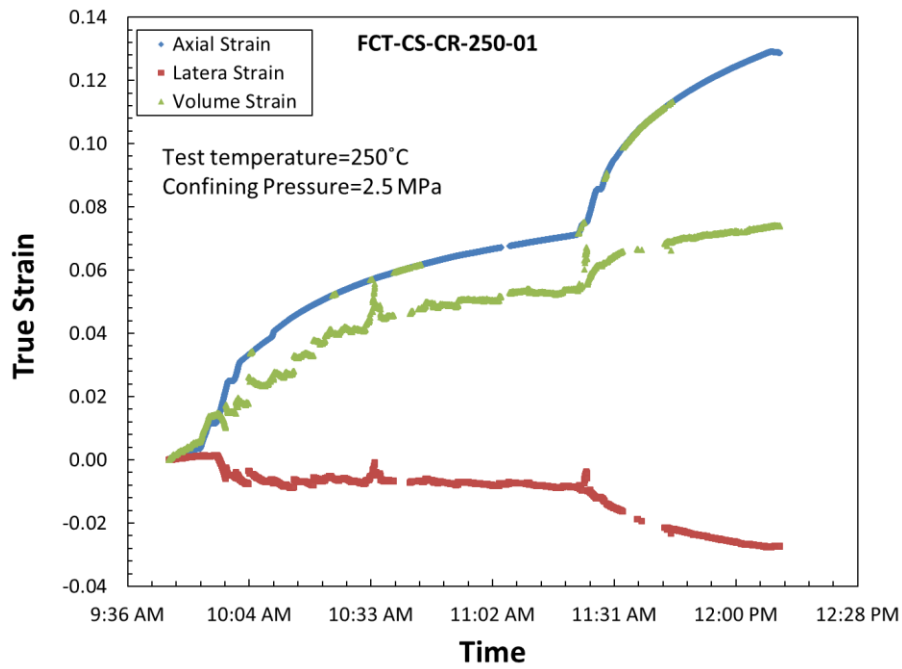
Figure 2-12 presents a comparison of true strain (axial, lateral, and volume) for the three test temperatures. In that the confining pressure (2.5 MPa) and differential stresses (2.5, 5.0 MPa) are the same for each temperature, the strain-time response elucidates the temperature effect upon compaction in shear deformation. The 100°C test ran for about five and a half days and is missing some early data due to a data logger malfunction, the 175°C ran for fourteen hours, and the 250°C ran for about five hours. It should be noted that the fractional density at the start of the shear portion of the test increased with increasing test temperature due to a greater amount of volume strain during the hydrostatic portion of the test. And, although the starting fractional density is greatest for the 250°C sample, it experiences the greatest strain at these differential stresses, the strains for the 175°C are intermediate, and the 100°C sample experiences the least strains.



(a)



(b)



(c)

Figure 2-12. True Strain Versus Time (a) 100°C, (b) 175°C, (c) 250°C.

The unload reload loops during shear tests are used to determine Young's modulus at intervals during the deformation. In Figure 2-13, normalized Young's modulus is plotted against the fractional density. Young's modulus appears to increase consistently with increasing fractional density at a given temperature. Also, the data suggest that Young's modulus decreases with increasing temperature; however, the data are too sparse to make definitive statements about the empirical relationships presented. The unload/reload loops were dependent on unload and reload rates because the porous salt aggregate was always creeping; the combination of experimental technique and ongoing deformation gave rise to the data scatter observed. Young's modulus was normalized based on experimental data for intact WIPP salt. For shear tests with higher confining pressures, Young's modulus increases. The specific values of Young's modulus used for the normalization process were 21, 27, and 43 GPa for confining pressures of 2.5, 5, and 10 MPa respectively.

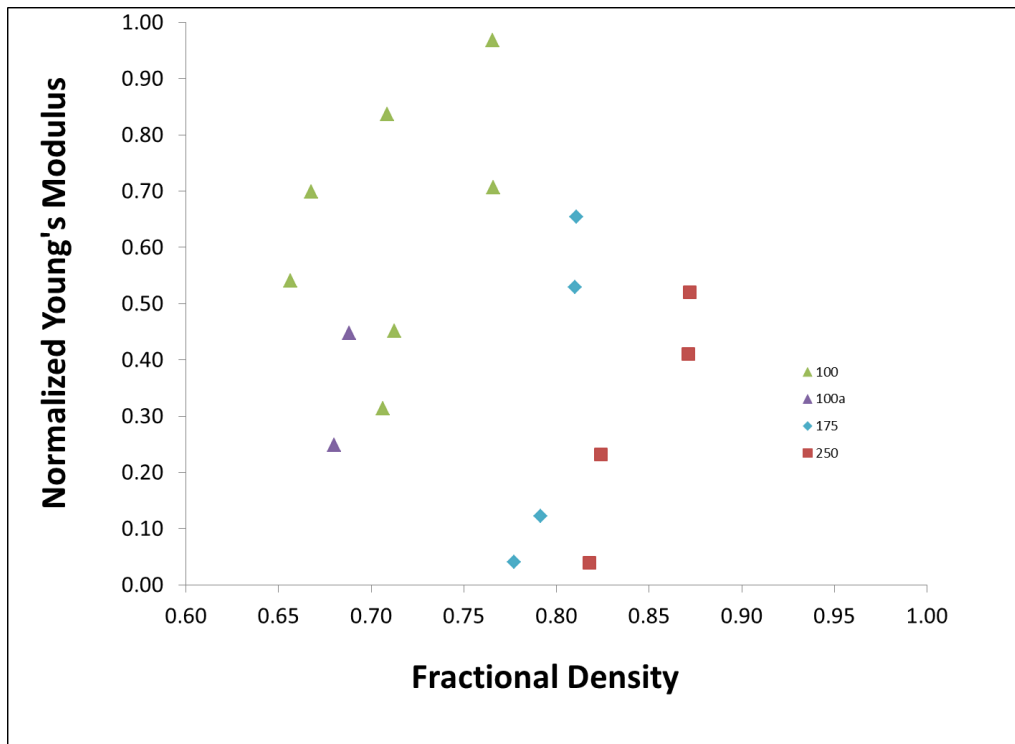


Figure 2-13. Fractional Density Versus Normalized Young's Modulus.

## 2.2 Summary and Conclusions

An experimental program was designed to systematically perform a qualitative evaluation of crushed salt consolidation as a function of stress and temperature conditions. The laboratory studies provide consolidation behavior for temperatures to 250°C and stresses to 20 MPa.

The test matrix includes isostatic, shear and creep tests in order to determine elastic properties as a function of temperature and fractional density. Determinations of elastic properties versus fractional density have been made, however the limited data constrains investigation of these relationships. The experimental stages of temperature, pressure, and shear were applied in order to acquire data for use in fitting the constitutive model with a minimum number of tests, while still exploring the full range of desired temperature, pressure and stress space.

An important observation during these tests is production of brine from the pore pressure port for 250°C tests during the heating phase when the specimen was unconfined. This observation suggests the existence of some amount of trapped water and has implications for assumptions of a dry environment for high level waste disposal in bedded salt.

Data will be evaluated in terms of the Callahan model in the following Chapter. The final volumetric strain and fractional density will be linked to the operative deformation mechanisms in Chapter 4.

The experimental program completed used a preliminary approach in a first-ever attempt to parameterize and evaluate the Callahan model with a data set at stress and temperature conditions that extend existing information into parameter space applicable to elements of high-level nuclear waste disposal. There were few if any repeat tests, as good experimental practice would usually dictate. An expeditious program required that many of the experiments provide data for multiple stress and temperature conditions, ideally each stress and temperature condition would be run individually with specific stress and temperature paths. More tests would be needed to better examine the Callahan model (see next chapter). Finally, tests run to extremely low porosities/high fractional densities were not completed. Properties of reconsolidating salt at low porosity are the most important to salt repository performance considerations.

### 3 CONSTITUTIVE MODELING

To model the mechanical behavior of reconsolidating granular salt in a repository setting, a constitutive model was developed to capture the major deformation components. The purpose of this chapter is to examine the ability of the model to represent the reconsolidation of granular salt at elevated temperatures because of the current interest in disposal of heat-generating nuclear waste. The model development evolution is documented in reports and publications including Callahan et al. (1995, 1996, and 1998), Hansen et al. (1999), and Callahan (1999). The constitutive model comprises nonlinear elastic and creep consolidation components. For the nonlinear elastic model, the functional forms for the elastic constants given by Sjaardema and Krieg (1987) were adopted (Callahan et al. 1995). Two mechanisms — dislocation creep and grain boundary diffusional pressure solution — were combined to form the basis for the constitutive model governing the creep consolidation portion of the model. Dislocation creep of intact salt has been characterized by the multimechanism deformation (M–D) model (Munson, 1979; Munson and Dawson, 1979; Munson et al., 1989). Thus, the equivalent inelastic strain rate measure for the dislocation creep portion of the crushed-salt model is taken to be the M–D material model. The only modification for application of the M–D model to crushed salt included replacing the intact salt effective stress measure with a newly developed effective stress measure for crushed salt that depends on mean stress and fractional density. Upon complete consolidation, the crushed-salt model reproduces identically the M–D model for intact salt. The pressure solution portion of the model was adopted from the grain boundary diffusional pressure solution model for wet crushed salt presented by Spiers and Brzesowsky (1993). The only modifications for application of the Spiers and Brzesowsky model to the crushed salt model included using the same effective stress measure as used for the M–D model and providing for an assumed small initial value of volumetric strain.

A database of crushed salt consolidation laboratory test results was assembled, analyzed, and reported by Callahan et al. (1995, 1996). Creation of the database was initiated with an extensive library search and compilation of potentially useful test results (Pfeifle, 1995). The test data were compiled from the original studies conducted by Holcomb and Hannum (1982), Pfeifle and Senseny (1985), Holcomb and Shields (1987), Zeuch et al. (1991), and Brodsky (1994). That compilation was reviewed to document those tests deemed inappropriate for parameter estimation, and the surviving tests formed the database for parameter estimation work (Callahan et al. 1995). Subsequently, six shear consolidation tests were added to the database for constitutive model evaluation and parameter estimation in two different studies: Callahan et al. (1996) — two tests and Hansen et al. (1998) — four tests. The database is constructed from two types of tests: isostatic (all three stress components are equal, often called hydrostatic) consolidation and shear consolidation. Nonlinear least-squares model fitting to the database produced two sets of material parameter values for the model — one for the shear consolidation tests and one for a combination of the shear and isostatic consolidation tests. Using the parameter values determined from the fitted database, the constitutive model was validated against three constant strain-rate tests. Based on the fitting statistics, the ability of the model to predict the test data, and the ability of the model to predict load paths and test data outside of the fitted database,

the model was determined to capture the creep consolidation behavior of crushed salt reasonably well.

Unfortunately the laboratory tests included in the experimental database were conducted predominately at room temperature. The database includes eight isostatic tests at temperatures of nominally 40°C, 60°C, 80°C, and 100°C conducted by Holcomb and Hannum (1982); however, the duration of the longest of these tests was 4.8 days. In this chapter, the granular salt reconsolidation model is evaluated to see how well the model represents consolidation behavior at elevated temperatures up to 250°C. The evaluation is accomplished based on the experiments described and presented in Chapter 2.

### 3.1 Model Temperature Dependencies

The granular salt reconsolidation model includes temperature functions in both the dislocation creep and pressure solution portions of the model. The exponential temperature functions provide significant accelerations in the strain rate with temperature increases. Unfortunately, reconsolidation behavior for temperatures up to 250°C is an extrapolation outside of the databases for both the pressure solution and dislocation creep temperature functions.

The pressure solution temperature dependency ( $G_{ps}$ ) is given by Spiers and Brzesowsky (1993) as

$$G_{ps}(T) = \frac{\exp\left(-\frac{Q_s}{RT}\right)}{T} \quad (1)$$

where

$$R = \text{universal gas constant} \left[ \frac{J}{\text{mol} \cdot K} \right]$$

$$T = \text{temperature} [K]$$

$$\frac{Q_s}{R} = 1,077.46 [K]$$

Spiers and Brzesowsky (1993) state that they evaluated the temperature function for temperatures from 20°C to 90°C. Therefore, 250°C is significantly outside of their database. Figure 3-1 shows the normalized value (i.e.,  $G_{ps}(T)/G_{ps}(T_0)$ ), where  $T_0 = 273.15$  K) of the temperature function given in Equation 1. The figure shows that at 250°C the pressure solution strain rate is about 3.4 times greater than the strain rate at 0°C.

Temperature dependency in the M-D model is included in the transient and steady-state portions of the model. For the transient part of the model, temperature dependency is included in the transient strain limit as

$$\varepsilon_t^f = K_0 \exp(cT) \left( \frac{\sigma_{eq}}{\mu} \right)^m \quad (2)$$

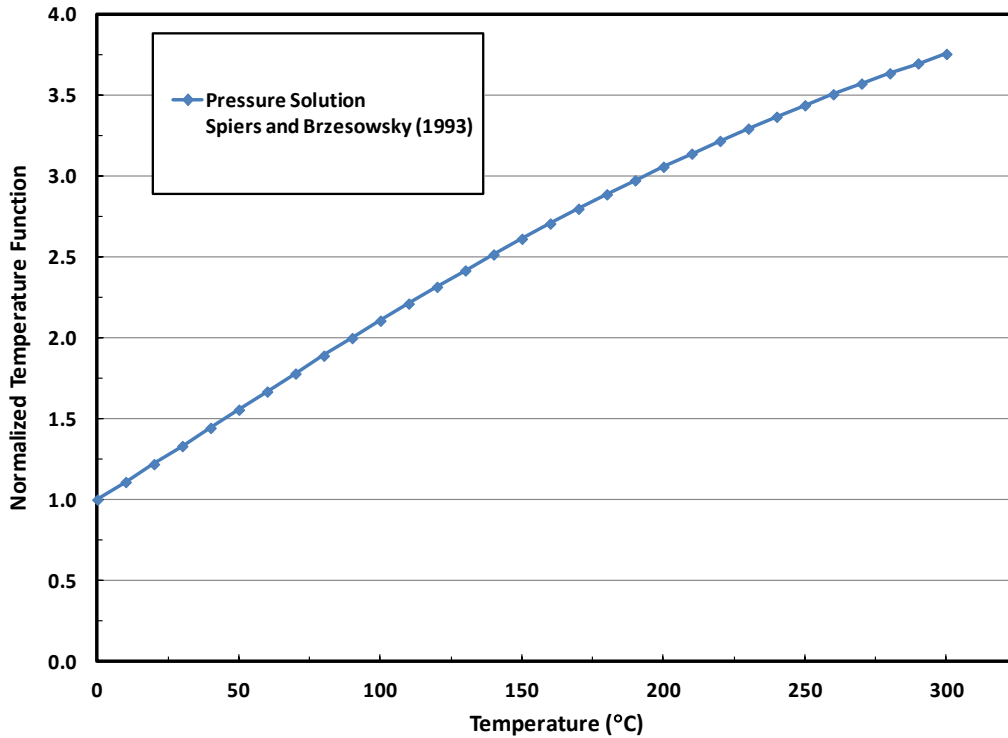


Figure 3-1. Normalized Creep Consolidation Temperature Functions.

where<sup>1</sup>

---

<sup>1</sup> For purposes of this report, parameter values for the M-D model are those assumed to be representative of clean WIPP salt (e.g., see Callahan, 1999, Table 4-1).

$\sigma_{eq}$  = the effective stress measure  
 $T$  = absolute temperature  
 $\mu$  = shear modulus  
 $K_0, c$ , and  $m$  = material parameters

Therefore, the M-D transient temperature dependency function is written as

$$H_t(T) = \exp(cT) \quad (3)$$

Figure 3-2 shows the normalized value (i.e.,  $H_t(T)/H_t(T_0)$ ) of the temperature function given in Equation 3. The figure shows that at 250°C the transient strain limit is about 10 times greater than the transient strain limit at 0°C.

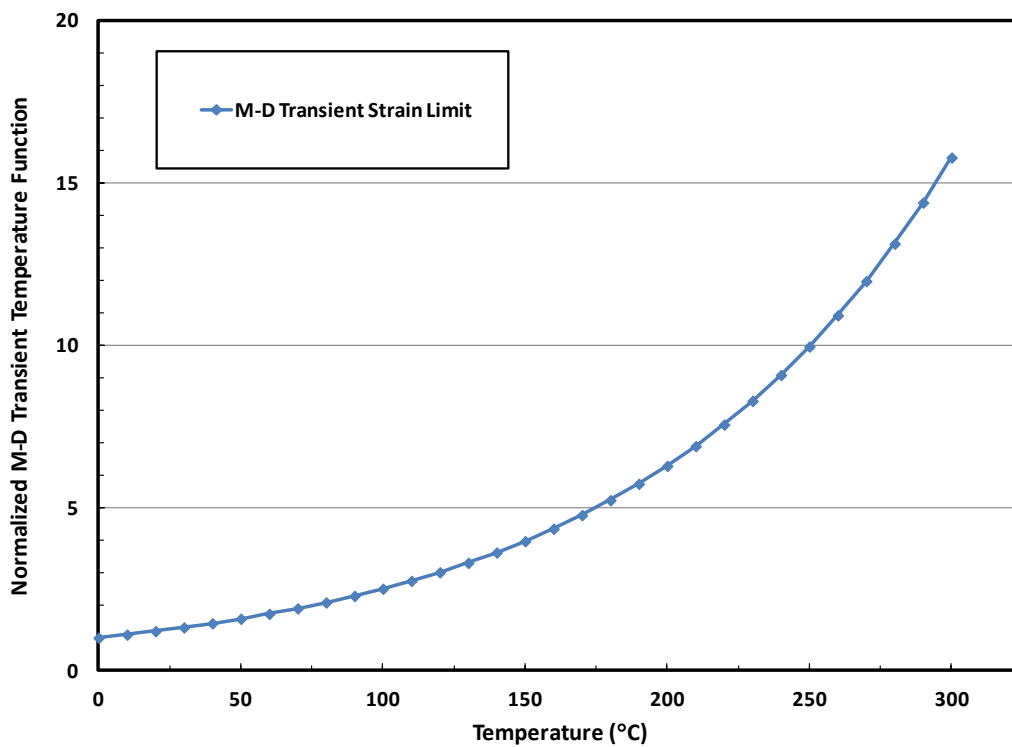


Figure 3-2. Normalized M-D Transient Temperature Function.

The M-D model includes three additive steady-state strain rate mechanisms each with temperature dependency given as

$$\dot{\epsilon}_{s_1} = A_1 \exp\left(-\frac{Q_1}{RT}\right) \left(\frac{\sigma_{eq}}{\mu}\right)^{n_1} \quad (4)$$

$$\dot{\epsilon}_{s_2} = A_2 \exp\left(-\frac{Q_2}{RT}\right) \left(\frac{\sigma_{eq}}{\mu}\right)^{n_2} \quad (5)$$

$$\dot{\epsilon}_{s_3} = \left( B_1 \exp\left(-\frac{Q_1}{RT}\right) + B_2 \exp\left(-\frac{Q_2}{RT}\right) \right) \sinh \left[ q \left( \frac{\sigma_{eq}^f - \sigma_0}{\mu} \right) \right] H(\sigma_{eq} - \sigma_0) \quad (6)$$

where  $A_1, A_2, B_1, B_2, n_1, n_2, Q_1, Q_2, q,$  and  $\sigma_0$  are material parameters. Therefore, the M-D steady-state temperature dependency functions may be written as:

$$H_{s_1}(T) = \exp\left(-\frac{Q_1}{RT}\right) \quad (7)$$

$$H_{s_2}(T) = \exp\left(-\frac{Q_2}{RT}\right) \quad (8)$$

$$H_{s_3}(T) = B_1 \exp\left(-\frac{Q_1}{RT}\right) + B_2 \exp\left(-\frac{Q_2}{RT}\right) \quad (9)$$

Figure 3-3 and Figure 3-4 show the normalized values (i.e.,  $H_{s_1}(T)/H_{s_1}(T_0), H_{s_2}(T)/H_{s_2}(T_0),$  and  $H_{s_3}(T)/H_{s_3}(T_0)$ ) of the M-D steady-state temperature functions given in Equations 7, 8, and 9. The two figures are identical except for the ordinate in that the Log of the normalized M-D steady-state temperature functions are plotted in Figure 3-3 and the actual values (scaled by one million) are plotted in Figure 3-4. Figure 3-4 clearly shows how dominant the first M-D steady-state function is at higher temperatures.

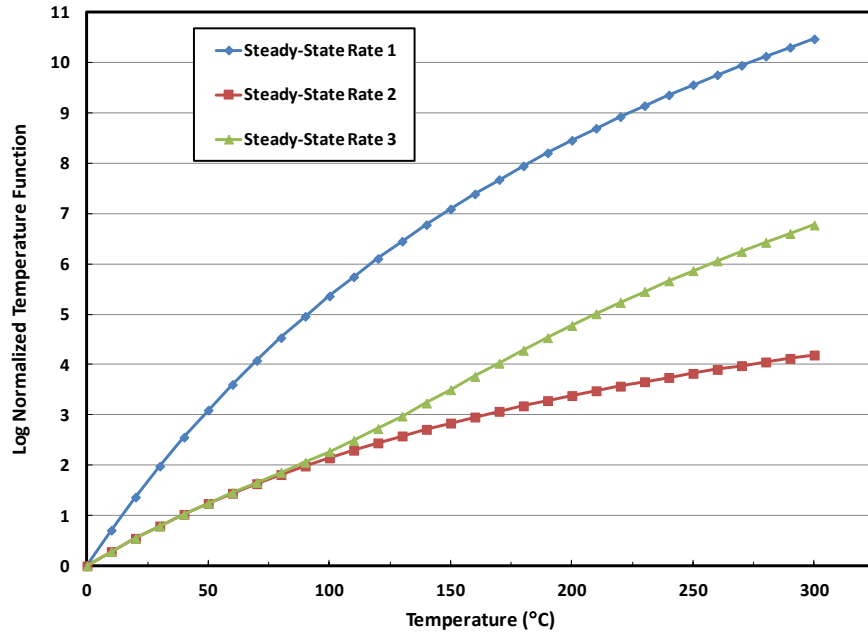


Figure 3-3. Log Normalized M-D Steady-State Temperature Functions.

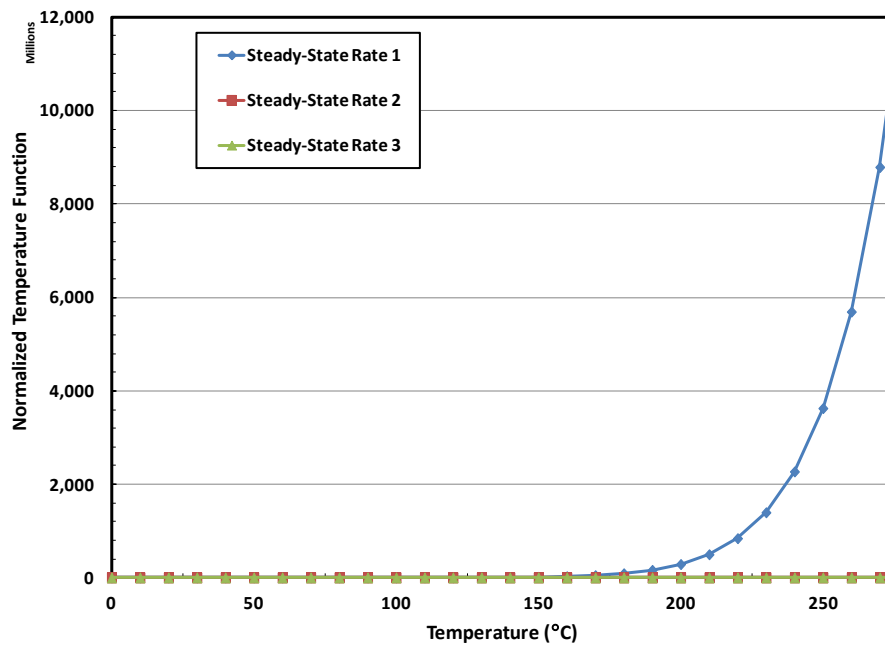


Figure 3-4. Normalized M-D Transient Temperature Function.

Figure 3-5 plots the percentage contribution to the total steady-state strain rate attributable to each of the steady-state strain rate mechanisms as a function of temperature for effective stress values of 5, 10, 20, and 25 MPa. The steady-state strain rate attributable to the third mechanism is zero for all cases except for the 25 MPa case because the value for the cut-off stress ( $\sigma_0$ ) is 20.57 MPa. Figure 3-5 shows that, regardless of effective stress value, the second steady-state strain rate mechanism is dominant for temperatures roughly less than 100°C and the first steady-state strain rate mechanism is dominant for temperatures roughly greater than 100°C. Figure 3-5 also shows at temperatures around 250°C and above that nearly all of the steady-state strain rate comes from the first steady-state strain rate mechanism unless the effective stress exceeds 20 MPa and the third steady-state strain rate mechanism contributes about 15 percent of the total steady-state strain rate.

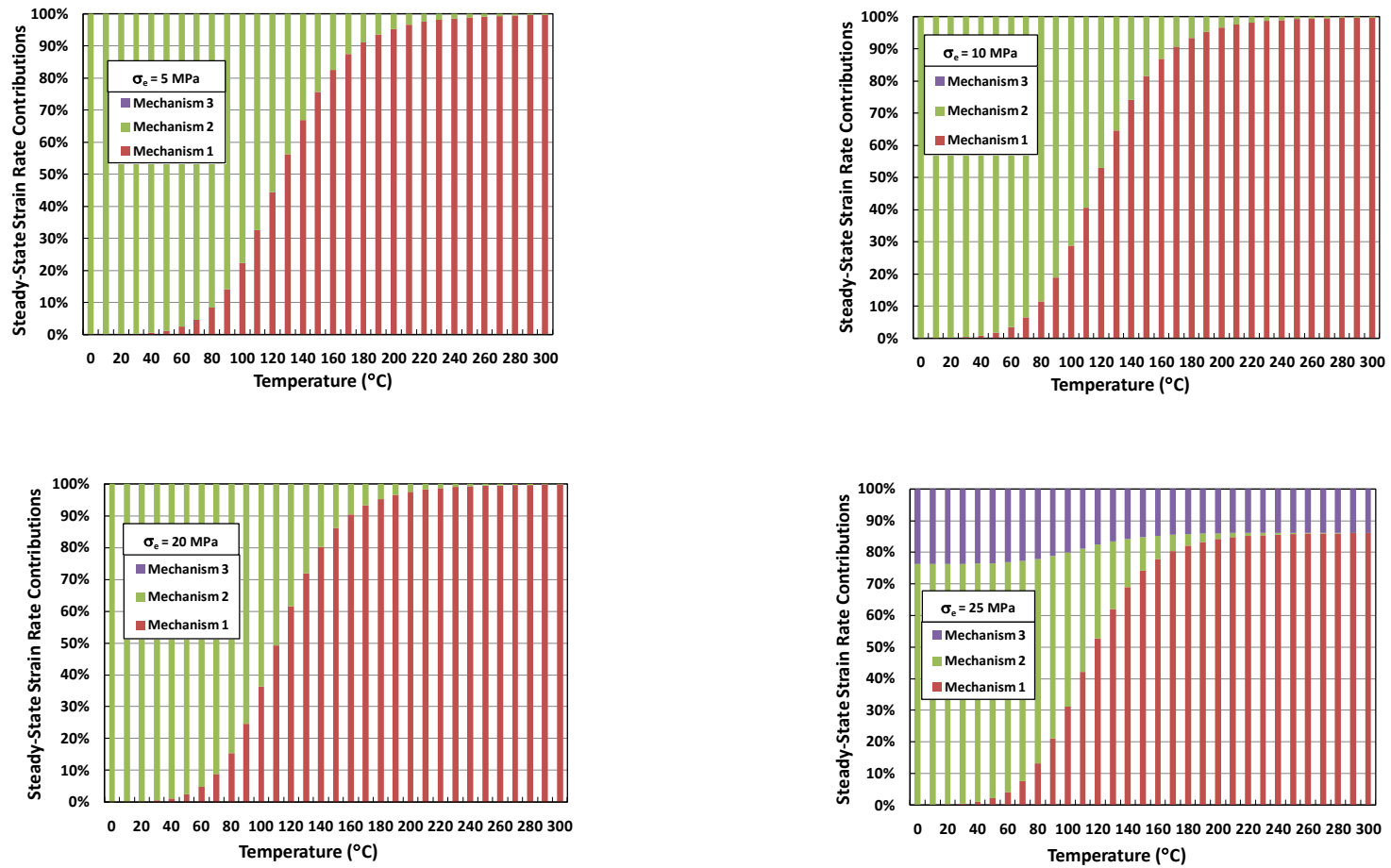


Figure 3-5. Contributions to the Total Steady-State Strain Rate by Each Mechanism as a Function of Temperature for Effective Stresses of 5, 10, 20, and 25 MPa.

### 3.2 Comparison with Experiments

Until now, there have been few experiments conducted to evaluate the crushed salt model's ability to represent granular salt's behavior at elevated temperatures. In this chapter, the granular salt reconsolidation model is evaluated to see how well the model represents consolidation behavior at elevated temperatures up to 250°C. The experiments discussed in Chapter 2 were designed to quantitatively evaluate consolidation as a function of stress ( $\sigma$ ) and temperature (T) with laboratory studies to temperatures of 250°C and stresses to 20 MPa. Table 3-1 shows laboratory tests discussed in Chapter 2 that were simulated using the crushed salt constitutive model.

**Table 3-1. Test Matrix for Salt Reconsolidation at Elevated Temperature**

Test Number	Test Type	T (°C)	Maximum Confining Pressure (MPa)	Stress Difference (MPa)	Axial Stress (MPa)	Mean Stress (MPa)	Description
2	Isostatic	100	20.0	0	20.0	20.0	Quasistatic
4	Isostatic	175	20.0	0	20.0	20.0	Quasistatic
6	Isostatic	250	20.0	0	20.0	20.0	Quasistatic
18	Isostatic/Shear	100	5.0	2.5/5.0	7.5/10.0	5.83/6.67	Quasistatic-Creep
13	Isostatic/Shear	175	2.5	2.5/5.0	5.0/7.5	3.33/4.17	Quasistatic-Creep
16	Isostatic/Shear	250	5.0	2.5/5.0	7.5/10.0	5.83/6.67	Quasistatic-Creep

The isostatic tests (Test Numbers 2, 4, and 6) are compared with the crushed salt model predictions in Figure 3-6. Model predictions in all instances were calculated using the finite element program SPECTROM-32 (Callahan et al. 1989). The length of time to conduct the laboratory tests was about 70 minutes for all three tests. For the model simulations of the tests, the time required to perform the unload/reload portions of the tests were deducted from the loading time for the simulations. Thus, the loading times for the test simulations were all about 55 minutes. In all cases, the simulations indicate that the model predicts greater compressibility ("softer" behavior) than shown by the laboratory test specimens and that the differences caused by temperature are not as large as obtained in the laboratory.

The database described in Callahan (1999) used to develop the material parameters for the crushed salt creep consolidation constitutive model has several areas where data gaps exist that may account for some of the differences between the laboratory test data and the model's predictions. The data gaps include test type, stress, temperature, and test duration. The database does not include any tests loaded to 20 MPa in about one hour. The database includes isostatic

tests that were loaded to a prescribed mean stress value, and the target mean stress was subsequently held for several days. These tests bias the model fitting to the longer-term performance while sacrificing the short-term behavior. The highest mean stress level in any of the tests in the database is 10.1 MPa; whereas, the current isostatic tests reach about 20 MPa. The model development database only includes eight tests at elevated temperatures (i.e., two tests at each nominal temperature of 40°C, 60°C, 80°C, and 100°C). The duration of the current isostatic laboratory tests is about one hour; whereas, the shortest test in the model development database is about 65 hours.

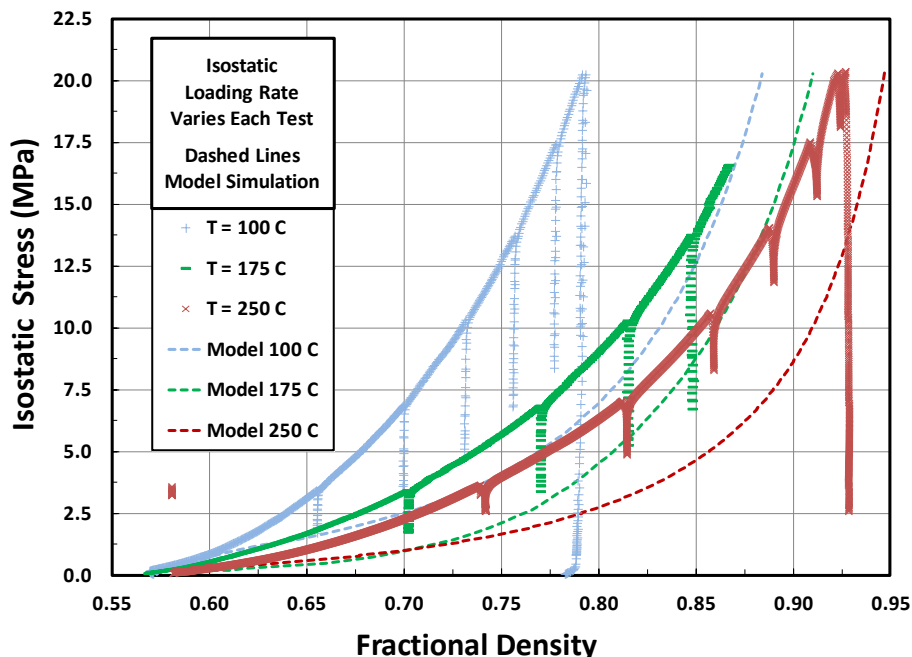


**Figure 3-6. Comparison of Model Predictions to Isostatic Laboratory Test Numbers 2 (100°C), 4 (250°C), and 6 (250°C).**

The isostatic/shear creep consolidation tests (Test Numbers 18, 13, and 16) are compared with the crushed model predictions in Figures 3-7 and 3-8. Although the loading durations of each portion of these tests varied from test to test, each test included the following stages following initial setup and temperature stabilization:

1. Isostatically load to the target confining pressure
2. Apply the differential stress for the first stage of creep consolidation
3. Continue shear consolidation creep to about 5 to 6 percent volumetric strain
4. Apply the differential stress for the second stage of creep consolidation
5. Continue the shear consolidation creep for an additional 5 to 6 percent volumetric strain
6. Unload test specimen terminating the test

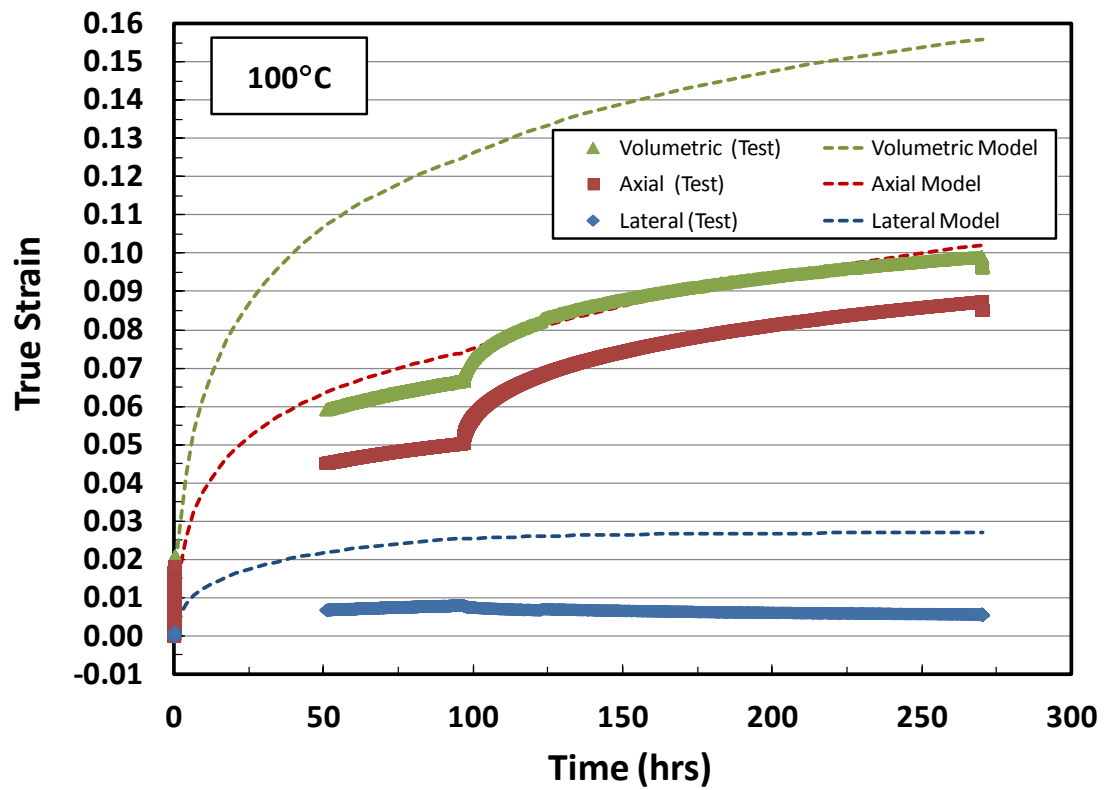
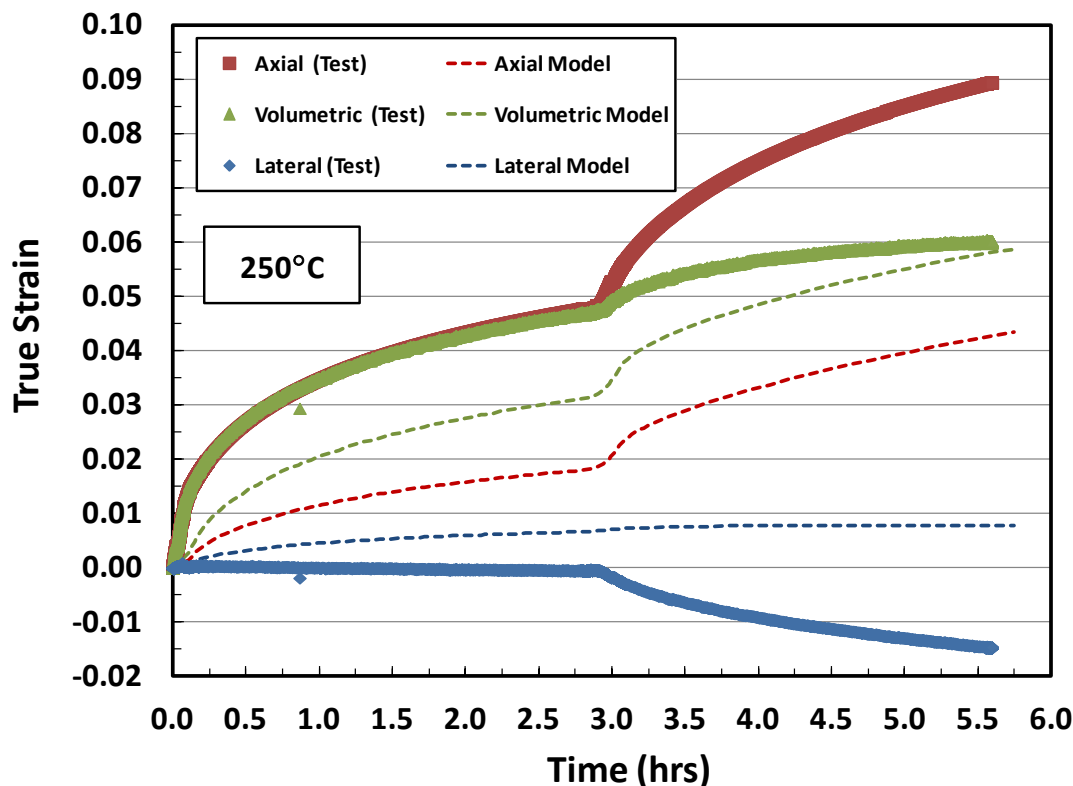


Figure 3-7. Comparison of Model Prediction to the Shear Stages of Laboratory Test Number 18 at 100°C.



**Figure 3-8. Comparison of Model Prediction to the Shear Stages of Laboratory Creep Consolidation Test Number 16 at 250°C.**

In each of the Figures 3-7 and 3-8, stages 2 through 5 enumerated above are plotted in the figures. Therefore, the initially isostatic loading to the desired mean stress level is not shown and most of the unloading is not shown. Time and strain data were translated so that the zero values occurred at the beginning of the first stress difference loading stage. The length of time to conduct the laboratory tests was about 270 hours, 12.5 hours, and 5.5 hours for Test Numbers 18, 13, and 16 respectively, which reflects the influence of temperature on the deformation of the crushed salt. The gap in the laboratory data shown in Figure 3-7 was caused by a malfunction in the data acquisition system.

The test simulation results are interesting in that the predicted volumetric strains are greater than the laboratory results at 100°C, the predicted volumetric strains are quite close to the laboratory results at 175°C, and the predicted volumetric strains are less than the laboratory results at 250°C. The model simulations are subject to the same data gap shortcomings discussed for the isostatic tests. However, these results are encouraging given the fact that the database contains no tests conducted above 100°C. Future test results on intact salt at elevated temperatures (upon which the temperature dependency of the crushed salt model is based) may provide general improvements on the model’s ability to predict elevated temperature results.

## 4 MICROMECHANICS

Design, analysis and performance assessment of potential salt repositories for heat-generating nuclear waste require knowledge of thermal, mechanical, and fluid transport properties of reconsolidating granular salt. Extensive research completed on the topic of compaction and hydraulic properties of crushed salt, including recent summary papers on the temporal evolution of salt compaction and permeability compiled for the Vorläufige Sicherheitsanalyse Gorleben (Popp and Salzer, 2011). Generic repository research supported by the Used Fuel Campaign in the US is making the case for applying repository science to practical design, operation and performance; therefore, the supporting research, as reviewed here, will attempt to demonstrate the bridge from theoretical and first order physics to real-world applications.

A number of excellent research papers provide engineering characteristics and practical application of granular salt reconsolidation properties (see for example Zhang et al., 2007; Popp and Salzer, 2011). An impressive series of papers by Spiers and co-workers (Franssen and Spiers, 1990; Spiers et al., 1990; Spiers and Brzesowsky, 1993) provides theory and microstructural observations of densification processes. Very recently, the 3<sup>rd</sup> US/German workshop on salt repository research, design and operation included salt reconsolidation as a special focus area. Updated information on salt repository sciences including salt reconsolidation efforts can be found on the following website: [http://www.sandia.gov/SALT/SALT\\_Home.html](http://www.sandia.gov/SALT/SALT_Home.html). Based on the considerable body of evidence including a summary of the research summarized in this report, densification mechanisms of both wet and dry granular salt have been demonstrated to be quite well understood. Given the interest in reconsolidating granular salt and the state of the art, a review paper with an emphasis on salt repository applications has been proposed as part of generic salt research sponsored by Fuel Cycle Research and Development.

From the perspective of shaft seal systems in salt, the Department of Energy WIPP program supported comprehensive and systematic, research, development and demonstration of salt compaction, reconsolidation, and micromechanics associated with the design and certification of the shaft seal design (Hansen, 1997). Large-scale demonstrations of possible shaft construction methods (Hansen and Ahrens, 1996) confirmed that mine-run salt with 1% water by weight added could be dynamically compacted to 90% of theoretical density. Thus, reconsolidation for shaft seal applications could start with an initial porosity of 10%. Consolidation from the initial construction conditions forward would occur as the surrounding salt formation creeps inward. The phenomena associated with consolidation under these conditions were established by laboratory testing on the dynamically compacted material, including measurement of permeability as a function of porosity. The scientific evidence framing ambient reconsolidation of granular salt with a small amount of moisture is underpinned by large-scale tests, laboratory consolidation measurements, and microscopic documentation of deformational processes (Brodsky et al., 1996). Permeability/density functions developed from the shaft seal experience also provide a reference point for drift sealing design, analysis or experimentation (Hansen and Knowles, 1999). However, large-scale reconsolidation under hot and potentially dry conditions has been less well described. Perspectives on these elements of salt reconsolidation are provided here.

### 4.1 Background

The salt repository community benefits from large amounts of pertinent information on granular salt consolidation ranging over a length scale from angstroms to tens of meters. Understanding

granular salt reconsolidation under a wide range of conditions is essential to establish certain performance bases for salt repositories for heat-generating nuclear waste. Historical information and experience are provided to set the stage for current research efforts.

#### 4.1.1 WIPP Shaft Seal Technological Advances

The proposed use of crushed salt as a functional seal element in the WIPP shafts gave rise to several technological advances. A large-scale dynamic compaction demonstration using mine-run salt produced a compacted mass having a fractional density of 0.9 and a permeability of  $9 \times 10^{-14} \text{ m}^2$ . Modeling evolution of crushed salt from these initial conditions to a high-density, low permeability seal required implementation of a suitable constitutive model, as discussed in Chapter 3. Refinement of model parameters, definition of the relationship between permeability and density and a solid understanding of the processes are required for use of reconsolidated salt as a repository sealing element. Implementation of a proper constitutive model, inclusion of a reliable permeability/density relationship for reconsolidating crushed salt, and a fundamental understanding of micromechanical processes assure credible design and analyses of the WIPP shaft seal system.

A large-scale dynamic compaction demonstration using mine-run WIPP salt (Hansen and Ahrens, 1996) established possible initial conditions of a compacted salt seal component. Hansen and Ahrens selected deep dynamic compaction as a construction technique because it provides the greatest energy application to the crushed salt of available techniques, is relatively easy to apply, and has an effective depth of compactive influence far greater than lift thickness (approximately 2 m). Transport of granular salt to the working level in a shaft can be accomplished by dropping it down a slickline. If desired, a small mist of additional water can be sprayed onto the crushed salt as it is placed at the shaft working horizon. The basic construction technique was demonstrated above ground; however, the concept is readily adaptable to existing shaft sinking procedures.

To enhance compaction, 1 wt. % water was added to the *relatively* dry mine-run salt. The large-scale compaction demonstration produced  $40 \text{ m}^3$  of compacted salt that had a uniform fractional density equaling 0.9 of natural intact salt. These results established the datum for shaft construction and basis for initial conditions of laboratory investigations. The permeability of compacting crushed salt is known to decrease as density increases (Brodsky, 1994) and the density of crushed salt in the seal increases with time during reconsolidation. An example of consolidation test results is given below in Figure 4-1. Test conditions included hydrostatic confining stress of 1 MPa and a pore fluid inlet pressure of 0.345 MPa. Two of the four curves on Figure 4-1 represent actual test measurements; the other two show calculated measurements. The curve labeled "Burette Measurement" is the total measured volume of brine collected at the vented end of the specimen, and the curve labeled "Volumetric Strain" is the test system measurement provided by the dilatometer. The data indicate that the saturated specimen is compacting; thus some volume of brine is being expelled from the vented end. The burette measurement has two components. One is the volume being expelled by consolidation, and the other is the volume of fluid migrating through the specimen. When the volume of expelled pore fluid derived from consolidation is subtracted from the burette measurement, the apparent permeability is found to decrease rapidly from an initial value of about  $5 \times 10^{-16} \text{ m}^2$  to zero flow after 10 days.

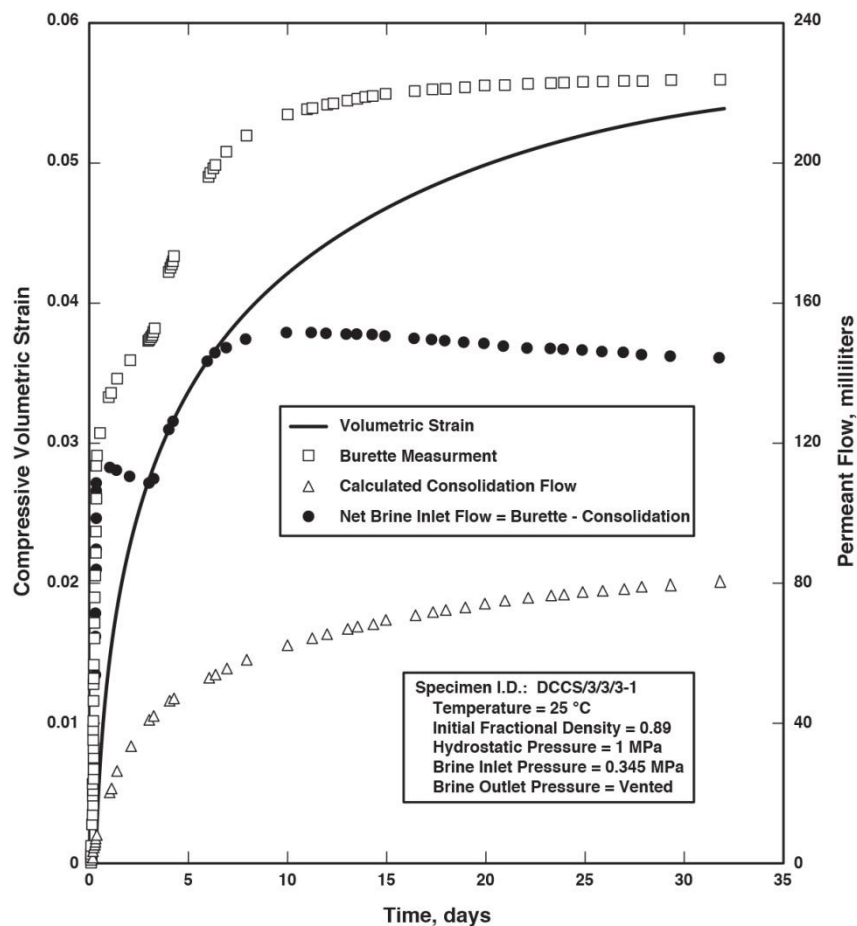


**Figure 4-1. Volumetric Strain and Brine Flow Measurements on Reconsolidating Granular Salt.**

Experimental difficulties, such as a plugged brine flow tube, could account for apparent loss of permeability. Therefore, as the test apparatus was disassembled, the confining pressure was carefully reduced to allow flow around the specimen, which demonstrated that no restriction to flow developed except for that presented by the specimen itself. Based on these convincing test results and results obtained by Brodsky (1994), it appears that brine permeation in dense reconsolidating salt is self-limiting.

In thin sections made after consolidation, a large percentage of the initial fine powder was removed by pressure-solution and re-precipitation. Confirmation of microprocesses was made by scanning electron microscopy. The initial state of dynamically compacted salt exhibited loose grain boundaries, while post-consolidation substructures were sutured by pressure solution. In addition, the fracture face exposed in the SEM showed grain boundary separation in the compacted salt and grain cleavage in the reconsolidated salt. The nature of the fracture surfaces demonstrated that the strength of grain boundaries after pressure-solution/precipitation is sufficient to favor crystalline fracture along cleavage planes rather than fractures along grain boundaries.

#### 4.1.2 BAMBUS II Evidence

The BAMBUS and BAMBUS II Project (Bechthold et al., 2004) provides the best available full-scale, long-term, thermomechanical information on granular salt reconsolidation. BAMBUS is an acronym for Backfilling and Sealing of Underground Repositories for Radioactive Waste in Salt. The principal scientific objective of the project was to extend the basis for optimizing the repository design and construction and for predicting the long-term performance of barriers, including the reconsolidation of crushed salt backfill.

In situ investigations were carried on in the Asse salt mine subsequent to completion of the large-scale TSDE (Thermal Simulation of Drift Emplacement, also discussed in Bechtold et al., 2004) in which the emplacement drift was electrically heated to between 170 and 200°C for more than 8 years. Characterization of the reconsolidated salt included microstructural petrofabrics and laboratory tests.

Sandia was a partner on the BAMBUS II in situ reconnaissance and performed permeability tests on the reconsolidated salt. The photograph shown in Figure 4-2 is the BAMBUS II setting as the test room was re-entered. The large heater is surrounded by reconsolidated granular salt, which had various porosities depending upon location. Most porosity measurements ranged from 20 to 25%. If an assumption is made that the porosity upon placement was of the order of 40%, then after ten years of in situ testing, porosity was reduced by 10 to 20 %. Thus, an additional 10 or 20 years under these conditions would be required to reduce the porosity sufficiently to produce a low permeability medium.



**Figure 4-2. Photograph of the BAMBUS II E Re-excavation.**

The photomicrographs in Figure 4-3 are a thin section in cross-polarized light (left) and surface image from a scanning electron microscope (right). These thin sections were taken directly from BAMBUS II salt extracted as shown in the field test photograph Figure 4-2. This particular sample has a measured porosity of 20.7% and a permeability of  $4.2 \times 10^{-13} \text{ m}^2$ . Brittle processes dominate, as can be seen from the small, sharply angular grains situated between larger grains, all of which exhibit cubic cleavage habit. The grain boundaries are not sutured as evidenced by the free surface in the right photograph shown in Figure 4-3. The grains have no evident cohesion when broken, as breakage was accommodated at the grain boundary and not through the grains. Grain boundaries show no evidence of healing processes and the flexural breakage was accommodated by separation of grain boundaries and not tensile failure of the grains themselves.

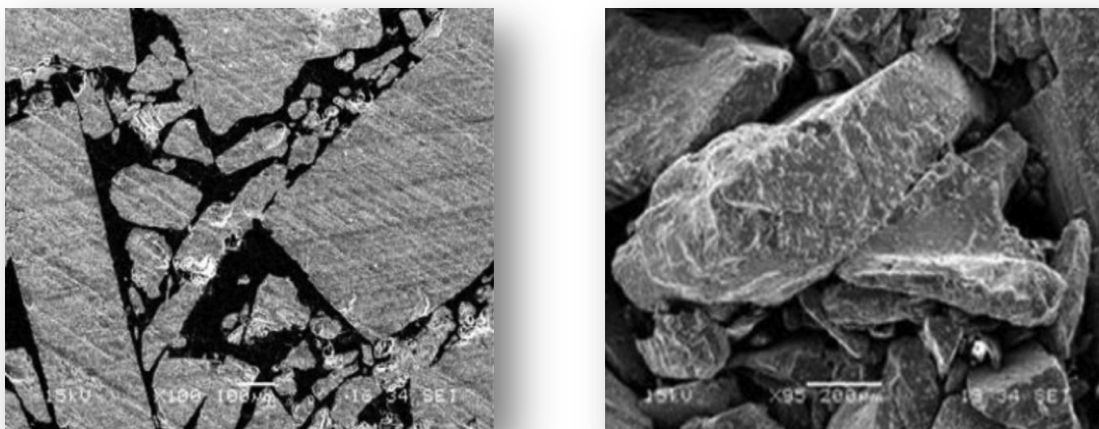


Figure 4-3. Reconsolidated Salt with 20.7% Porosity.

## 4.2 Observational Techniques

Techniques developed in previous studies, such as the WIPP shaft seal investigations (Chapter 4.1.1) and the observational work completed for the final BAMBUS II report (Chapter 4.1.2) were revitalized and extended for the research reported here. This type of observational work has not been performed in US repository programs for many years. Methods employed include optical microscopy on thick-thin sections and etched cleavage chips. Scanning electron microscopy was used to examine freshly broken surfaces and coated thick-thin sections. An optical “thick-thin” section is about 5mm thick, which allows for optical observations on the surface, along grain boundaries and through the crystal structure.

After the samples were successfully consolidated in the laboratory experiment, they were cut in half length-wise using a low-damage diamond wire saw and subsequently quartered as shown in the photographs in Figure 4-4. Optical slides were made for most material, but much more observational petrofabric work could be done. An example thick-thin section is also shown in Figure 4-4. The blue color is low-viscosity epoxy that is drawn into the porosity by vacuum. The quarter-round subsections are broken by hand to expose a surface of the compacted material. These fresh surfaces are sputter-coated and examined by SEM. A unique technique was successfully attempted here for the first time, which involved plucking single grains from the consolidated mass, and then cleaving, etching and examining them. The results are remarkable.



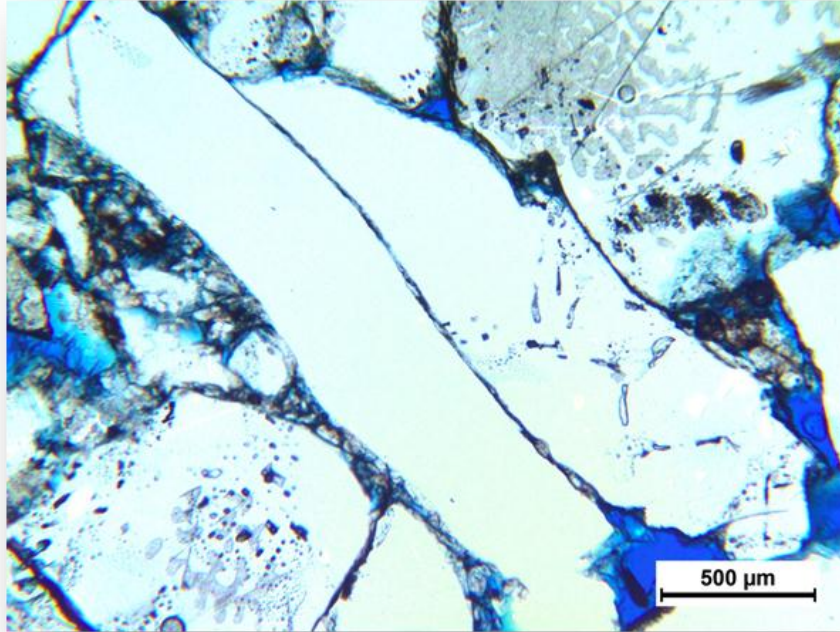
**Figure 4-4. Sawn Samples and an Optical Thick-Thin Section**

Consolidation processes at high porosity involve instantaneous grain rearrangement and microfracture, which can proceed only so far before grain boundary processes and crystal plastic mechanisms begin to dominate further porosity reduction. As porosity is reduced, plastic deformation proceeds, which with attendant and immediate increase in dislocation density is accommodated by slip along the dodecahedral  $\{110\}$  planes. Salt plasticity promoted by slip or glide along the  $\{110\}$  has been well documented in many laboratory tests on intact salt (e.g., Hansen, 1985) but was not observed in the studies reported here owing to the limited numbers and conditions of the specimens examined. The petrographic evidence shown in this report is largely from tests that were taken to  $<10\%$  porosity.

Extraordinary crystal deformation is shown in Figure 4-5. This image is taken in transmitted light on a thick-thin section prepared from granular salt reconsolidated to low porosity at  $250^{\circ}\text{C}$ . The exceptional crystal plasticity and compatible grain boundaries between the elongate grains in the center of the frame can be fully appreciated when compared to the salt grains in Figure 4-3, which have consolidated to approximately 21% porosity. Note fluid inclusions in the relatively large equant grains in the lower left and upper right quadrants of the field of view in Figure 4-5. Then, note the absence of fluid inclusions in the paired grains that display the tight boundary and exceptional elongation. Under these conditions at low porosity the densification processes involve plasticity coupled pressure solution (Spiers and Brzesowsky, 1993).

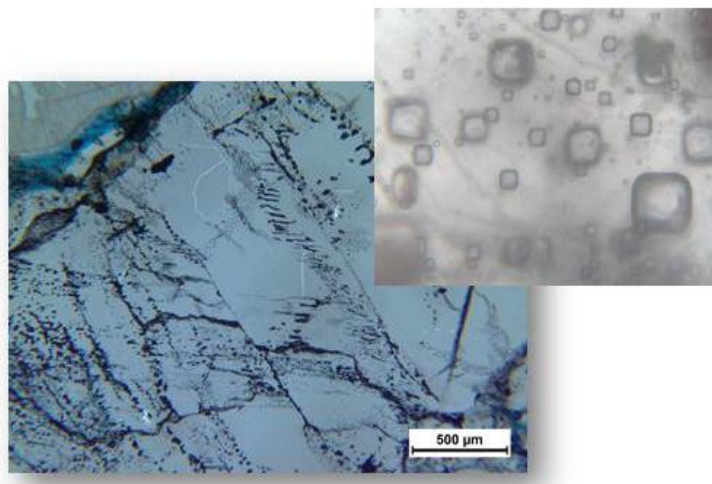
Also portrayed in the photomicrograph in Figure 4-5 are the pulverized grains clustered on the left lower area of view. All similar minute grains have been completely consumed between the two elongate grains. Elongation facilitated by slip on  $\{110\}$  planes apparently has moved nearly all the internal fluid inclusions to the grain boundaries. The fluid thereby made available to the

grain-boundary promoted rampant pressure solution and consumption of the fine grains previously occupying the boundary. Upon close inspection, vestige micrograins can be seen on the very tight grain boundary.



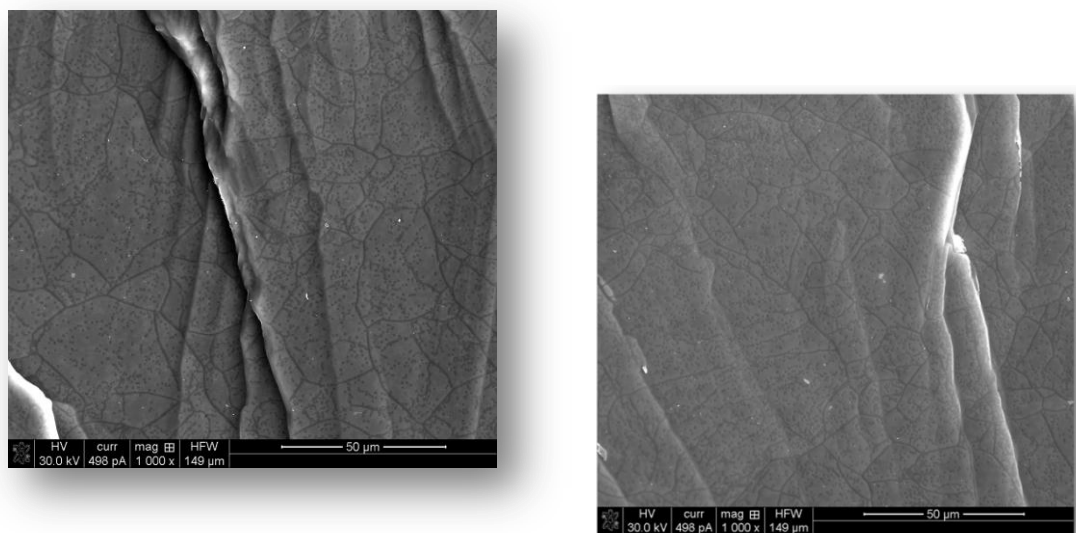
**Figure 4-5. Extensive Grain Deformation During Reconsolidation at 250°C.**

A similarly dramatic photomicrograph is shown in Figure 4-6, in which the motion of internal fluid inclusions is captured on  $\{110\}$  planes and very tightly closed grain boundaries. Magnification is the same as the micrograph above and the blue hue is caused by epoxy impregnation. Fluid inclusions tend to collect along the tight grain boundaries, as might be expected as the fluid itself promotes creation of the grain boundary. The abundance of fluid inclusions typical of Permian bedded salt and their undisturbed cubic habit are shown at a greater magnification in the inset photograph. The and the high degree of mobility of the inclusions can be seen in the dark images at an angle to the grain boundaries (presumably along  $\{110\}$ ).



**Figure 4-6. Glide of Fluid Inclusions Along Slip Planes 250°C.**

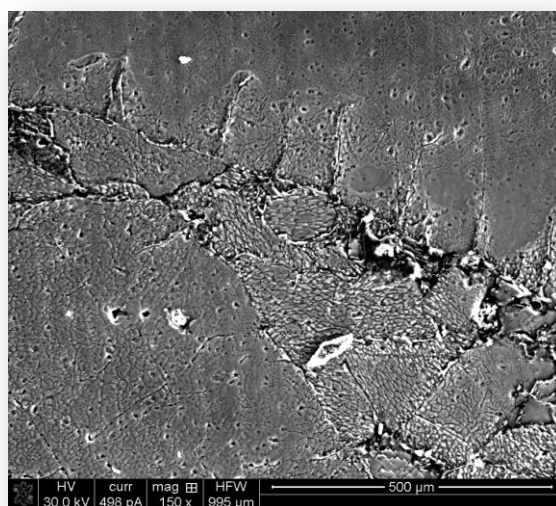
The two photomicrographs shown in Figure 4-7 show material extricated from the reconsolidated sample. The fresh face of the broken quarter-round samples provided an opportunity to pluck out a few grains approximately 3-5 mm in diameter. These highly distorted grains were cleaved with some difficulty. One can appreciate the internal grain deformation of the cleaved chips by comparing the fabric of these surfaces to the Miller Indices  $\{100\}$  planes of native Permian salt, which cleaves nearly perfectly planer and exhibits few cleavage steps. By contrast to the undeformed salt, the cleavage plane  $\{100\}$  itself is highly warped. This gives the surface an undulatory fabric with the appearance of folds, like a curtain hanging from a horizontal rod. After these grains were extracted, they were etched in methanol saturated with  $\text{PbCl}_2$  and stopped in butanol. The results exhibit arrays of well-developed subgrains indicative of thermally activated climb recovery. In addition, the free-dislocation density within the polygons is very low, also indicating rampant recovery by climb.



**Figure 4-7. Etched Cleavage Chips from Samples Consolidated at 250°C.**

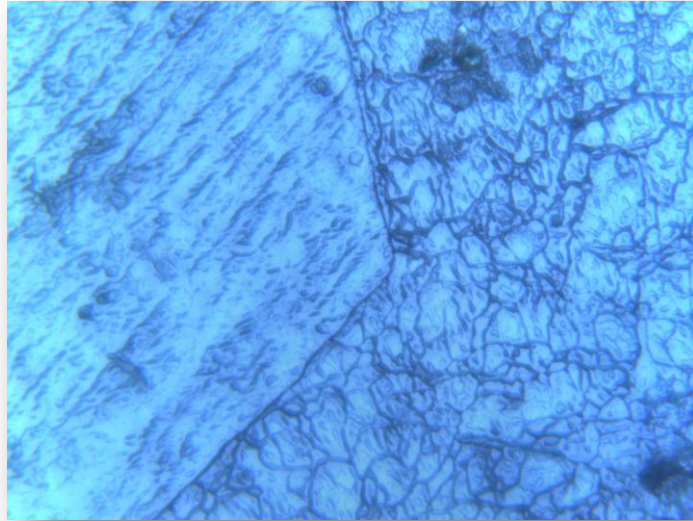
The samples in Figure 4-7 are SQ-250-01 and SQ-250-02 from Table 2. These samples were consolidated at 250°C to measured volumetric strains of 31% (left) and 37% (right). The maximal differential stresses were 6.3 MPa and 11.5 MPa, respectively. Based on previous research summarized by Carter et al. (1982) deformed salt substructure displays a relationship between the applied steady state stress difference and subgrain size. The average subgrain size in these micrographs is approximately 25  $\mu\text{m}$ , which according to (Carter et al., 1982) equates to a stress difference of roughly 7 MPa .

Figure 4-8 is an etched section that has been sputter coated and examined in the SEM. Note the rampant crystal plasticity via polygonization. The small equant grains in the central area exhibit small, tight substructures indicative of high stress difference. The smaller grains are soon to be consumed by solution transfer driven by gradients in chemical potential associated with strain gradients developed between grain contacts and pore walls (Spiers and Brzesowsky, 1993).



**Figure 4-8. Plasticity Coupled Pressure Solution.**

The final micrograph in Figure 4-9 shows an etched cleavage chip confirming classic recrystallization with the relatively clear new grain (left) consuming the highly polygonized grain (right). The horizontal field of view is 500  $\mu\text{m}$ . The strain energy is reduced in the process, which can move at high velocity (Poirier, 1985). Based on previous observational petrofabric research, one might expect more clear evidence of recrystallization, but it was rare in the limited number of samples examined here. Microscopy techniques are tedious and require a level of experience to execute and interpret. Hopefully, additional substructural work can be completed on these very interesting reconsolidated salt samples to elucidate salt substructure features at each temperature. The temperature dependent deformation mechanisms might then be linked to the constitutive model.



**Figure 4-9. Recrystallization.**

## 5 RECOMMENDATIONS AND CONCLUSIONS

This chapter provides a summary of recommendations and conclusions, particularly emphasizing application to salt repository science. Overall, the challenging experimental program proved very successful. The experimental program was systematically designed to perform a qualitative evaluation of crushed salt consolidation as a function of stress and temperature conditions. The laboratory studies provided consolidation behavior for temperature to 250°C and stress to 20 MPa. The test matrix included isostatic, shear, and creep tests, which provided elastic properties as a function of temperature and fractional density. Determinations of elastic properties versus fractional density were made; however, the data remain limited. An important observation during these tests was production of water from the pore pressure port for 250°C tests during the heating phase, despite drying the granular salt at 100°C to constant mass. This observation may have implications for heat-generating waste in salt repositories.

The experimental program comprised a limited number of tests and therefore the matrix conditions were carefully considered, incorporating review and suggestions from international collaborators. There were fewer repeat tests than desirable. To maximize information derived from few experiments, multiple stress and temperature conditions were applied during one test set-up. Ideally each stress and temperature condition would be run individually with specific stress and temperature paths. Additional tests run to extremely low porosities/high fractional densities would be of considerable interest.

The constitutive model developed for crushed salt embodies the observed micromechanisms important for the deformation of crushed salt over a wide range of porosity, stress, loading rate, and moisture content. However, the existence of few elevated temperature tests during development of the model biases its predictive ability to temperatures below 100°C. In addition, the model does not appear to represent short-term crushed salt deformation at high stresses very well, but the occurrence of this type of loading condition in the field is not expected for any salt repository situation. The model components (dislocation creep and pressure solution) include exponential temperature functions that significantly increase strain rates with temperature increases. Although no attempt was made at this point to use the limited number of tests to determine parameter values or develop new temperature dependencies for the model, the laboratory tests conducted and reported here provide a good foundation for the dataset that will ultimately be needed to further develop the temperature dependencies for the model. Because the presence of moisture is extremely important in crushed salt deformation, evaluation of moisture presence and changes during the tests will be important. Regardless of the lack of a complete high temperature database for development of model parameters, overall the model does reasonably well predicting the tests at temperatures of 100°C, 175°C, and 250°C.

As with much cutting-edge science, certain areas remain where additional research could add value. From the laboratory point of view, loading variations, differing stress paths and some repeated load cycles could help quantify results. A variety of parameter excursions would characterize temperature and porosity influences. With additional testing, selection could be made of certain samples at various states of consolidation for microstructural observations. Additional examination and documentation of substructures would help more clearly and fully understand the consolidation mechanisms from initial stages with high porosity to the dense stages as porosity is minimized. Additional substructural microscopy could illuminate governing deformational processes at intermediate temperatures, porosity and other factors—such as the

nature of water availability. Notwithstanding these recommendations for additional investigations, granular salt consolidation has an impressive fundamental scientific basis and the research reported here substantially advances our understanding of granular salt reconsolidation at high temperatures.

The recent 3rd US/German Workshop on Salt Repository Research, Design and Operations highlighted the special topic of granular salt reconsolidation. One recommendation considered by the international experts is creation of a state-of-the-art review paper that addresses salt repository applications, such as geotechnical barriers, while illustrating the operating mechanisms. Mechanistically, the consolidation model behavior in the high porosity range is not well constrained, but for seal system design, analysis and performance, these conditions are relatively less imperative than the low porosity range, which may not be sufficiently validated and calibrated in salt repository applications. Not all of these recommendations can be addressed by additional laboratory and microscopy studies; there is a need for systematic reviews of industry experience and forensics of salt reconsolidation from operating salt mines. In some respects up-scaling consolidation behavior measured at the laboratory scale to field-scale magnitudes is essential.

In terms of application of granular salt reconsolidation to salt repositories, the following conclusions can be made:

- Shaft seal construction methods can readily place mine-run salt in a vertical shaft to 90% theoretical density. Thereafter, compression of the surrounding formation will readily reduce the porosity and attendant permeability. Relatively low pressure is needed to affect low porosity and permeability. Ambient reconsolidation is well understood in terms of design, construction and performance.
- Evidence convincingly demonstrates that fluid aided consolidation processes will govern low-porosity consolidation for bedded salt, even when mine-run salt is purposefully dried.
- Drift seal system elements present a greater construction and performance assessment challenge because of the difficulty associated with placement of granular salt to relatively high density in a horizontal configuration.
- Overall, the preponderance of scientific information, empirical evidence, industry practice, micromechanics, and modeling provide confidence in granular salt seal element performance in repository applications.

## 6 REFERENCES

Aubertin, M. and H.R. Hardy. 1996. The Mechanical Behavior of Salt, Proceedings of the Fourth Conference. Montreal Canada. Trans Tech Publications. ISBN 0-87849-103-1.

Bauer, S.J. 2012. *Consolidation of Crushed Salt at Temperatures up to 250°C under Hydrostatic and Shear Stresses, Rev. 1*. SNL-FCT-TP-11-0001. Sandia National Laboratories, Albuquerque, NM.

Bechthold, W., E. Smailos, S. Heusermann, W. Bollingerfehr. B. Ba-Zargan Sabot, T. Rothfuchs, P. Kamlot, J. Grupa, S. Olivella, F.D. Hansen, 2004. *Backfilling and Sealing of Underground Repositories for Radioactive Waste in Salt (BAMBUS II-Project)*, Final report, EUR 20621 EN, Nuclear Science and Technology, European Commission, Brussels.

Brodsky, N.S. 1994. *Hydrostatic and Shear Consolidation Tests With Permeability Measurements on Waste Isolation Pilot Plant Crushed Salt*. SAND93-7058, prepared by RE/SPEC Inc., Rapid City, SD, for Sandia National Laboratories, Albuquerque, NM.

Brodsky, N.S., F.D. Hansen, and T.W. Pfeifle. 1996. *Properties of Dynamically Compacted WIPP Salt*. Proceeding of the 4th Conference on the Mechanical Behavior of Salt, Trans Tech Publications, Clausthal-Zellerfeld, Germany. SAND96-0838C.

Callahan, G.D. 1999, *Crushed Salt Constitutive Model*, SAND98-2680. Sandia National Laboratories, Albuquerque, NM.

Callahan, G.D., A.F. Fossum, and D.K. Svalstad. 1989. *Documentation of SPECTROM-32: A Finite Element Thermomechanical Stress Analysis Program*. DOE/CH/10378-2, prepared by RE/SPEC Inc., Rapid City, SD, for the U.S. Department of Energy, Chicago Operations Office, Argonne, IL, Vol. I and II.

Callahan, G.D., M.C. Loken, L.D. Hurtado, and F.D. Hansen. 1996. *Evaluation of Constitutive Models for Crushed Salt*, Proceeding of the 4th Conference on the Mechanical Behavior of Salt, Trans Tech Publications, Clausthal-Zellerfeld, Germany. SAND96-0791C.

Callahan, G.D., M.C. Loken, L.L. Van Sambeek, R. Chen, T.W. Pfeifle, J.D. Nieland, and F.D. Hansen. 1995. *Evaluation of Potential Crushed-Salt Constitutive Models*. SAND95-2143, prepared by RE/SPEC Inc., Rapid City, SD, for Sandia National Laboratories, Albuquerque, NM.

Callahan, G.D., K.D. Mellegard, and F.D. Hansen. 1998. *Constitutive Behavior of Reconsolidating Crushed Salt*. International Journal of Rock Mechanics and Mining Sciences, Vol. 35, No. 4/5, Paper No. 029.

Carter, N.L., F.D. Hansen, and P.E. Senseny. 1982. *Stress Magnitudes in Natural Rock Salt*, Journal of Geophysical Research, Vol. 87, pp. 9289-9300.

DOE. 2011. *A Management Proposal for Salt Disposal Investigations with a Field Scale Heater Test at WIPP*. DOE/CBFO-11-3470. June 2011. U.S. DOE Carlsbad Field Office

Franssen, R.C.W. and C.J. Spiers. 1990. *Deformation of Polycrystalline Salt in Compression and in Shear at 250-350°*. Geological Society Special Publication No. 45.

Hansen, F.D. 1985. *Deformation Mechanisms of Experimentally Deformed Salina Basin Bedded Salt*. Battelle Memorial Institute. Office of Nuclear Waste Isolation. Columbus, OH. BMI/ONWI-552.

Hansen, F.D. 1997. *Reconsolidating salt: Compaction, Constitutive Modeling, and Physical Processes*. Int. J. Rock Mech. & Min. Sci. Vol 34, No. 3-4.

Hansen F.D. and E.H. Ahrens. 1996. *Large-Scale Dynamic Compaction of Natural Salt*. Proceeding of the 4th Conference on the Mechanical Behavior of Salt, Trans Tech Publications, Clausthal-Zellerfeld, Germany. SAND96-0792C.

Hansen, F.D. and C.D. Leigh. 2011. *Salt Disposal of Heat-generating Nuclear Waste*, SAND2011-0161. Sandia National Laboratories, Albuquerque, NM.

Hansen, F.D. and M.K. Knowles. 1999. *Design and Analysis of a Shaft Seal System for the Waste Isolation Pilot Plant*. Sandia National Laboratories, Albuquerque, NM. SAND99-0904J.

Hansen, F.D., G.D. Callahan, M.C. Loken, and K.D. Mellegard. 1998. *Crushed-Salt Constitutive Model Update*. SAND97-2601, prepared by RE/SPEC Inc., Rapid City, SD, for Sandia National Laboratories, Albuquerque, NM.

Holcomb, D.J. and D.W. Hannum. 1982. *Consolidation of Crushed Salt Backfill under Conditions Appropriate to the WIPP Facility*. SAND82-0630. Sandia National Laboratories, Albuquerque, NM.

Holcomb, D.J. and M. Shields. 1987. *Hydrostatic Creep Consolidation of Crushed Salt with Added Water*. SAND87- 1990. Sandia National Laboratories, Albuquerque, NM.

Holcomb, D.J. and D.H. Zeuch. 1990. *Modeling the Consolidation of a Porous Aggregate of Dry Salt as Isostatic Hot Pressing*, *J. Geophys. Res.* V. 95, p. 15611-15622.

Munson, D.E. 1979. *Preliminary Deformation-Mechanism Map for Salt (With Application to WIPP)*. SAND79-0076. Sandia National Laboratories, Albuquerque, NM.

Munson, D.E. and P.R. Dawson. 1979. *Constitutive Model for the Low Temperature Creep of Salt (With Application to WIPP)*. SAND79-1853. Sandia National Laboratories, Albuquerque, NM.

Munson, D.E., A.F. Fossum, and P.E. Senseny. 1989. *Advances in Resolution of Discrepancies Between Predicted and Measured In Situ WIPP Room Closures*. SAND88-2948. Sandia National Laboratories, Albuquerque, NM.

Pfeifle, T.W. 1995. *WIPP Crushed-Salt Database for Constitutive Model Evaluations*. Calculation File 325/04/03, prepared by RE/SPEC Inc., Rapid City, SD, for Sandia National Laboratories, Albuquerque, NM.

Pfeifle, T.W., and P.E. Senseny. 1985. *Permeability and Consolidation of Crushed Salt from the WIPP Site*. Topical Report RSI-0278. Prepared for Sandia National Laboratories, Albuquerque, NM. Rapid City, SD: RWSPEC Inc. (Copy on file in the Sandia WIPP Central Files, Sandia National Laboratories, Albuquerque, NM as WPO#36824.)

Poirier, J.P. 1985. *Creep of Crystals*. Cambridge University Press.

Popp, T. and K. Salzer. 2011. *Diskussionbeitrag zum Kompaktionsverhalten und den hydraulischen Eigenschaften von Salzgrusversatz*, Institut für Gebirgsmechanik GmbH Leipzig Germany.

Sjaardema, G.D. and R.D. Krieg. 1987. *A Constitutive Model for the Consolidation of WIPP Crushed Salt and Its Use in Analyses of Backfilled Shaft and Drift Configuration*. SAND87-1977. Sandia National Laboratories, Albuquerque, NM.

Spiers, C.J. and R.H. Brzesowsky. 1993. *Densification Behaviour of Wet Granular Salt: Theory versus Experiment*. 7<sup>th</sup> Symposium on Salt. Vol. I. Elsevier Science Publishers B.V. Amsterdam.

Spiers, C.J., P.M.T.M. Schutjens, R.H. Brzesowsky, C.J. Peach, J.L. Liezenberg, and H.J. Zwart. 1990. *Experimental Determination of Constitutive Parameters Governing Creep of Rocksalt by Pressure Solution*. Geological Society Special Publication No. 54.

Wallner, M., K-H Lux, W. Minkley, and H.R. Hardy. 2007. *The Mechanical Behavior of Salt, Proceeding of the Sixth Conference*. Hannover Germany. Balkema. ISBN 13: 978-415-444398-2.

Zeuch, D.H., D.J. Zimmerer, and M.E. Shields. 1991. *Interim Report on the Effects of Brine-Saturation and Shear Stress on Consolidation of Crushed, Natural Rock Salt from the Waste Isolation Pilot Plant (WIPP)*. SAND91-0105. Sandia National Laboratories, Albuquerque, NM.

Zhang, C.-L., T. Rothfuchs, and J. Droste. 2007 *Post-Tests on Thermo-Mechanically Compacted Salt Backfill*. 6<sup>th</sup> Conference on the Mechanical Behavior of Salt. Hannover, Germany.



## Appendix A

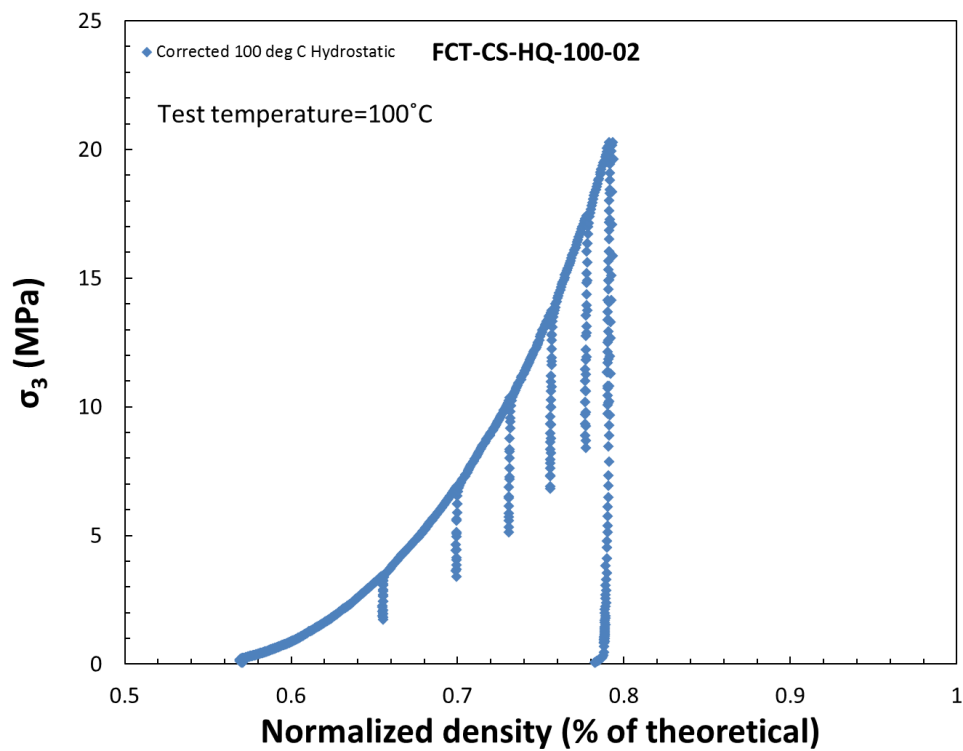
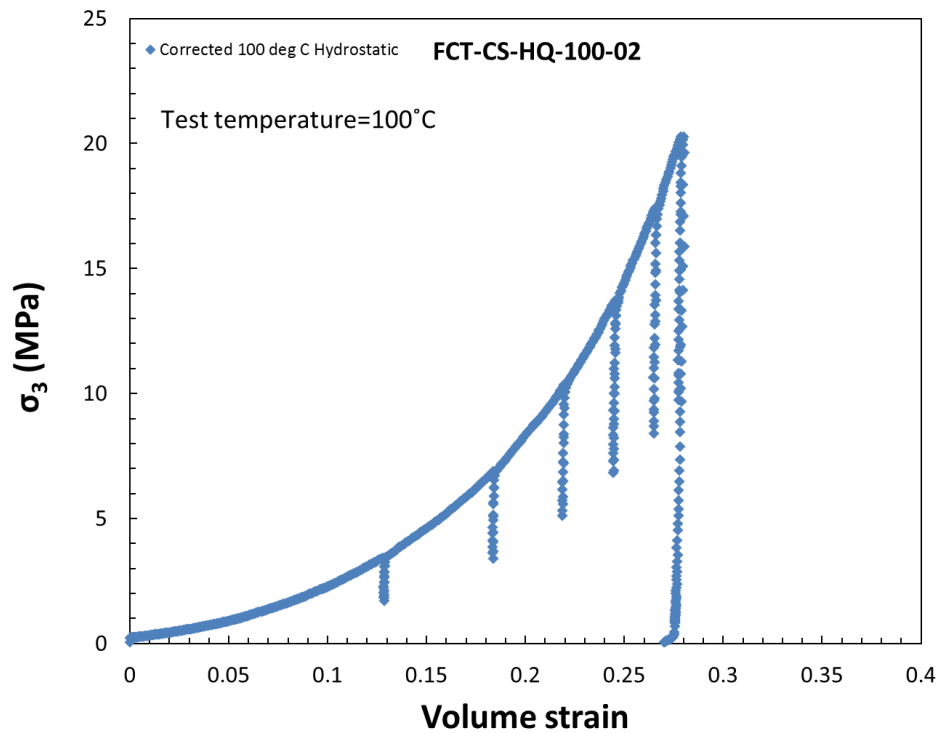
### MECHANICAL PROPERTY TEST RESULTS

Appendix A contains plots of all experiments completed.

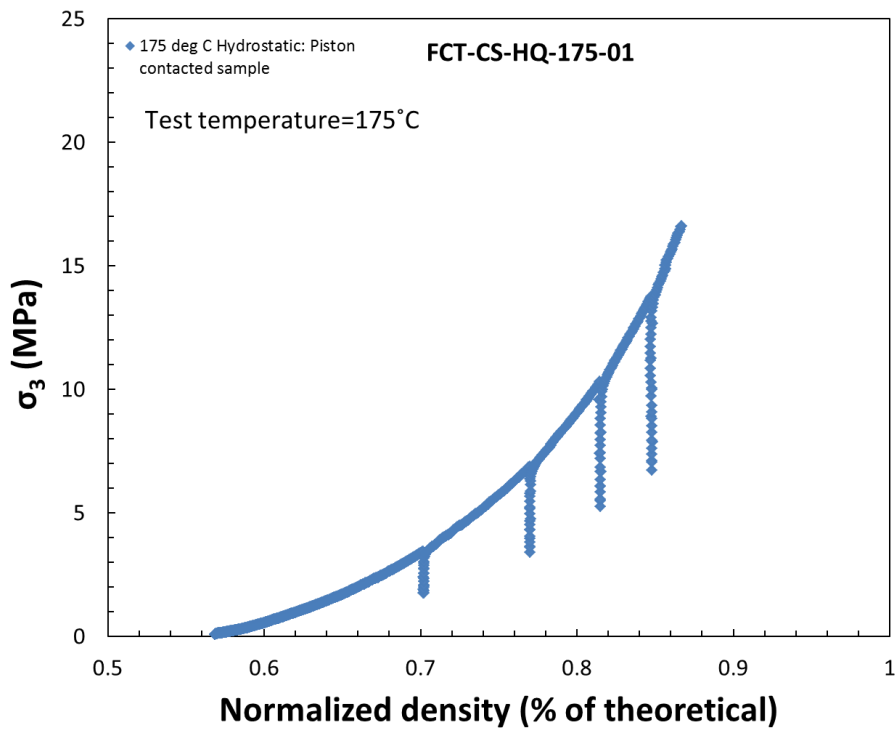
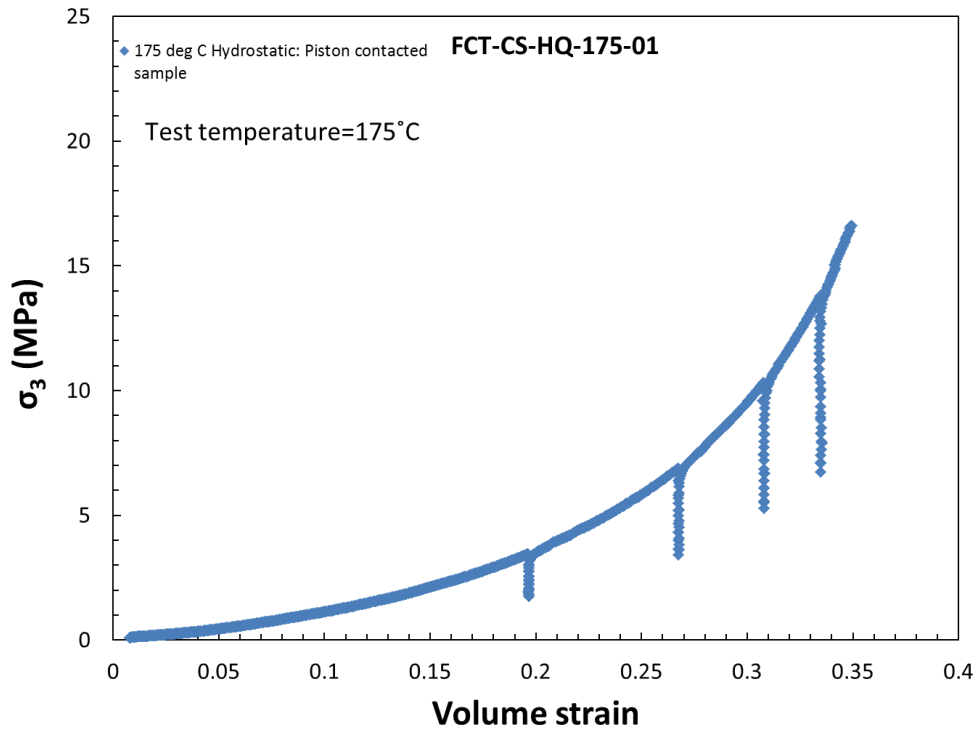
- Experiments FCT-CS-HQ-100-02, FCT-CS-HQ-175-0, and FCT-CS-HQ-250-02 are isostatic
- Experiments FCT-CS-SQ-250-0 and FCT-CS-SQ-250-02 are isostatic and quasistatic shear
- Experiments FCT-CS-CR-250-01, FCT-CS-CR-175-01, FCT-CS-CR-175-01, FCT-CS-CR-175-02, FCT-CS-CR-100-01, FCT-CS-CR-250-05, FCT-CS-CR-100-02, and FCT-CS-CR-100-03 are isostatic and quasistatic shear and creep
- Experiments FCT-CS-HQ-ALL-01 and FCT-CS-HQ-ALL-02 are multi-temperature isostatic
- List of Experiments:

FCT-CS-HQ-100-02.....	A-2
FCT-CS-HQ-175-01.....	A-3
FCT-CS-HQ-250-02.....	A-4
FCT-CS-SQ-250-01.....	A-5
FCT-CS-SQ-250-02.....	A-7
FCT-CS-CR-250-01.....	A-8
FCT-CS-CR-175-01.....	A-9
FCT-CS-CR-175-02.....	A-11
FCT-CS-CR-100-01.....	A-12
FCT-CS-CR-250-05.....	A-14
FCT-CS-CR-100-02.....	A-15
FCT-CS-CR-100-03.....	A-17
FCT-CS-HQ-ALL-01.....	A-18
FCT-CS-HQ-ALL-02.....	A-19

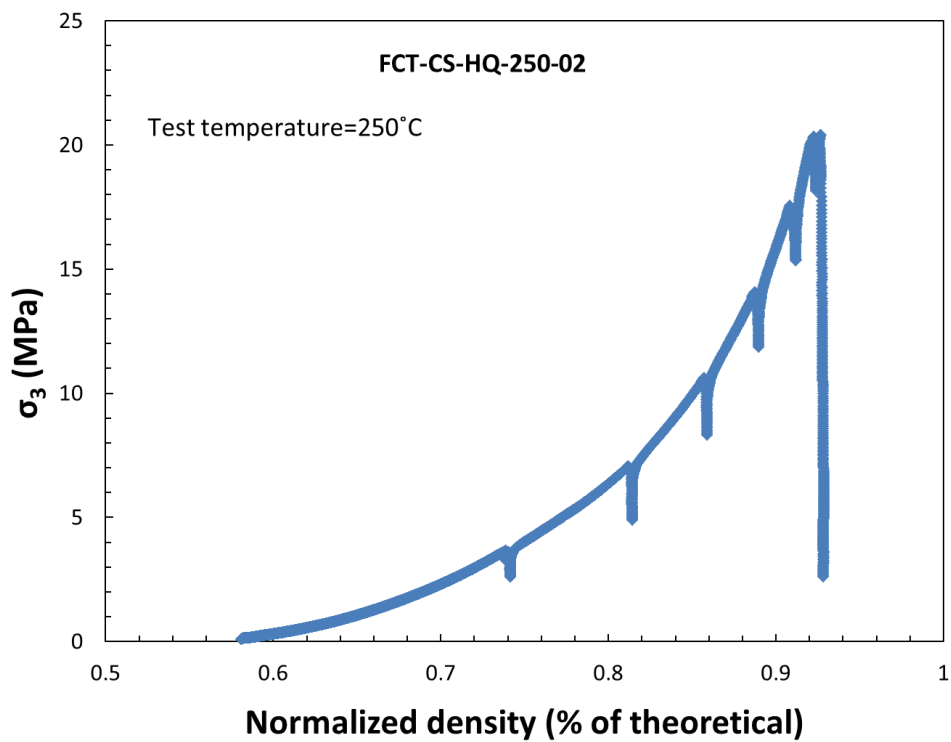
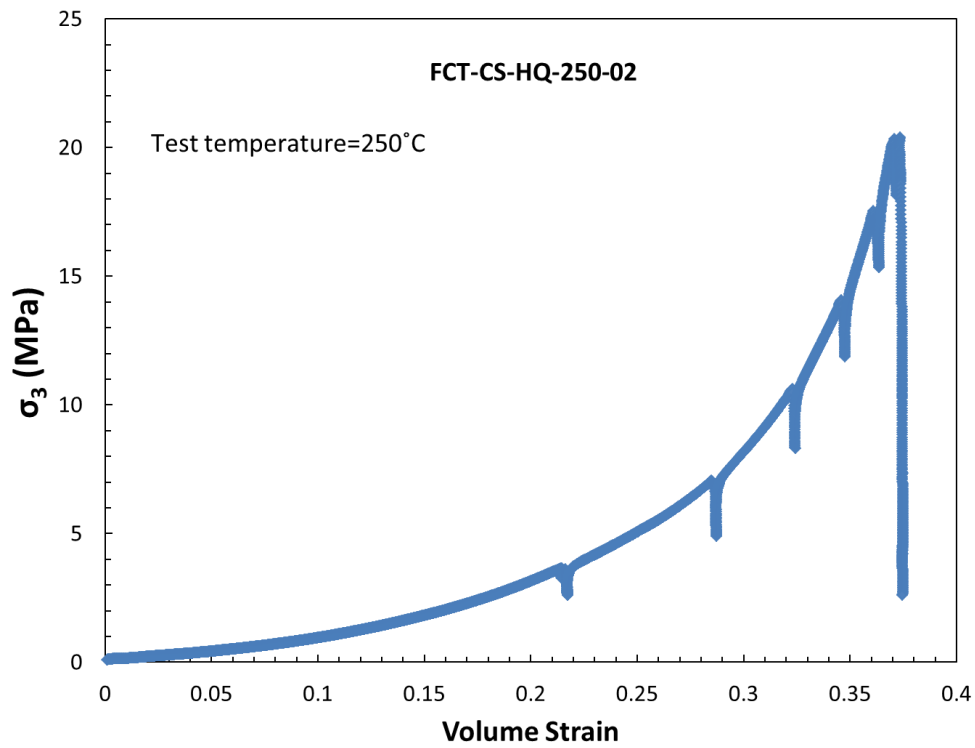
## A-1. FCT-CS-HQ-100-02

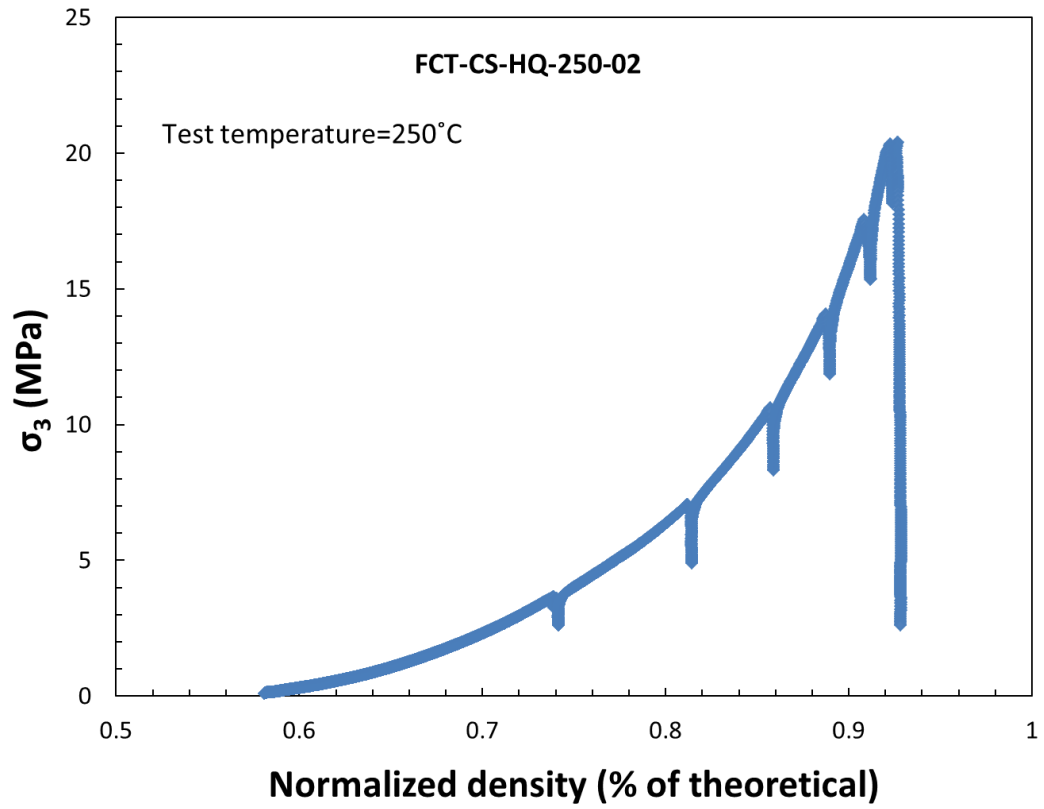


## A-2. FCT-CS-HQ-175-01

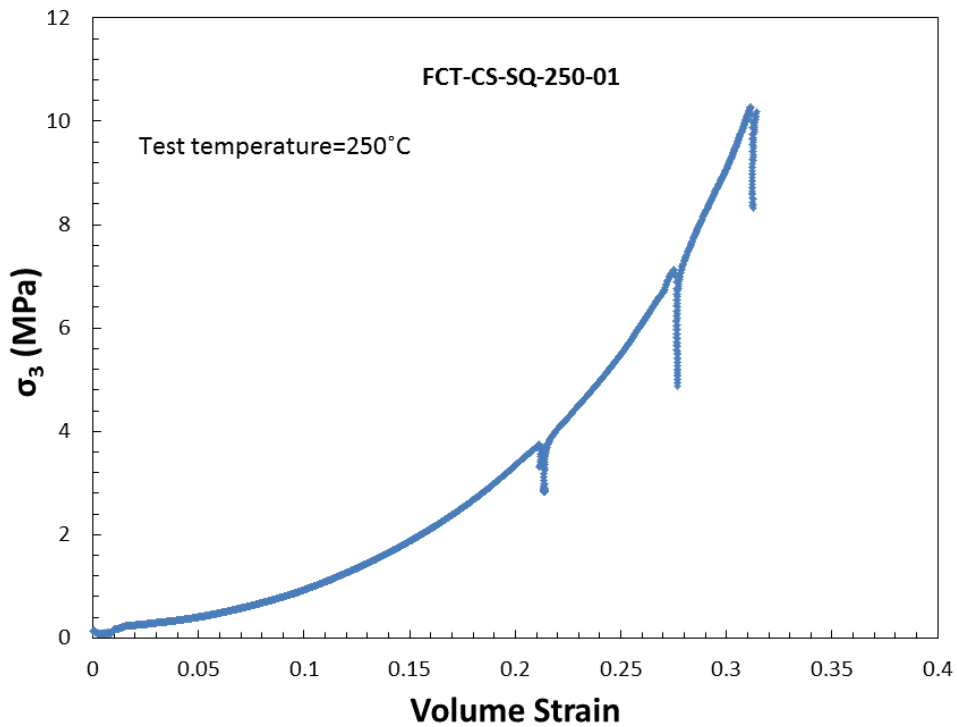


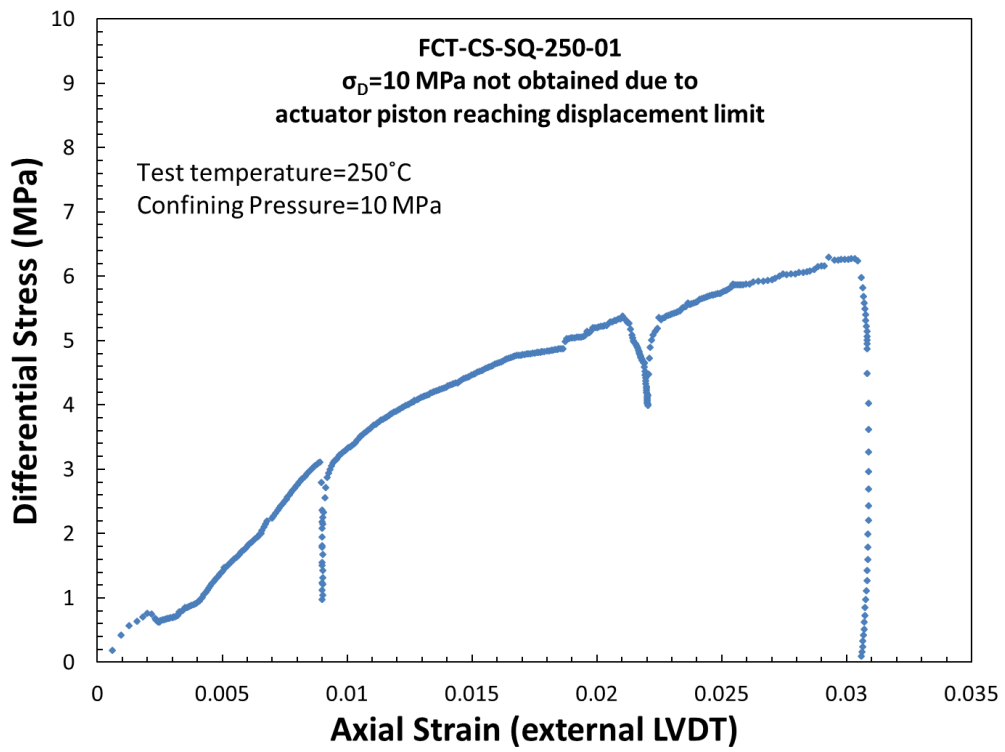
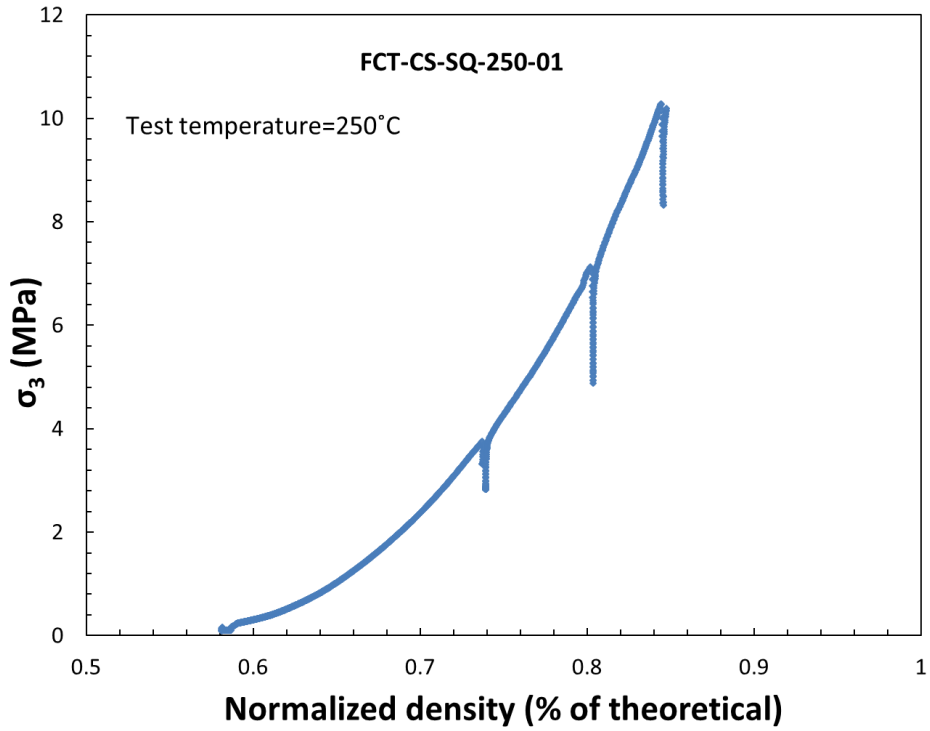
## A-3. FCT-CS-HQ-250-02



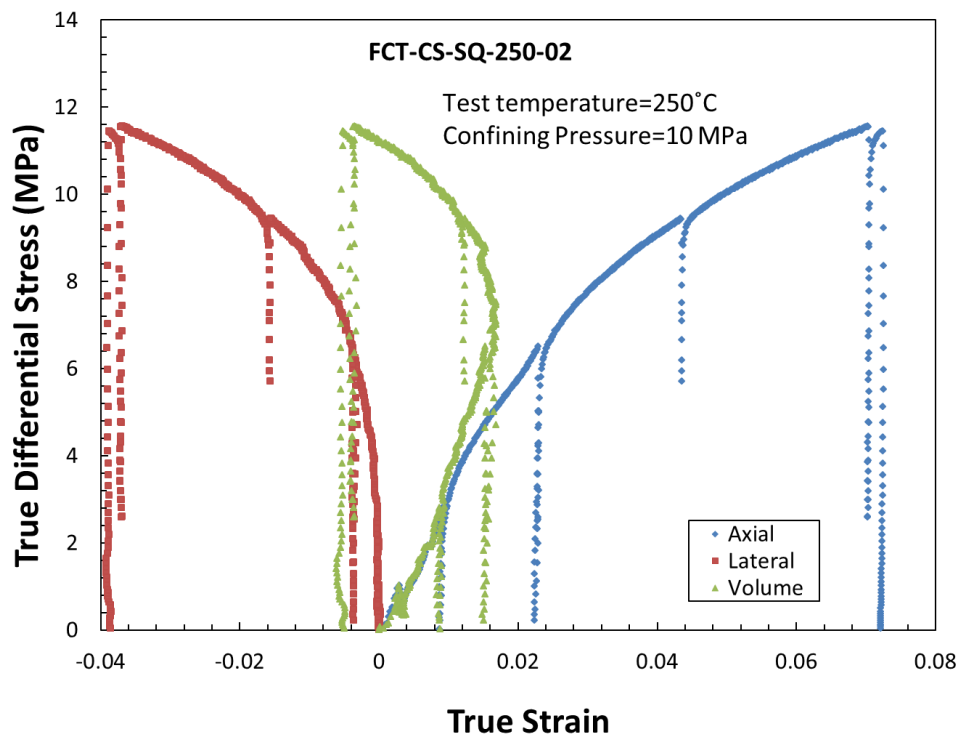
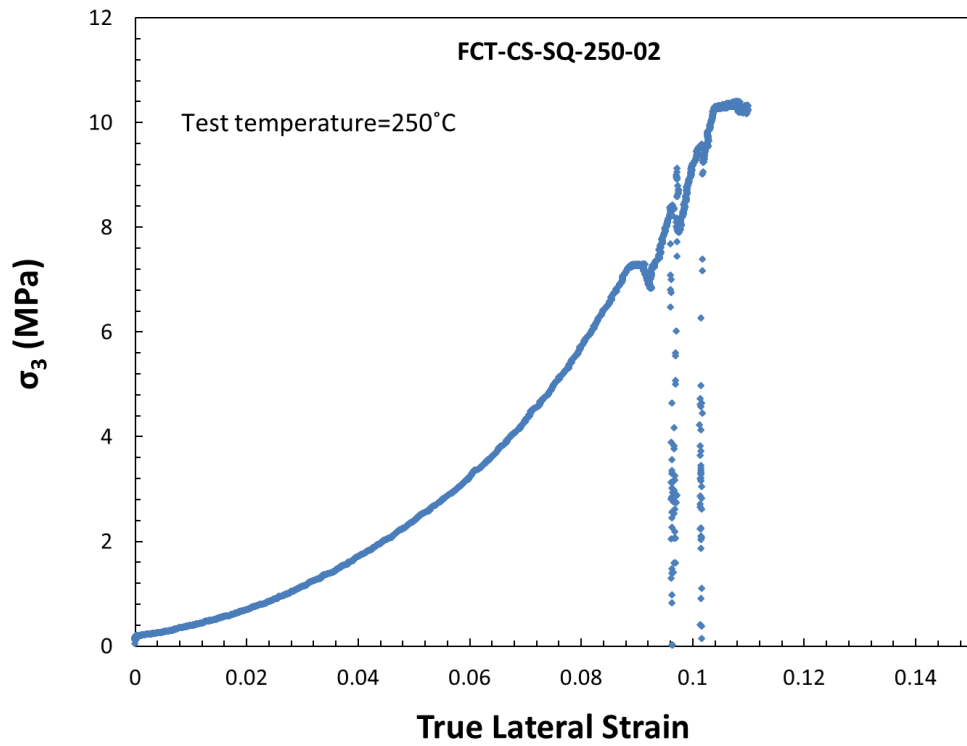


**A-4. FCT-CS-SQ-250-01**

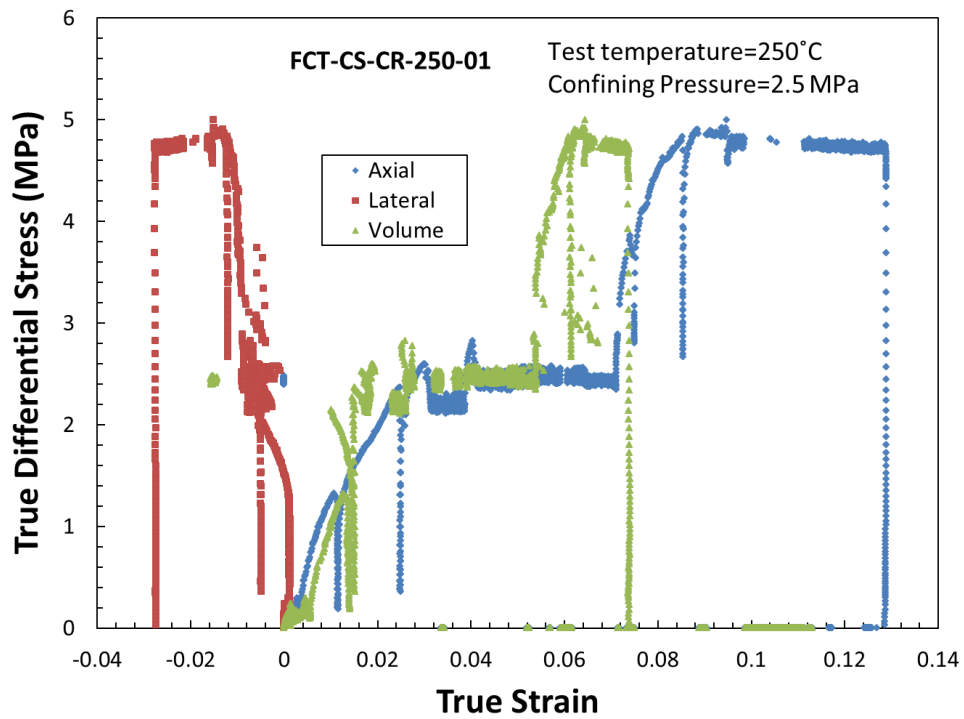
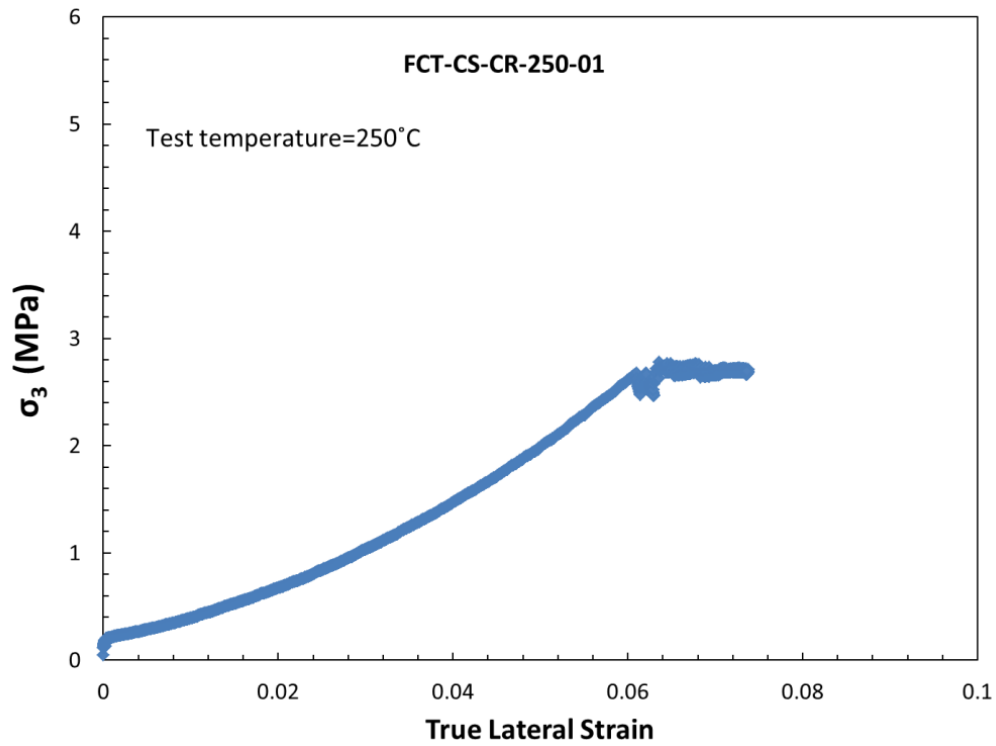


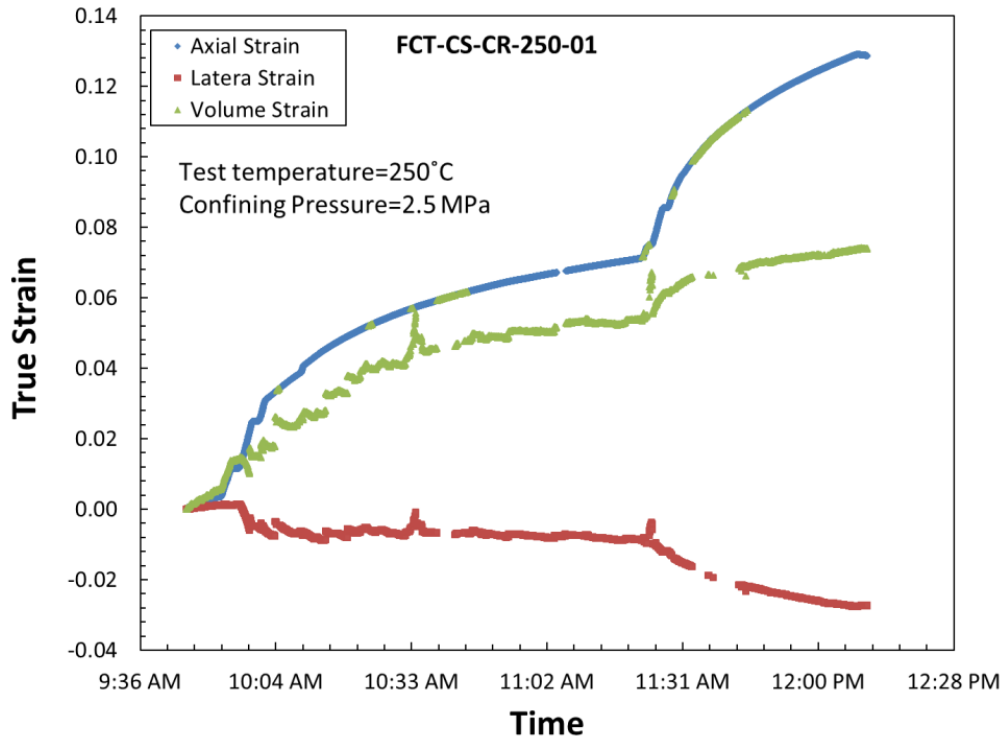


### A-5. FCT-CS-SQ-250-02

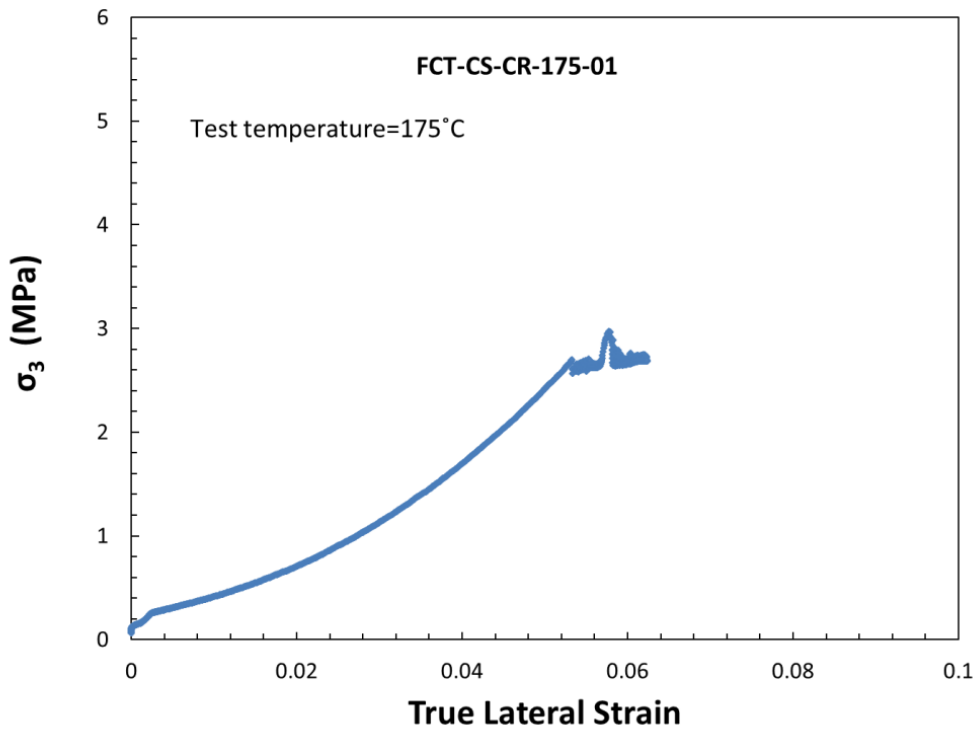


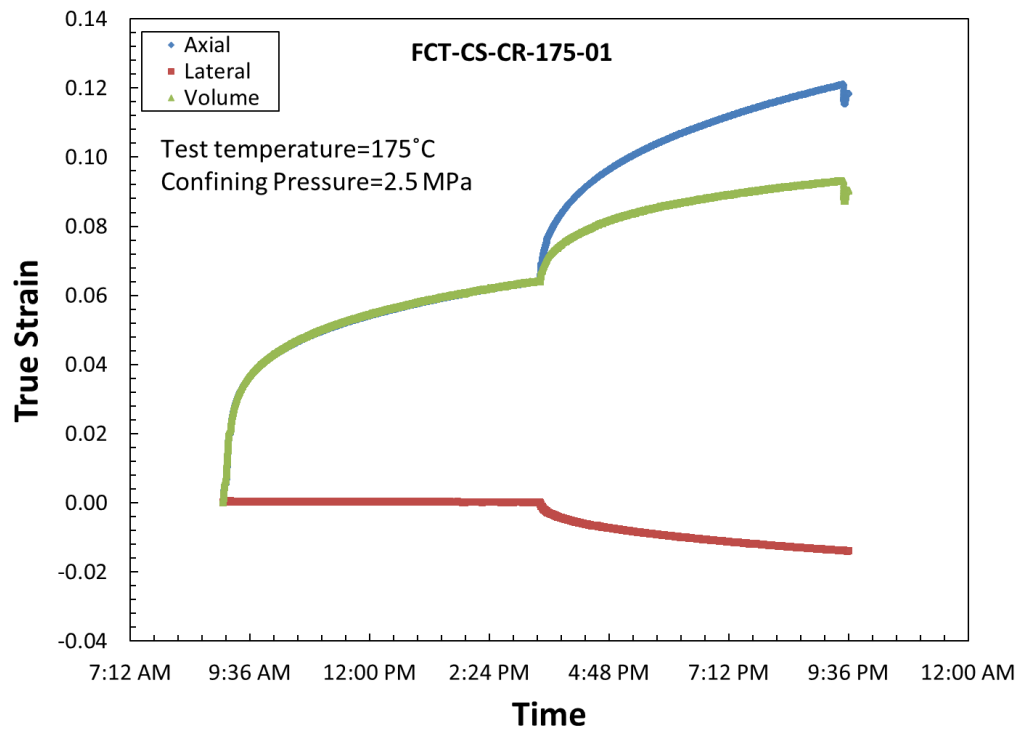
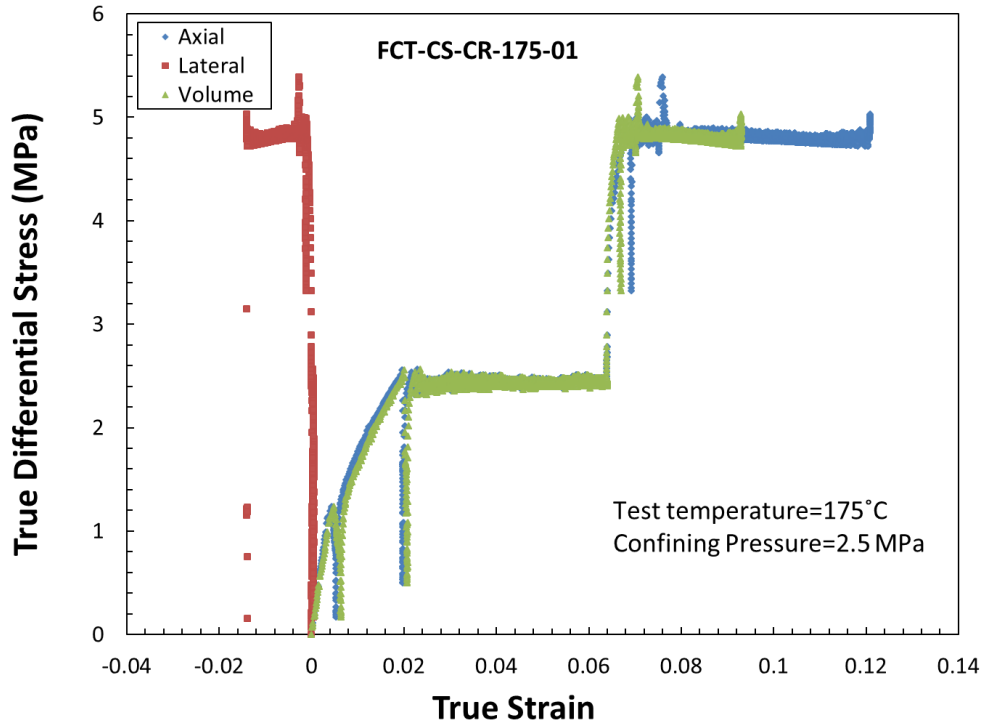
## A-6. FCT-CS-CR-250-01



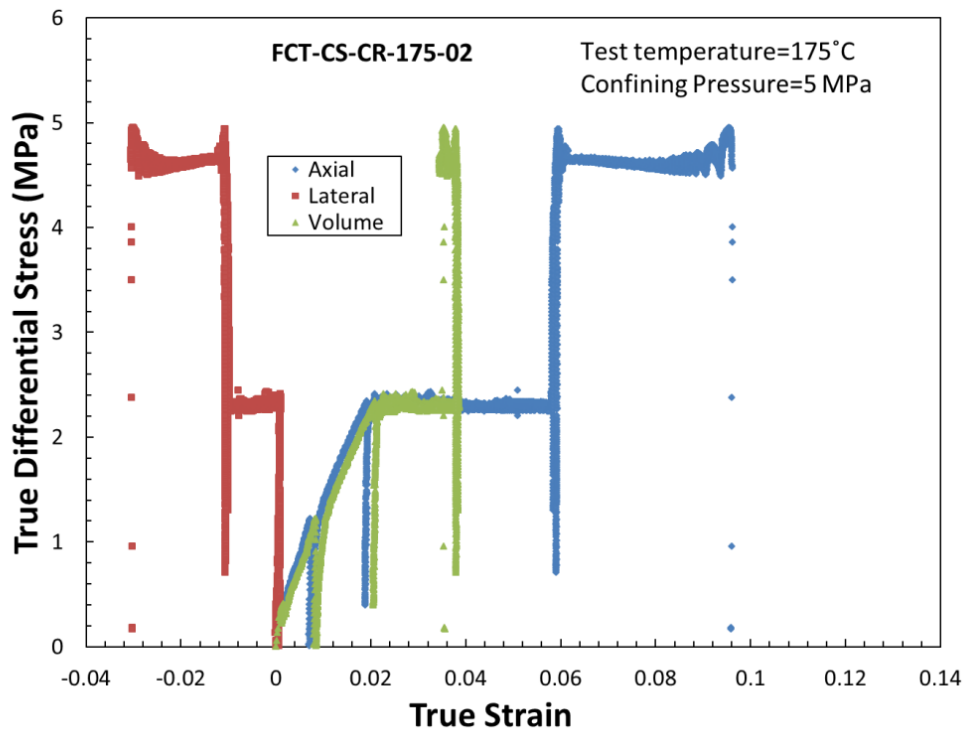
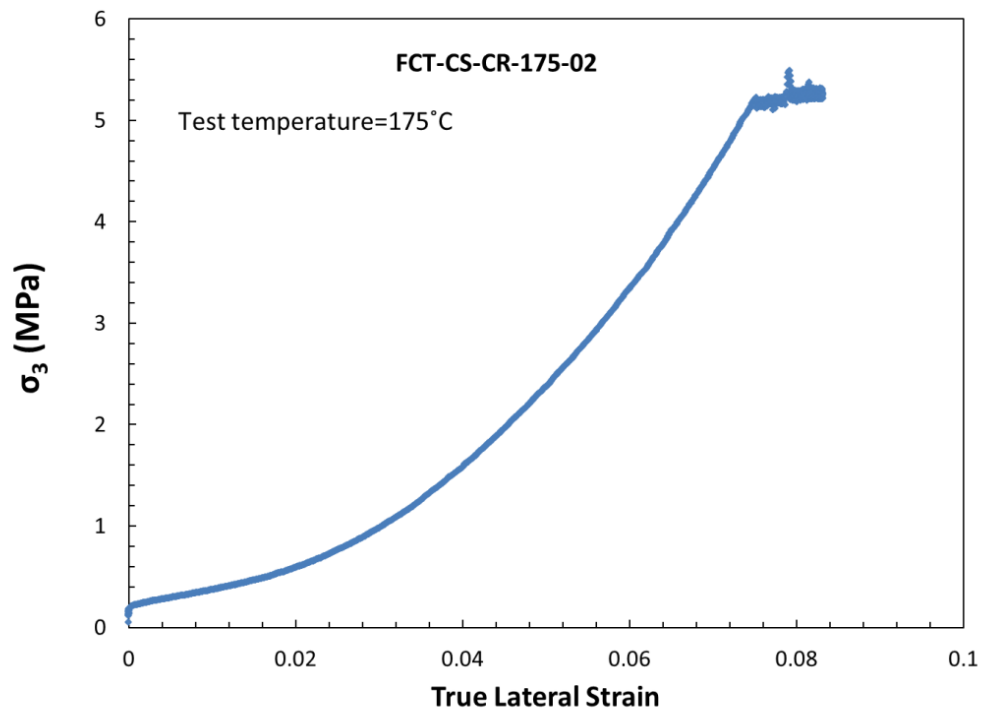


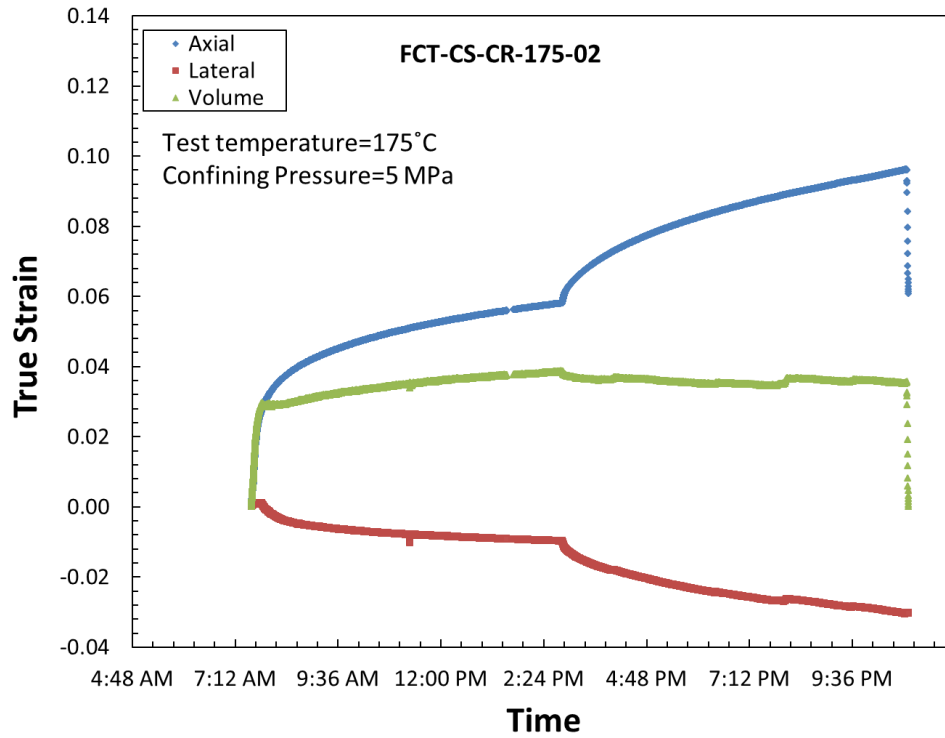
**A-7. FCT-CS-CR-175-01**



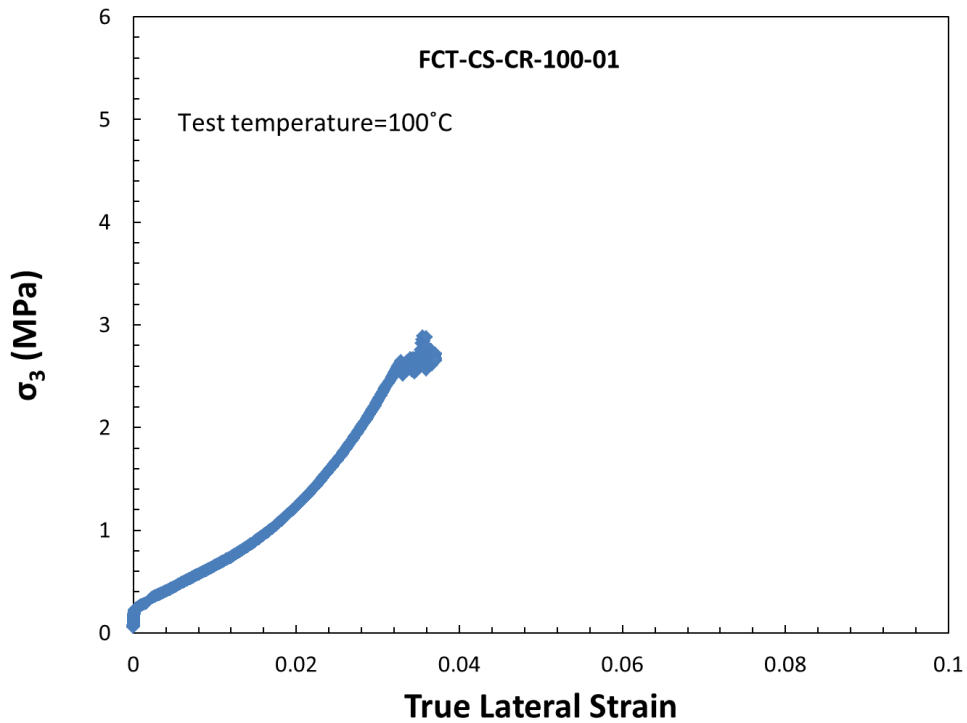


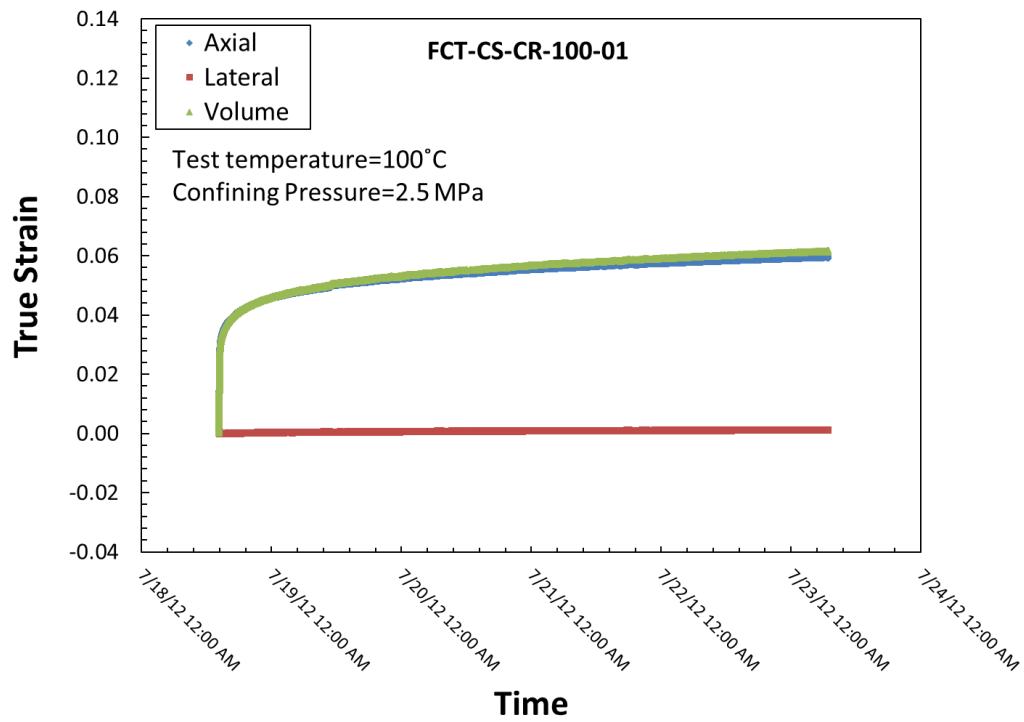
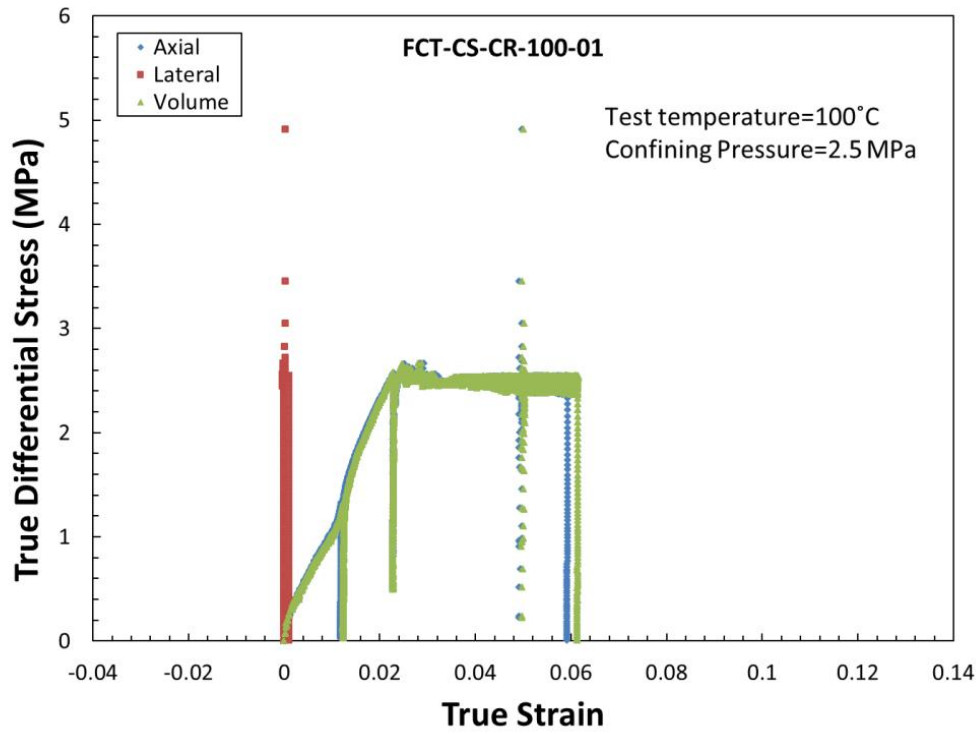
### A-8. FCT-CS-CR-175-02



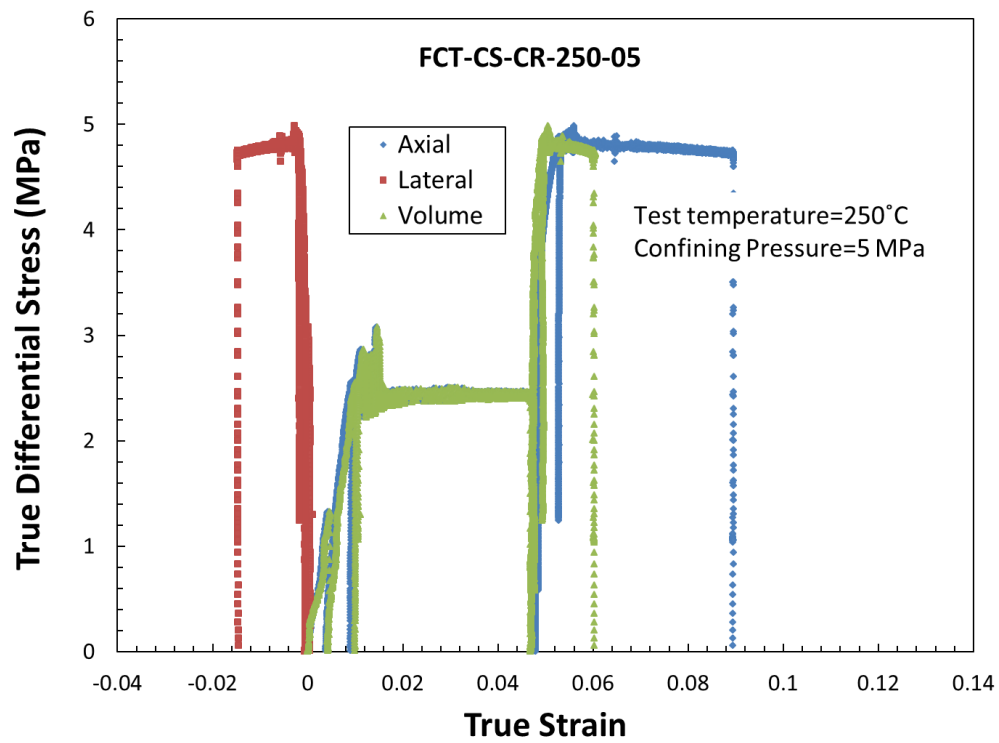
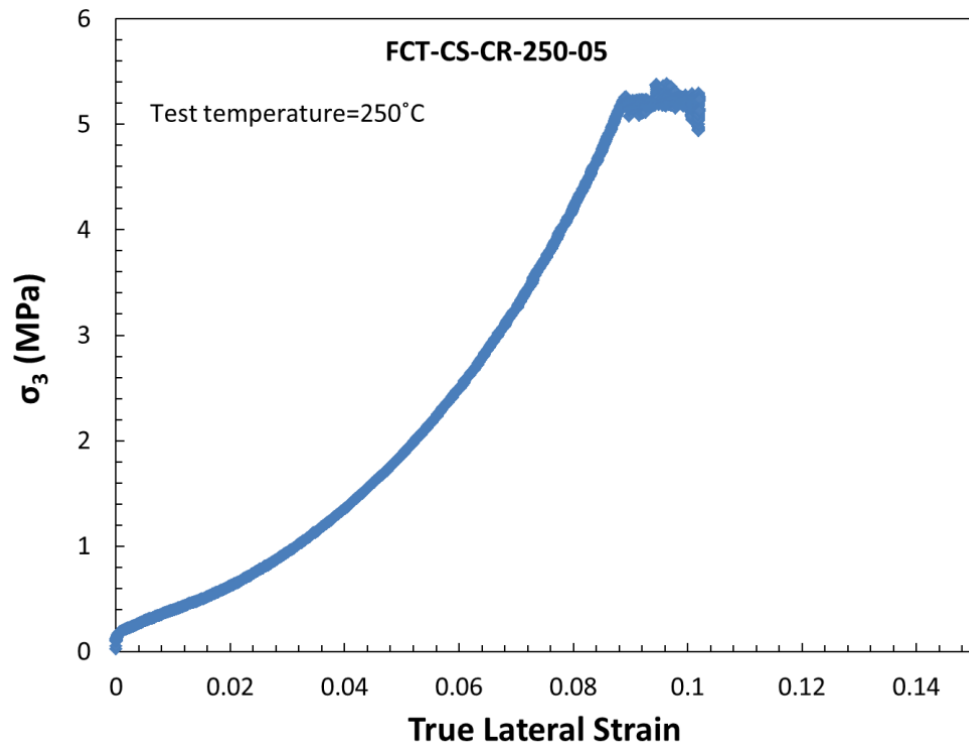


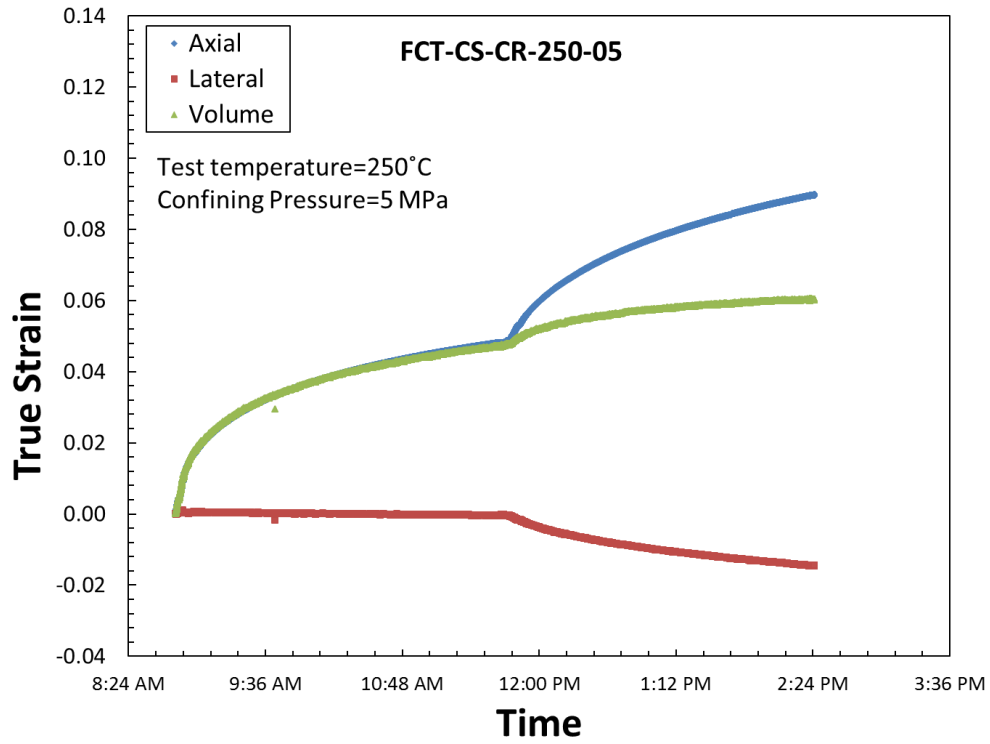
**A-9. FCT-CS-CR-100-01**



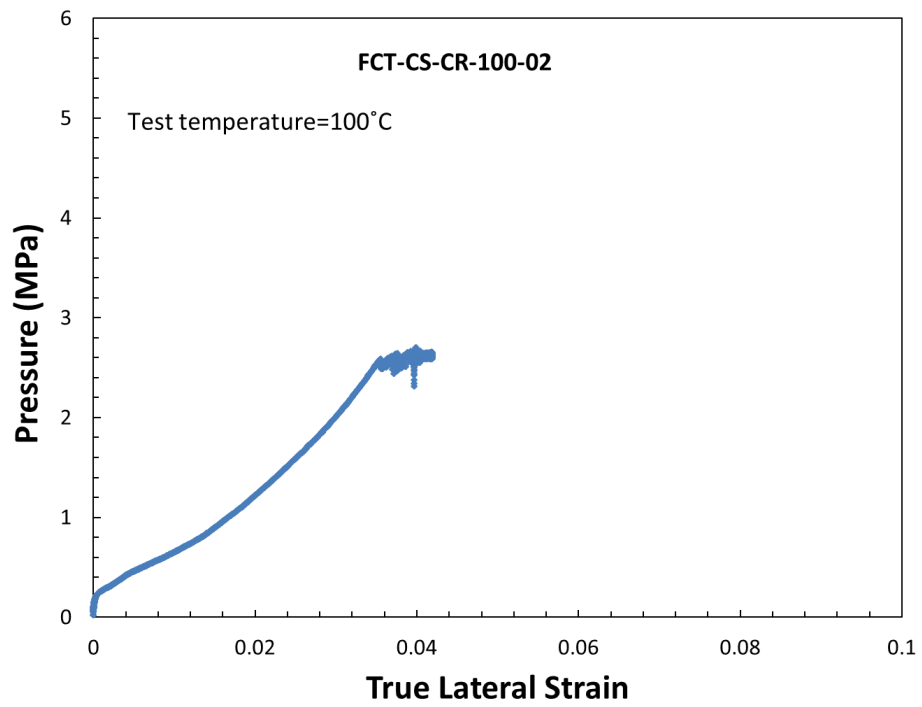


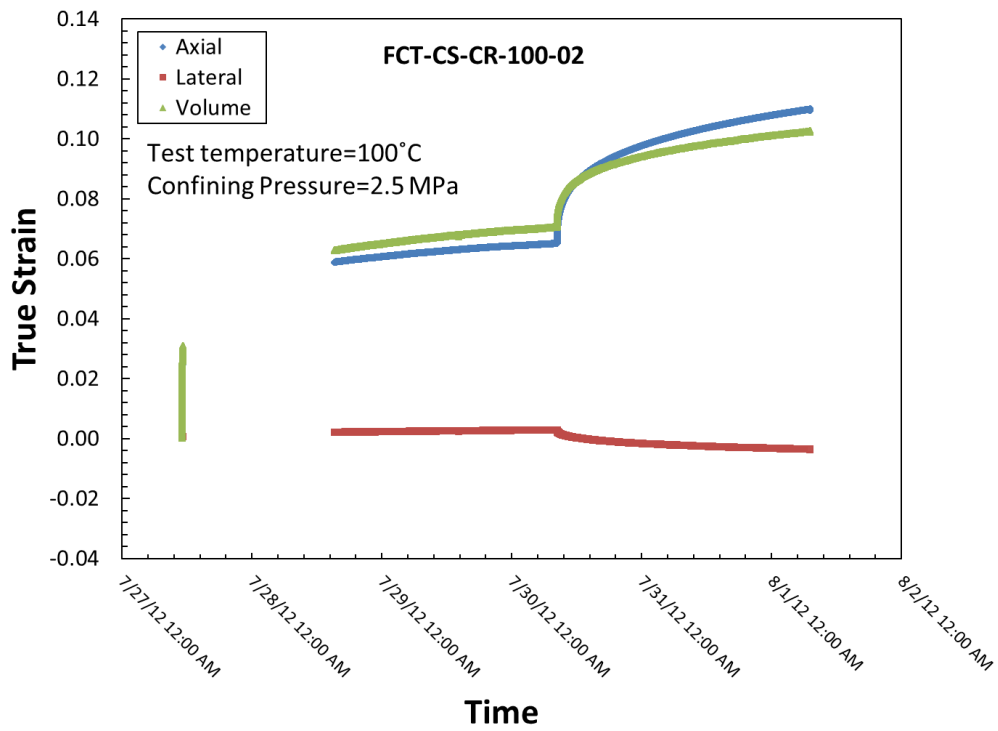
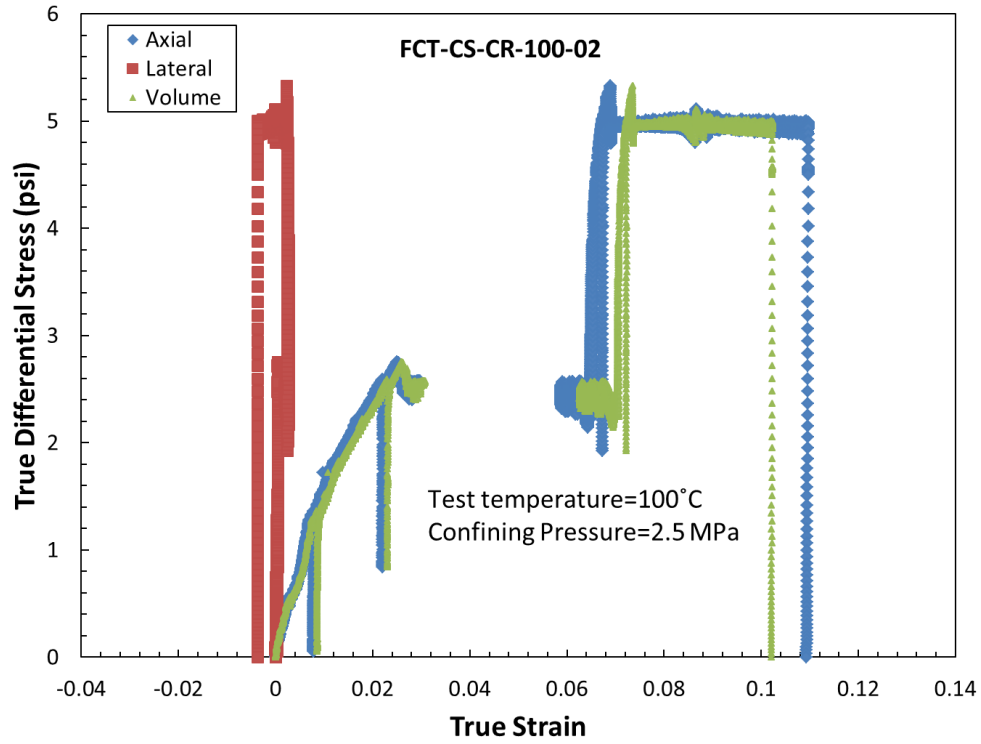
## A-10. FCT-CS-CR-250-05



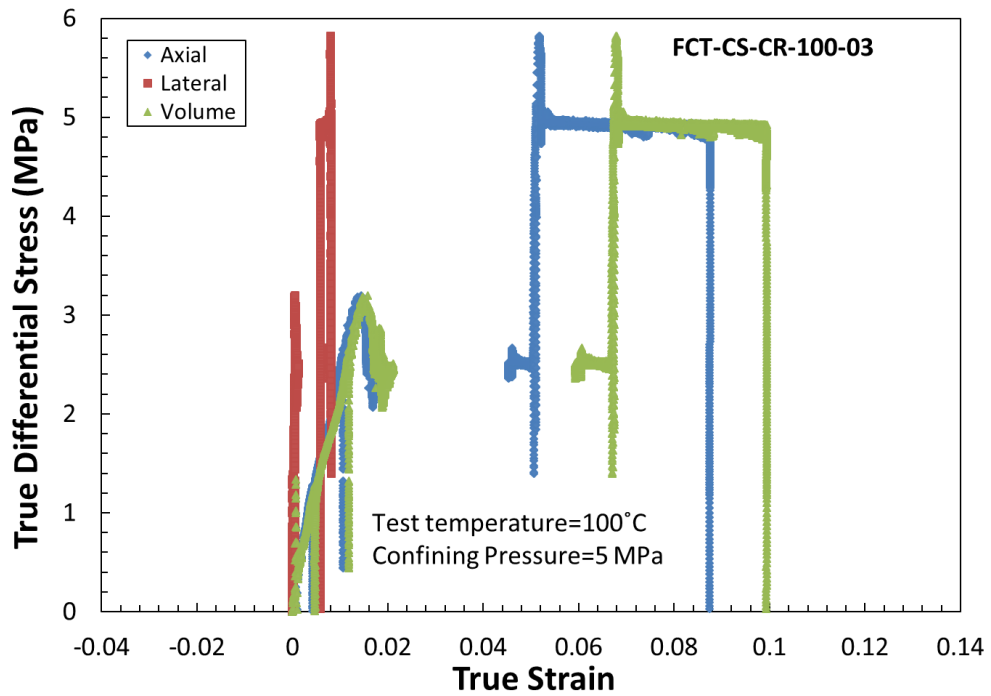
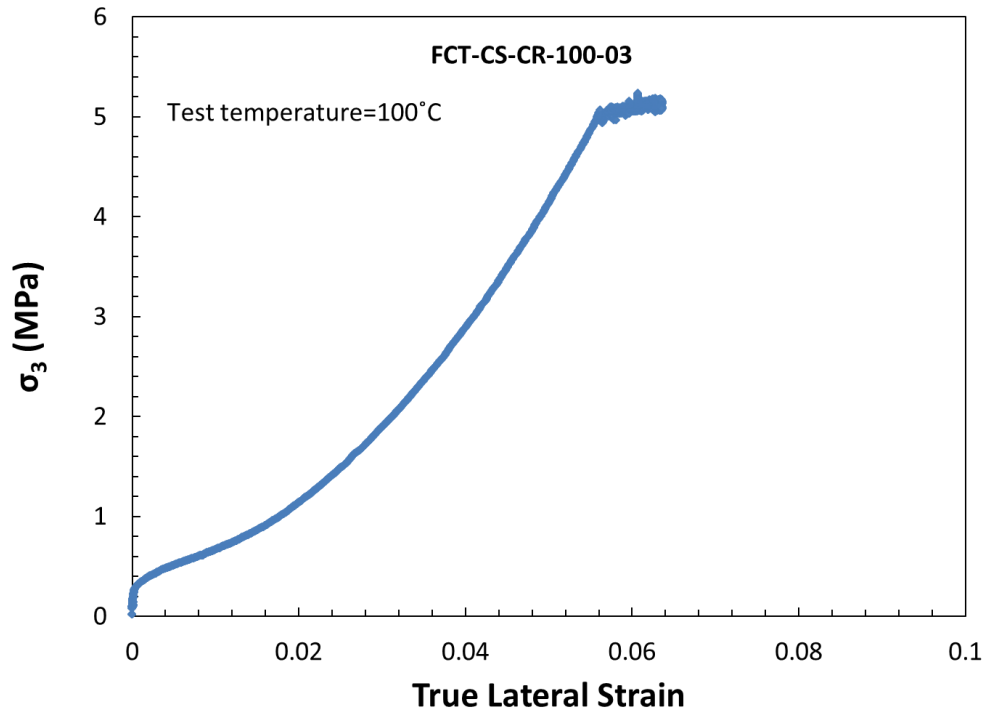


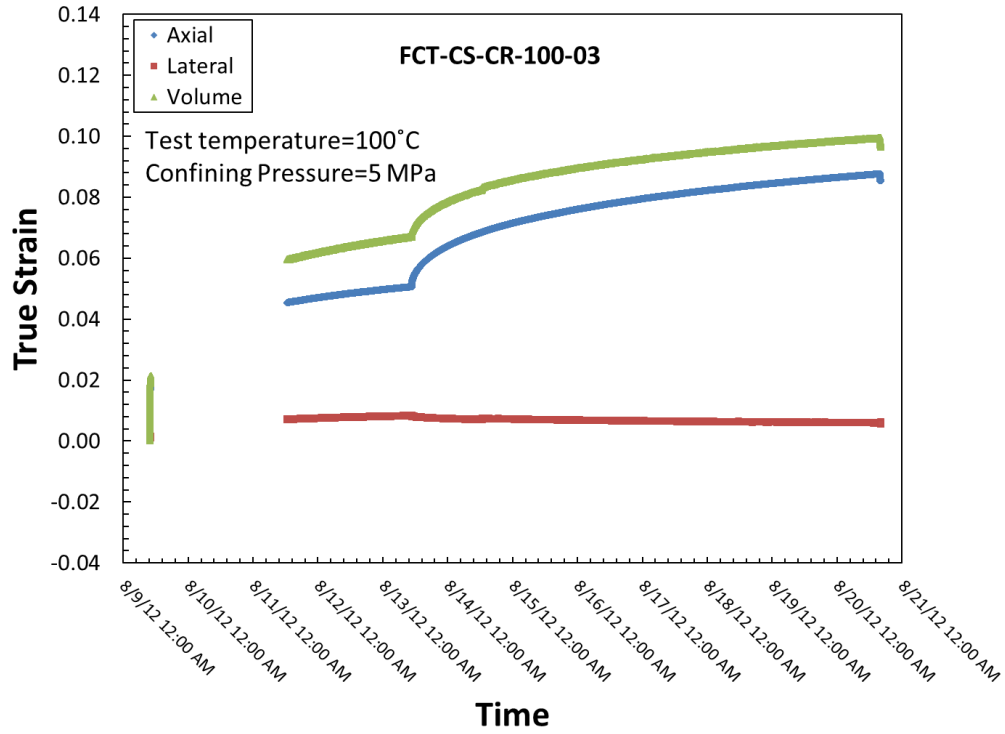
**A-11. FCT-CS-CR-100-02**



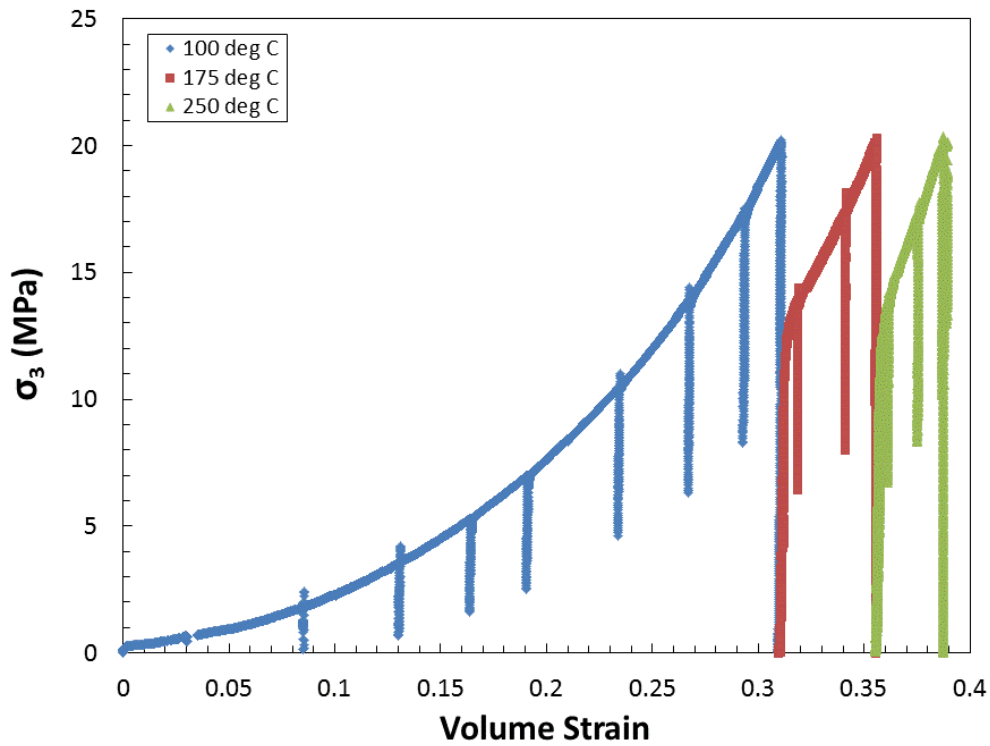


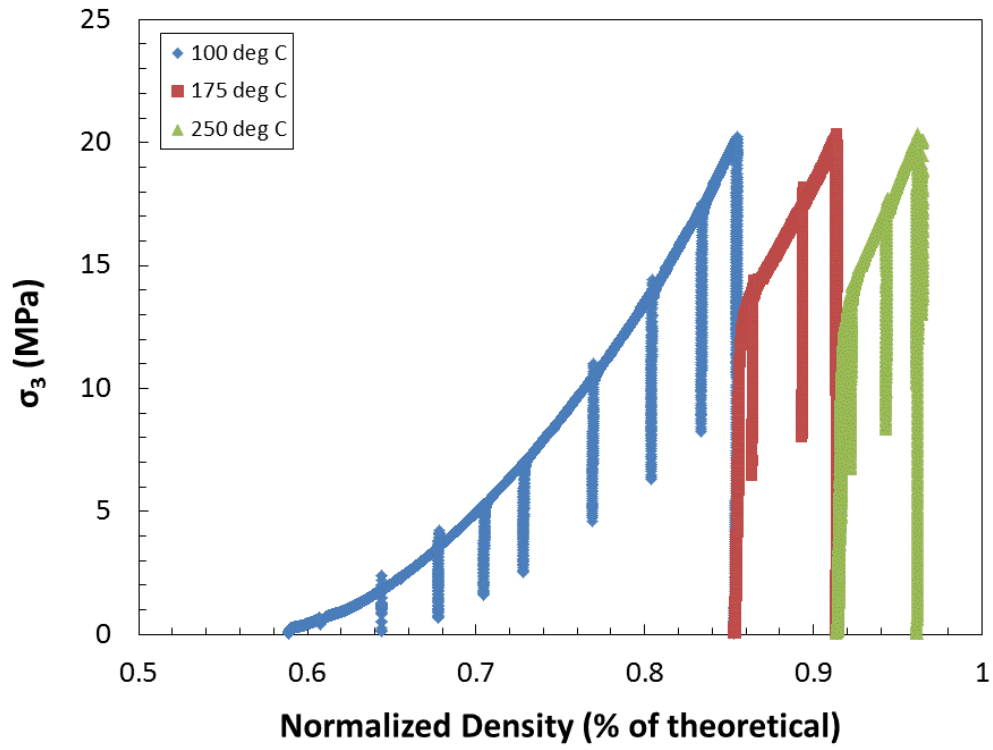
### A-12. FCT-CS-CR-100-03





**A-13. FCT-CS-HQ-ALL-01**





**A-14. FCT-CS-HQ-ALL-02**

